Semiclassical Quantization in a Smooth Potential Using Bogomolny's Quantum Surface of Section

by

Michael Richard Haggerty

Submitted to the Department of Physics
in partial fulfillment of the requirements for the degree of

Doctor of Philosophy in Physics

at the

MASSACHUSETTS INSTITUTE OF TECHNOLOGY

February 1994

Author .....
Department of Physics
13 September 1993

Certified by .....
Michel Baranger
Professor
Thesis Supervisor

Accepted by .....
George F. Koster
Chairman, Departmental Committee on Graduate Students

Semiclassical Quantization in a Smooth Potential Using Bogomolny's Quantum Surface of Section

by

Michael Richard Haggerty

Submitted to the Department of Physics
on 13 September 1993, in partial fulfillment of the
requirements for the degree of
Doctor of Philosophy in Physics

Abstract

An exploratory application of Bogomolny's recently proposed quantum surface of section method to the motion of a particle in a two-dimensional smooth potential is reported. In this method, a surface of section (SOS) is drawn through the system's classical phase space. The evolution of a wavefunction perpendicular to the SOS is computed semiclassically, by integrating an ensemble of classical trajectories from one crossing of the SOS to the next. That information is then summed into a transfer operator T, which is diagonalized to get its eigenvalues and eigenvectors. Eigenstates of the full quantum system occur at values of the parameters (like E or $\hbar$) for which T has an invariant state (an eigenvector with eigenvalue 1).

It is shown that T can be computed through a simple numerical integral over initial conditions of classical trajectories, with no problems of divergences. A technique is presented for taking advantage of a mirror symmetry present in the model system used. The algorithmic complexity of the method is estimated, as well as its dependence on system dimension and degree of chaos, and the number of eigenstates desired. In addition, the technique of solving for eigenvalues of $\hbar$ at constant energy is discussed at length, including its labor-saving advantages over solving for eigenenergies at fixed $\hbar$.

The numerical experiment involved the computation of hundreds of semiclassical eigenvalues of $\hbar$, along with the exact values, in both classically regular and classically chaotic energy regimes. Bogomolny's method was found to predict these values straightforwardly and in most cases unambiguously, with comparable errors in the two regimes. Neither do the errors seem to get worse for highly excited states. As a fraction of the ever-shrinking mean level spacing, however, the worst semiclassical errors increase with excitation number; nevertheless, the few hundred levels computed all have errors which have not yet reached one mean level spacing.

The two regimes are found to show marked differences in the behavior of the eigenvalues of the T operator. First, in the regular regime the eigenvalues follow smooth curves which connect quantum states with similar SOS properties; in the chaotic regime, the curves are bent and kinked and states on a single curve do not

share common properties. Second, the T operator eigenvalues are roughly grouped into two classes: those near the unit circle, which are associated with true quantum states, and those near the origin, which are not. In the chaotic regime, eigenvalues make the transition from one group to the other very quickly; in the regular regime, the transition is more gradual, with the result that the authenticity of a few percent of the semiclassical predictions is uncertain.

The surface of section wavefunctions are also computed and compared to the exact SOS wavefunctions, with good agreement.

Finally, a way to extract information about the actions of classical trajectories which contribute to a particular quantum state is discussed, and many examples of such "action spectra" are shown.

Thesis Supervisor: Michel Baranger
Title: Professor

Acknowledgments

I would like to thank my thesis advisor, Michel Baranger, for his inspiration, support, and creative suggestions during the course of this work. His warm personality and enthusiasm for subjects inside and outside of physics have done much to make the last couple years such a pleasure.

I would also like to thank Dawn Meredith, Bent Lauritzen, and Daniel Provost for many interesting discussions and much useful feedback. Our periodic get-togethers were engaging and educational, hopefully not only for me.

I want to express my appreciation to OS/2 programmer extraordinaire Eberhard Mattes, who is responsible for the excellent, free ports of both the GNU C++ compiler and the TEX compiler that were used extensively in the production of this thesis.

I am indebted to my family; they have always stood behind me and, even across great geographical distance, their support is unfailing.

Finally, I would like to thank Pia Kaiser. In my years at MIT, my most important discovery was Pia, my most rewarding collaboration our relationship, and my most inspiring revelation our love.

Contents

List of Figures

List of Tables

Chapter 1

Introduction

Semiclassical methods of quantizing certain types of Hamiltonian systems have been known since the discovery of quantum mechanics. Specifically, if a Hamiltonian is classically integrable (if it has as many constants of motion as degrees of freedom) then its trajectories are constrained to invariant tori, and EBK quantization can be applied. Quantization occurs when the action integrated along any closed loop on one of these tori satisfies:

$$\oint_{C_i} p \cdot dq = 2\pi\hbar(n_i + \mu_i/4),$$

where μ_i is an integer that counts the number of caustics along the trajectory. For 1-D Hamiltonians (all of which are integrable), the tori are just the periodic orbits, and the analogous WKB method can be applied; it yields accurate results with little effort, even for the ground state. However, integrable systems form only a subset of measure zero of all Hamiltonians systems; the fact that most famous, textbook examples are of the integrable sort is because they are easier to handle, not because nonintegrable systems are intrinsically less interesting.

Steps towards understanding how to quantize generic, *nonintegrable* systems semiclassically are more recent. The approach which currently dominates the field is the trace formula of Gutzwiller, which sums purely classical information about periodic orbits into an expression for the quantum mechanical density of states; the poles of

the expression indicate quantum eigenenergies [1, 2, 3, 4]. However, the number of periodic orbits increases exponentially with period—faster than the contributions of individual orbits decrease; thus the sum does not converge absolutely. A large volume of current research is devoted to developing clever tricks to reorder the sum in such a way that it converges to a useful answer, but the problem is not yet satisfactorily solved.

Recently, Bogomolny proposed an entirely different scheme to obtain eigenstate information in the semiclassical limit by using a quantum surface of section (SOS) [5]. His method, which is the primary topic of this thesis, will be specified precisely and discussed at length in subsequent chapters; for now, we will try to present a conceptual overview while avoiding unnecessary details.

A quantum surface of section is akin to the classical Poincaré surface of section, which has proven so useful to classical dynamicists both practically and theoretically. A classical Poincaré SOS is a surface drawn through a system's phase space; the trajectory of interest is computed and each time that it pierces the surface in a prespecified direction, the point where the crossing occurred is noted. The pattern of points produced by a succession of crossings gives information about the nature of the trajectory—for example whether it is periodic, quasi-periodic, or chaotic. SOS's are most useful for systems that have two degrees of freedom; such a system has a four dimensional phase space and a three dimensional energy shell, but only a two dimensional surface of section (the most convenient dimensionality for plotting and viewing).

Bogomolny's quantum surface of section is similarly a surface drawn through the configuration space of the corresponding classical Hamiltonian. Again classical trajectories are integrated from one crossing until the next same-direction crossing of the surface. But now, instead of only marking the points where the trajectories cross the surface, one also notes the semiclassical phase $\exp(iS/\hbar)$ which has accumulated since the previous crossing ($S = \int \vec{p} \cdot d\vec{q}$ is the action accumulated along the trajectory). Such information, for all classical orbits of one Poincaré mapping and some energy E, is summed together and projected onto the coordinate part of the

SOS into a *transfer operator* T which will be defined below. The projection process discards the momentum information normally associated with a classical surface of section, and T correspondingly operates on functions of one variable fewer than the number of degrees of freedom in the system (namely, the Poincaré section's position coordinates).

Since T only requires information about trajectories of one Poincaré mapping, it is well defined in terms of only finite quantities. Therefore, there are no problems at all, neither theoretical nor practical, with divergences in Bogomolny's technique. The T matrix can be computed to arbitrary accuracy, requiring (as we shall see) only a two dimensional numerical quadrature of finite-time orbits. This very attractive attribute is one which is not posessed by the Gutzwiller trace formula, which is plagued by the exponentially growing number of periodic orbits of increasing period.

Conceptually, T gives the evolution of a quantum mechanical wave function from one intersection with the SOS to the next. In this regard T is akin to a Green function in the energy representation. T operates on functions $|\psi\rangle$ which live on the coordinate part of the surface of section:

$$|\psi'\rangle = T\,|\psi\rangle\,.$$

$|\psi\rangle$ has the value of the full quantum mechanical wavefunction where the latter intersects the surface of section. T applied to $|\psi\rangle$ produces, roughly speaking, the image of $|\psi\rangle$ after one Poincaré mapping. Eigenstates of the quantum system occur for values of adjustable parameters (which we call α, but could be for example E or $\hbar$) for which T_α has an invariant state:

$$T_\alpha\,|\psi\rangle = |\psi\rangle \tag{1.1}$$

i.e. they occur whenever T_α has an eigenvalue which is equal to unity. So to find the eigenstates of a quantum mechanical system, one computes T, diagonalizes it to find its eigenvalues, and plots those eigenvalues in the complex plane for a range of α. Whenever one of the eigenvalues crosses through 1, then *at the corresponding set of parameters α, the quantum mechanical system is predicted to have an eigenstate.*

We know of four other calculations to date that use Bogomolny's technique. Lau-

ritzen [6], by resorting to a stationary phase integral, showed that Bogomolny's quantization condition (1.1) reduces to EBK quantization for integrable systems in general, and the rectangular billiard in particular. Bogomolny and Carioli [7] applied the method to a "surface of constant negative curvature" with vanishing potential energy; this is a billiard-type chaotic system whose orbits can also be written down explicitly.

Szeredi, Lefebvre, and Goodings [8] used the quantum SOS in their study of the wedge billiard, a scalable system bounded on two sides by straight hard walls and confined in the open direction by a uniform downward gravity-like force. This system has four types of orbits of one Poincaré mapping, which can be written down; they summed these orbits into a T matrix in a basis of position-space cells and were able to reproduce the first twenty quantum eigenvalues with an average RMS error of 6.5% of the mean level spacing.

Finally, Boasman in his thesis [9] thoroughly investigates, in a largely analytic way, the asymptotic accuracy that Bogomolny's method achieves for billiard problems, and supports his predictions with evidence from numerical calculations.

Each of the previous calculations were restricted to non-generic systems—integrable systems or billiards (or integrable billiards). There is, of course a reason for preferring billiards: they are scalable systems whose classical trajectories are the same regardless of energy, many chaotic billiards are known, and, most importantly, one can write down explicit formulas for the classical trajectories connecting any two points on the surface of section. On the other hand, billiards are thought to have different convergence properties than do smooth potentials. Moreover, smooth potentials—not billiards—are the kind typically encountered in models of natural systems, so it is interesting to know how well they can be handled with new methods.

Therefore, we chose to undertake our research in this more challenging laboratory—the smooth Hamiltonian system. The centerpiece of this thesis is a computational application of Bogomolny's method to the Nelson_2 potential (see Appendix B),

a smooth, bounded, nonlinear oscillator with Hamiltonian

$$H = \tfrac{1}{2}\left(p_x^2 + p_y^2\right) + \tfrac{1}{2}\omega^2 x^2 + \tfrac{1}{2}\left(y - \tfrac{1}{2}x^2\right)^2$$

The system is non-scalable, and has a rich periodic orbit structure [10]. For low energies, it approaches a 2-D anisotropic harmonic oscillator, and is predominantly regular; as the energy is increased, the degree of chaos increases and eventually dominates the phase space; we will present computations in both regimes to illuminate the similarities and differences.

This paper is organized as follows: Section 2.1 outlines the idea of Bogomolny that is the subject of this paper. Section 2.2 develops various expressions for T which offer a somewhat different perspective on its operation, and which translate directly into an algorithm for computing T. Section 2.3 shows how to take advantage of a mirror symmetry when computing T. Section 2.4 estimates the effort needed to apply Bogomolny's method, as compared with traditional methods. Section 2.5 explains a trick which enables Bogomolny's theory to be verified with less numerical effort than a naive approach would require. Chapter 3 discusses the nature of eigenclassicity problems in general, and provides details of how the exact eigenclassicity spectrum was calculated for the Nelson_2 system. Section 4.1 introduces the model system to which we applied Bogomolny's method. Section 4.2 gives some of the behind-the-scenes details about our implementation of the semiclassical computation. Section 4.3 qualitatively describes the behavior of the eigenvalues of the T operator. Section 4.4 presents the eigenclassicity spectra produced by Bogomolny's method, and compares them to exact spectra in both the regular and the chaotic regime. Section 4.5 tells how the surface of section wavefunctions can be obtained from the theory, and makes some comments about how well they are predicted. Finally, Chapter 5 discusses a way to extract information about which classical trajectories have the strongest influence on particular quantum eigenstates.

A comment about nomenclature: we will be dealing with two related but distinct eigenproblems—Bogomolny's condition on the T_α operator (Eq. (1.1), and the time

independent Schrödinger equation for the full quantum mechanical system. In order to reduce confusion, we assume the following naming convention: the terms *eigenvalues* and *surface of section eigenfunctions* in this paper always refer to quantities obtained from diagonalizing the T_α operator. It should be kept in mind that T_α and its eigenvalues can be computed for any choice of parameters α, whether or not an eigenstate of the quantum system exists for those parameters. The words *eigenenergies*, *eigenclassicities* (explained below), and *eigenstates* all refer to energy eigenstates of the full quantum mechanical Hamiltonian. These eigenstates only exist for special values of the parameters α—in fact, only those for which T has a unit *eigenvalue*, according to Bogomolny's theory.

Chapter 2

Theory

2.1 The results of Bogomolny

Bogomolny [5] gives an expression for the transfer operator T for systems of any dimension and using any surface of section. Our interests are narrower, since the systems for which we will be doing computations are symmetric about the y-axis, and the y-axis will be used as the surface of section. In this case, the expression for T can be written:

$$\langle y'|\, T\, |y\rangle = \frac{1}{(2\pi i\hbar)^{1/2}} \sum_{\text{cl.tr.}} \left| \frac{\partial^2 S(y',y)}{\partial y\, \partial y'} \right|^{1/2} e^{-i\pi\nu/2} \exp i\frac{S(y',y)}{\hbar} \tag{2.1}$$

T can be calculated for any chosen value E of energy. The sum is over all classical trajectories which have that energy, and which start at $(0,y)$ and end at $(0,y')$ one Poincaré mapping later (that is, with no intervening same-direction piercings of the SOS). (See figure 2-1.) $S(y',y) \equiv \int_y^{y'} \vec{p}\cdot d\vec{q}$ is the classical action along the trajectory considered. The second derivative of S which appears gives the degree of focusing of nearby trajectories onto the current trajectory. The focusing switches sign each time that there is a perfect re-convergence of nearby trajectories, which would lead to a branch cut ambiguity when its square root is taken; therefore, its absolute value is taken and the phase is put in separately through the Maslov index ν, which counts the number of sign changes in the focusing (note: its role is a bit subtler in higher

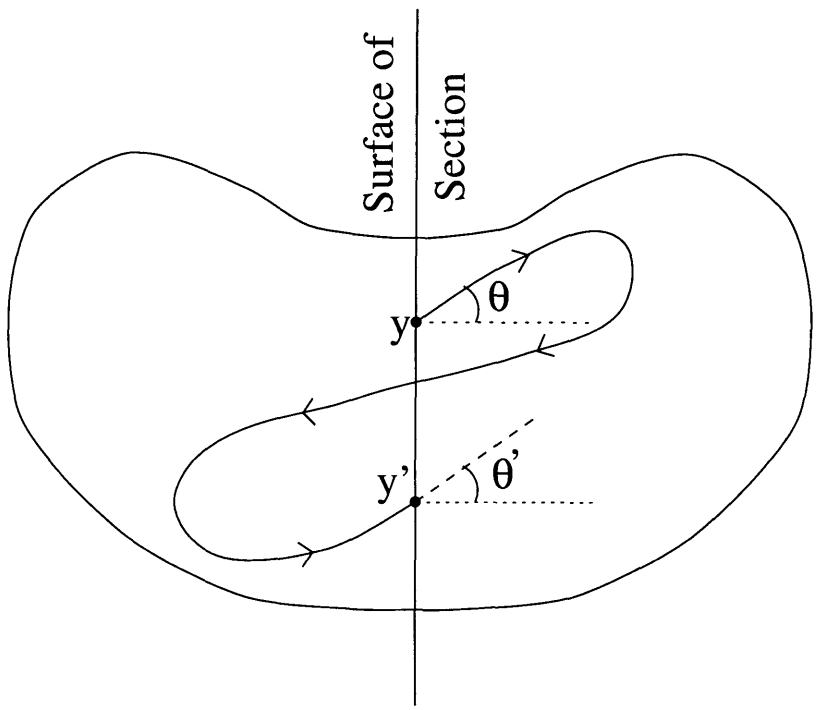

Figure 2-1: Orbits which contribute to the semiclassical transfer operator. In Bogomolny's construction, the trajectories which contribute are those of one complete Poincaré section: they are integrated from one intersection with the y-axis until the next intersection that occurs in the same direction.

dimensions; see [11]).

Bogomolny's construction of the T operator begins by dividing the allowed portion of phase space into two subregions "1" and "2", one on either side of the surface of section. In each half, a Green function $G_{1,2}$ is constructed which (i) obeys Schrödinger's equation in that subregion, (ii) is arbitrary on the SOS, and (ii) obeys the same boundary conditions as the true wavefunctions on the remainder of the boundary of that subregion. The next step is to write the wavefunctions in terms of the Green functions and a source function $\psi_{1,2}(y)$ on the surface of section:

$$\Psi_{1,2}(x,y) = \int_\Sigma dy'\, G_{1,2}(x,y;y';E)\psi_{1,2}(y').$$

This equation, plus the demand that Ψ_1 and Ψ_2 match on the SOS and satisfy the Schrödinger equation in region 1 or 2 respectively, lead to the self-consistency requirement that $\psi_1(y)$ satisfy

$$\int_\Sigma dy'\, \tilde{G}(x,y;y';E)\psi_1(y') = 0 \tag{2.2}$$

where

$$\begin{aligned}\tilde{G}(x,y;y';E) \quad &= \frac{\hbar^2}{2}\int_\Sigma dy' \\ &\times \left(G_1(0,y;y';E)\frac{\partial}{\partial n}G_2(x,y;y';E) - G_2(x,y;y';E)\frac{\partial}{\partial n}G_1(0,y;y';E)\right)\end{aligned}$$

and n is the outward-directed normal at point $(0,y)$.

For points on the surface of section, it is straightforward to write down the expression for $\tilde{G}$ in the semiclassical limit in terms of a sum over classical trajectories of one Poincaré mapping:

$$\begin{aligned}\tilde{G}(y'';y';E) \;&=\; \sum_{\text{cl.tr.}} \frac{1}{i\hbar(2\pi i\hbar)^{1/2}}\left|\frac{1}{|p''|\,|p'|}\frac{\partial^2 S}{\partial y''\partial y'}\right|^{1/2} \\ &\times \exp\left(\frac{i}{\hbar}S(y'',y';E) - i\frac{\pi}{2}\nu\right)\end{aligned}$$

A few more unilluminating steps transform the consistency condition (2.2) into

$$\det(1 - T) = 0,$$

where T is given by equation (2.1).

Bogomolny also gives some of the properties of the T operator, and proves them in the classical limit $\hbar \to 0$. His most important of these subsidiary claims is that the T operator is unitary; that is, in the limit $\hbar \to 0$,

$$TT^{\dagger} = 1.$$

This is, to be sure, a strange sort of unitarity, in light of his other claim that the dimension of T varies smoothly with parameters (such as energy); specifically, he says that

$$\dim T_{\alpha} = \frac{\text{volume of allowed phase space on the Poincaré surface}}{(2\pi\hbar)}. \tag{2.3}$$

The mechanism by which these two phenomena coexist will be examined in detail in the context of our numerical experiment (Sec. 4).

There are other interesting subjects covered in Bogomolny's paper, such as the relationship between T and the Selberg zeta function, and his prescription for computing full quantum mechanical eigenfunctions; we will not address those challenges in this paper, beyond presenting computations of *surface of section* wavefunctions predicted by the theory and comparing them to the exact SOS wavefunctions.

2.2 Computing the T operator: Avoiding the shooting problem

Each of the coordinate-space matrix elements of T in expression (2.1) above is a sum over classical trajectories of energy E which go from $(0, y)$ to $(0, y')$ in one Poincaré mapping. But to find these trajectories, it would be necessary to find all values of the

initial momentum $\vec{p} = (p\cos\theta, p\sin\theta)$ that cause a trajectory launched from y to next intersect the SOS at y'. Even though the momentum magnitude $p = \sqrt{2(E - V(0,y))}$ is fixed by the choice of energy, one would still have to solve a shooting problem—a (numerical) search in θ space to find the launching angles which cause the particle to end up at y'.

But this can be avoided. Consider: any properly chosen surface of section has the property that every trajectory eventually pierces it. As a function of initial conditions (on the SOS), call the next crossing point $Y'(y,\theta,E)$. It follows that *every* trajectory of the appropriate energy contributes to T; if it starts at $(0,y)$ with angle θ, for example, it contributes to $\langle Y'(y,\theta,E)|\, T\,|y\rangle$. This observation suggests that we transform (2.1) from a sum over endpoints into an integral over initial conditions.

Executing the desired transformation is possible and indeed straightforward. First we write a more useful expression for the partial derivative which appears in Eq. (2.1), being explicit about which variables are held constant:

$$\begin{aligned}
\frac{\partial^2 S(y',y)}{\partial y\,\partial y'} &\equiv \left[\frac{\partial}{\partial y'}\left(\frac{\partial S(y',y)}{\partial y}\right)_{y'E\Sigma}\right]_{yE\Sigma} \\
&= \left[\frac{\partial}{\partial y'}(-p_y)\right]_{yE\Sigma} \\
&= -\left[\frac{\partial y'}{\partial p_y}\right]^{-1}_{yE\Sigma}
\end{aligned}$$

Here we use a subscript of "Σ" to remind ourselves that the surface of section is meant to be fixed during the differentiation—in our case, $x = x' = 0$. The second line follows from the well-known identity $(\partial S/\partial y)_{y'E} = -p_y$.

As a function of initial conditions y and θ,

$$\left[\frac{\partial y'}{\partial p_y}\right]_{yE\Sigma} = \left[\frac{\partial Y'(y,\theta,E)}{\partial p_y}\right]_{yE\Sigma} = \left[\frac{\partial Y'}{\partial \theta}\right]_{yE\Sigma}\left[\frac{\partial \theta}{\partial p_y}\right]_{yE\Sigma} = \frac{1}{p_x}\left[\frac{\partial Y'}{\partial \theta}\right]_{yE\Sigma}.$$

Substituting into Eq. (2.1) and integrating out the basis states on the LHS, we have

$$T = \frac{1}{(2\pi i\hbar)^{1/2}} \int dy \int dy' \sum_{\text{cl.tr.}} |p_x|^{1/2} \left| \frac{\partial Y'}{\partial \theta} \right|_{yE\Sigma}^{-1/2} e^{iS/\hbar - i\pi\nu/2} \, |y'\rangle \langle y| \,. \tag{2.4}$$

Now we notice that the sum over classical trajectories which go from y to y' in one Poincaré mapping is equivalent to a sum over the discrete values θ_i which solve the shooting problem $y' = Y'(y, \theta_i, E)$ for the present values of y, y', and E. Schematically, we express that statement with the following equalities, which hold no matter what expression is inserted in the braces:

$$\begin{aligned} \sum_{\text{cl.tr.}} \left\{ \cdots \right\} &\equiv \sum_i \left\{ \cdots \right\} \Big|_{\theta_i} \\ &= \int d\theta \sum_i \delta(\theta - \theta_i) \left\{ \cdots \right\} \Big|_{\theta} \\ &= \int d\theta \left| \frac{\partial Y'(y, \theta, E)}{\partial \theta} \right|_{yE\Sigma} \delta(y' - Y'(y, \theta, E)) \left\{ \cdots \right\} \Big|_{\theta} . \end{aligned}$$

When we apply this identity to equation (2.4), the δ-function allows us to do the y' integral immediately:

$$\begin{aligned} T &= \frac{1}{(2\pi i\hbar)^{1/2}} \int dy \int d\theta \; |p_x|^{1/2} \left| \frac{\partial Y'(y, \theta, E)}{\partial \theta} \right|_{yE\Sigma}^{1/2} \\ &\quad \times \exp\left(i \frac{S(y, \theta)}{\hbar} - i \frac{\pi}{2} \nu \right) |Y'(y, \theta, E)\rangle \langle y| \end{aligned} \tag{2.5}$$

The result is an expression for T which can be evaluated without solving any shooting problems—a reduction of numerical effort. Moreover, this expression more closely represents our intuitive picture of the effect of T than does Eq. (2.1); that is, when T is applied to an initial surface of section wavefunction $|\psi\rangle$,

1. it breaks up $|\psi\rangle$ into its components at each position y;

2. each of these components becomes an ensemble of classical particles, launched in all directions θ;

3. the particles follow the classical equations of motion (accumulating quantum

mechanical phase as they go) until they hit the surface of section again;

4. the phases of the particles are summed together (with a weighting factor) to yield the new SOS wavefunction $|\psi'\rangle$.

It is equation (2.5) which formed the starting point for our numerical work.

Note that the partial derivative appearing in equation (2.5) is not computed directly, but rather from elements of the linearized tangent matrix, which can be computed efficiently using techniques similar to those described by Eckhardt and Wintgen [12] for computing the monodromy matrix. (The slight difference is that the monodromy ("once around") matrix only applies to periodic orbits, but we need to calculate stabilities at arbitrary times on non-periodic orbits.)

2.3 Removing symmetries

Remember that the T operator as defined above gives the evolution of a SOS wavefunction from one crossing of the SOS to the next *same-direction* crossing. But one might think that it would be also possible to write T as the composition of two operators: a T_1, which performs the evolution to the first crossing of the surface of section (which is in the *"wrong"* direction), followed by a T_2, which performs the second half of the evolution (to the second crossing, which is the first *"proper,"* same-direction crossing). See figure 2-2. The proof of this fact is the subject of the present section; effectively, we need to unravel the last part of Bogomolny's derivation of the T operator.

We begin by writing the expressions for two operators T_1 and T_2, the forms of which are exactly analogous to Eq. 2.1 (though we rearrange them for convenience):

$$\begin{aligned} T_1 &= \frac{1}{(2\pi i\hbar)^{1/2}} \int dy_1' \int dy_1 \sum_{y_1 \to y_1'} \left| \frac{\partial^2 S_1(y_1', y_1)}{\partial y_1 \, \partial y_1'} \right|^{1/2} e^{-i\pi\nu_1/2} \\ &\quad \exp\left(i \frac{S_1(y_1', y_1)}{\hbar} \right) |y_1'\rangle \langle y_1| \\ T_2 &= \frac{1}{(2\pi i\hbar)^{1/2}} \int dy_2'' \int dy_2' \sum_{y_2' \to y_2''} \left| \frac{\partial^2 S_2(y_2'', y_2')}{\partial y_2' \, \partial y_2''} \right|^{1/2} e^{-i\pi\nu_2/2} \end{aligned}$$

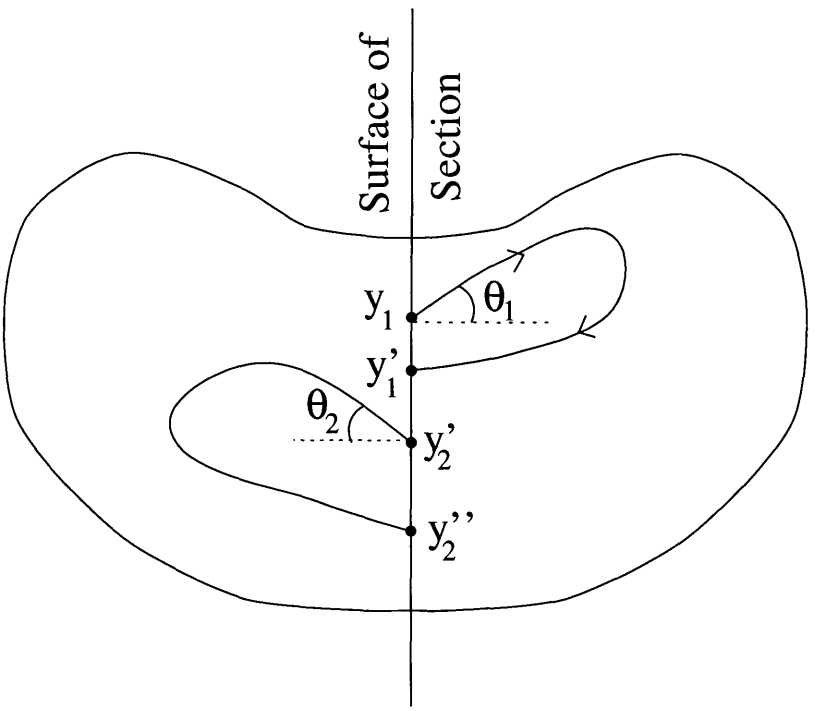

Figure 2-2: Half-Poincaré mapping trajectories which contribute to T_1 and T_2. In the text it is shown that, to within a stationary phase approximation, the transfer operator T can be written as the product of T_1 and T_2, each of which is a sum over "half-Poincaré mapping" trajectories on one side or the other of the SOS, such as those drawn here. The stationary phase approximation tells us that the strongest contributions to the product will come from pairs of half trajectories which join smoothly at the surface of section into a full-mapping trajectory.

$$\exp\left(i\frac{S_2(y_2'',y_2')}{\hbar}\right)|y_2''\rangle\langle y_2'|$$

where the classical trajectories $y_1 \to y_1'$ and $y_2' \to y_2''$ are on opposite sides of the SOS and correspond to "half" Poincaré mappings (that is, from one SOS crossing to the next, *opposite direction*, crossing). See Fig. 2-2.

Now we show that the product T_2T_1 is equal to T. The δ-function $\langle y_2'|\, y_1'\rangle$ allows us to perform one of the integrals immediately (and then drop the subscripts on the y's), yielding:

$$\begin{aligned} T_2T_1 &= \frac{1}{2\pi i\hbar}\int dy''\int dy'\int dy \sum_{y'\to y''}\sum_{y\to y'}\left|\frac{\partial^2 S_2(y'',y')}{\partial y'\,\partial y''}\right|^{1/2}\left|\frac{\partial^2 S_1(y',y)}{\partial y\,\partial y'}\right|^{1/2} \\ &\quad \times e^{-i\pi(\nu_2+\nu_1)/2}\exp\frac{i}{\hbar}\left(S_2(y'',y')+S_1(y',y)\right)|y''\rangle\langle y| \end{aligned} \tag{2.6}$$

We next do the y' integration using the stationary phase approximation; the only significant contribution is when

$$\begin{aligned} 0 &= \frac{\partial}{\partial y'}\left[S_2(y'',y')+S_1(y',y)\right]_{y,y'',E} \\ &= \left[-p_{2,y}'+p_{1,y}'\right] \end{aligned} \tag{2.7}$$

which requires that the final momentum of the first part of the trajectory equals the initial momentum of the second part. In other words, only classical trajectories smoothly connecting $y \to y''$ contribute significantly to the full transfer matrix T (as expected). At those points, the stationary phase approximation gives an additional factor of

$$\left|\frac{\partial^2}{\partial y'^2}\left[S_2(y'',y')+S_1(y',y)\right]_{y,y'',E}\right|^{-1/2}$$

in the integrand of equation (2.6).

It remains only to show that the new combined prefactor of Eq. (2.6) matches that of Eq. (2.1); i.e. that

$$\frac{\frac{\partial^2 S_1}{\partial y\,\partial y'}\frac{\partial^2 S_2}{\partial y''\,\partial y'}}{\frac{\partial^2 S_1}{\partial y'^2}+\frac{\partial^2 S_2}{\partial y'^2}} \stackrel{?}{=} \pm\frac{\partial^2 S(y'',y)}{\partial y\,\partial y''}. \tag{2.8}$$

To this end we define the function $Y'(y, y'')$ which gives the values of y' for classical trajectories smoothly connecting y to y'' in one Poincaré mapping. We then note that equation (2.7) is valid for any values of y and y'' as long as we evaluate it at $y' = Y'(y, y'')$, and so we write down that equation's derivatives with respect to y and y'':

$$0 = \left(\frac{\partial^2 S_1}{\partial y'^2} + \frac{\partial^2 S_2}{\partial y'^2}\right)\frac{\partial Y'}{\partial y} + \frac{\partial^2 S_1}{\partial y\,\partial y'} \tag{2.9}$$

$$0 = \left(\frac{\partial^2 S_1}{\partial y'^2} + \frac{\partial^2 S_2}{\partial y'^2}\right)\frac{\partial Y'}{\partial y''} + \frac{\partial^2 S_2}{\partial y''\,\partial y'} \tag{2.10}$$

In the current nomenclature, the action that enters the expression for T is

$$S(y'', y) = S_2(y'', Y'(y, y'')) + S_1(Y'(y, y''), y);$$

we will need its second partial derivative, which we can obtain using the chain rule and Eq. (2.7):

$$\frac{\partial^2 S(y'', y)}{\partial y\,\partial y''} = \frac{\partial^2 S_1}{\partial y\,\partial y'}\frac{\partial Y'}{\partial y''} + \frac{\partial^2 S_2}{\partial y''\,\partial y'}\frac{\partial Y'}{\partial y} + \left(\frac{\partial^2 S_1}{\partial y'^2} + \frac{\partial^2 S_2}{\partial y'^2}\right)\frac{\partial Y'}{\partial y}\frac{\partial Y'}{\partial y''} \tag{2.11}$$

Using Eqs. (2.7), (2.9), (2.10), and (2.11), it is trivial to establish that the equality holds in (2.8) when the minus sign is chosen. Therefore we have established that, to within a stationary phase approximation,

$$T \overset{\text{SPA}}{=} T_2 T_1.$$

Thus T can be decomposed into "half-Poincaré mapping operators" T_1 and T_2, as we hoped.

There will be a numerical efficiency gain from using this decomposition for any chaotic potential, regardless of symmetry, for the following reason. The computation of T requires doing an integral over the initial conditions y and θ. The integrand, however, involves functions such as $Y'(y, \theta)$, which is the point that a trajectory next intersects the SOS. To get better than Monte-Carlo quality convergence of the integral, these functions must be sampled on a fine enough mesh that their variation as

a function of initial conditions is sampled. In a chaotic regime, where nearby trajectories diverge exponentially in time, the divergence of nearby half trajectories will be roughly the square root of the divergence of full trajectories, and so, roughly, only the square root of the number of mesh points will need to be used. Thus two coarser meshes of half-length classical trajectories will be adequate to compute T_1 and T_2, and then those operators (in the form of matrices) can be multiplied to yield T. In fact, we suspect that the product T_2T_1 will yield even *better* estimates of the eigenvalues of the system due to the fact that it is "one stationary phase approximation closer" to the exact Feynman path integral underpinning the semiclassical approximations.

We use the T_2T_1 approach in our numerical computations below. In our case we realize an even more dramatic increase in numerical efficiency when we use the T_2T_1 approach: because our potential is symmetric with respect to reflection about the surface of section, $T_1 \equiv T_2$. Therefore in addition to the less dense mesh of trajectories that need to be calculated, the second half of the trajectories need *never* be calculated! Moreover there is no need to multiply $T_1 \cdot T_1$; our criterion that T have an eigenvalue of 1 is equivalent to the requirement that T_1 have an eigenvalue of $+1$ *or* -1. The sign of the eigenvalue tells us the parity of the associated eigenstate of the system with respect to reflection about the SOS.

Formally this reduction to the fundamental domain is equivalent to solving the half-domain problem with two different boundary conditions: first with a soft wall at the SOS, and second with a hard wall. The latter case is the one which produces odd-parity eigenstates, as follows: each trajectory has one reflection from the wall, and thus an additional phase of π appears through its Maslov index; this makes $T_{\text{hard}} = (-1)T_1$. In this picture quantization occurs when T_{hard} has an eigenvalue of 1, so, as above, these odd-parity states occur when T_1 has an eigenvalue of (-1).

Throughout the rest of the paper, we use the desymmetrized transfer operator T_1 in our computations, and we drop the subscript.

It is interesting to comment that another stationary phase approximation, similar to the one which established that $T = T_2T_1$, would produce the Gutzwiller periodic orbit formula, the better-known device for semiclassically quantizing chaotic systems.

From this vantage point it is easy to conjecture that the transfer matrix approach, which is "one stationary phase approximation closer" to Feynman path integration than is the periodic orbit formula, will yield correspondingly better estimates of quantum properties of the system than does the trace formula for a comparable amount of effort or a comparable number of input classical trajectories. Unfortunately the implementations of the two methods differ so completely that comparisons based on "equal effort" will be tricky and this conjecture will not be tested in the present paper.

2.4 Algorithmic complexity of method

The algorithm which needs to be followed to compute a system's spectrum follows from equation (2.5). We now give a crude estimate of the computational effort required to get the first N eigenstates of a d-degree of freedom system which has instability exponent λ—more precisely, we give the scaling of the effort with those quantities. We ignore the common situation that the degree of classical chaos varies with excitation number N because the nature of this interdependence is very system-specific. The lack of dependence assumed here is, incidentally, appropriate in the case of our own numerical experiment, in which energy is held constant (as will be explained in section 2.5); however, a specialized trick that we use means that the work that our experiment requires is less than the estimates developed in this section anyway. In character with the rest of this section, we will not attempt to give a precise definition of λ, except to say that it should measure the "typical" separation of two nearby orbits during one Poincaré mapping, as follows:

$$|\vec{y}_2' - \vec{y}_1'| \sim e^{\lambda} |\vec{y}_2 - \vec{y}_1|$$

The Nth excited state has a de Broglie wavelength which is $\lesssim \mathcal{O}(N^{-1/d})$, the estimate coming from counting the number of nodes that would fit in a container with rigid walls. Computing T requires that enough classical trajectories be calculated to capture the dynamics of the full energy shell with a resolution comparable to the

de Broglie wavelength of the Nth state: if the trajectories are started from a mesh of initial conditions with spacings in positions and momenta proportional to Δ, we need

$$\mathcal{O}(\Delta \cdot e^{\lambda}) \lesssim \mathcal{O}(N^{-1/d})$$

so

$$\Delta \lesssim \mathcal{O}(N^{-1/d} e^{-\lambda})$$

The mesh needs to include all trajectories of energy E which start on the SOS, a surface of dimension $(2d-2)$. This is thus also the dimension of the mesh of initial conditions, so the number of classical trajectories which need to be calculated is

$$\mathcal{O}(\Delta^{-2(d-1)}) \sim \mathcal{O}(N^{2(1-1/d)} e^{2\lambda(d-1)}).$$

Each trajectory must in general be integrated numerically. The number of time steps necessary depends on the details of the potential; a reasonable estimate is that it also scales like the reciprocal of the mesh spacing, $\mathcal{O}(\Delta^{-1})$. Thus the computational effort of computing the necessary trajectories is the number of trajectories times the number of time steps per trajectory, or

$$\mathcal{O}(\Delta^{-(2d-1)}) \sim \mathcal{O}(N^{2-1/d} e^{\lambda(2d-1)}).$$

Then the T operator must be constructed from the information about the trajectories. T operates on functions on the spatial part of the surface of section; these functions have $(d-1)$ dimensions—one fewer than eigenstates of the full quantum system. In practice, the matrix elements $\langle n_1 | T_\alpha | n_2 \rangle$ will be calculated in some basis fine enough to capture details the size of the de Broglie wavelength, in $(d-1)$ dimensions—that requires $\dim T \sim \mathcal{O}(N^{1-1/d})$ basis states, so that T has the square of that or $\mathcal{O}(N^{2(1-1/d)})$ matrix elements. If T is to be calculated in a generic basis, then each of its matrix elements needs to be updated for each trajectory; a job of complexity $\mathcal{O}(N^{4(1-1/d)} e^{2\lambda(d-1)})$. We can reduce this if we choose trajectories and basis sets more carefully:

If the mesh of initial conditions is rectangular, the job becomes somewhat easier because we can compute

$$T\,|\vec{y}\rangle$$

for each initial $\vec{y}$ as an integral over initial momenta, and only then sum the whole row into the T matrix; this optimization reduces the complexity to $\mathcal{O}(N^{3(1-1/d)}e^{2\lambda(d-1)})$.

Even better is to choose to compute T in a position basis (that is, positions covering the surface of section). In this case, a particular trajectory only contributes to a single matrix element of T (or at most a few depending the rounding scheme). Thus updating the T matrix need not take more than constant time for each trajectory, and this part of the algorithm is reduced from being fatally expensive to being almost incidental—only $\mathcal{O}(N^{2(1-1/d)}e^{2\lambda(d-1)})$.[1]

Next the T matrix needs to be diagonalized, with effort that goes with the cube of the size of the matrix, $\mathcal{O}(N^{3(1-1/d)})$. In this step Bogomolny's method has an advantage over a brute-force diagonalization of the Hamiltonian, which requires a matrix with size $\mathcal{O}(N)$ and effort $\mathcal{O}(N^3)$.

Finally, α must be scanned to find parameter values which yield eigenstates. This procedure requires $\mathcal{O}(N)$ repetitions of each of the above steps.

A grand total of the computational effort required to apply Bogomolny's method incorporates all of the above estimates:

$$\begin{aligned} \text{effort} &\sim \mathcal{O}([\underbrace{N^{2-1/d}e^{\lambda(2d-1)}}_{\text{calc. trajectories}} + \underbrace{N^{2(1-1/d)}e^{2\lambda(d-1)}}_{\text{update } T} + \underbrace{N^{3(1-1/d)}}_{\text{diagonalize } T}] \cdot \underbrace{N}_{\text{scan } \alpha}) \\ &\sim \mathcal{O}(N^{3-1/d}e^{\lambda(2d-1)} + N^{4-3/d}) \end{aligned} \tag{2.12}$$

(the second line summarizes the terms that dominate in different limits). Understanding this expression gives us important information about the practicality of Bogomolny's method.

First, the time needed to diagonalize the T matrix does not dominate when cal-

[1] Unfortunately, although we used the first optimization, we didn't notice the second one until our computations (in an oscillator basis) were finished, so updating the T matrix was the most expensive part of the computational cost—though not prohibitively so.

culating highly excited states of two degree of freedom systems; this is contrasted to the case of matrix mechanics where diagonalizing the Hamiltonian is virtually *all* of the work. The reason is that the T matrix is smaller than the Hamiltonian; it operates on functions which have one dimension fewer than the full quantum mechanical eigenstates so a smaller basis set is adequate. However, for systems with more than two degrees of freedom, diagonalizing T is the dominant part of the work of the algorithm; the advantage of smaller matrix size is overtaken by the disadvantage that the matrix must be diagonalized $\mathcal{O}(N)$ times.

Second, the effort of implementing the semiclassical method increases with increasing chaos (λ), a fact which should be obvious given that the method relies on classical trajectories. By contrast, the dependence of the effort of a direct diagonalization of H on λ is less explicit. As the degree of chaos is increased, it typically becomes necessary to include more and more quantum mechanical basis states in the matrix representation of the Hamiltonian in order to get the same number of eigenenergies to converge. Therefore, in practice matrix mechanics also becomes more effort as the degree of chaos is increased. Nevertheless, a quantitative estimate of the scaling would be tricky and will not be attempted here.

Third, comparing expression (2.12) against the matrix mechanical result of $\mathcal{O}(N^3)$, we see that Bogomolny's method should be *faster* than matrix diagonalization at getting high-N states when $d = 2$, comparable when $d = 3$, and poorer for $d \geq 4$.

2.5 Searching for eigen*classicities* instead of eigenenergies

So far we have been coy about specifying what we mean by the parameters denoted by α. In fact, α can represent any external parameters which enter the Schrödinger equation—E, $\hbar$, or parameters affecting the form of the Hamiltonian itself. The key point is that the quantization condition (1.1) is not attainable for arbitrary parameters; it can only be satisfied when there happens to be an eigenstate at that choice of parameters. So T_α can only show the presence or absence of a quantum eigenstate

(by respectively having or not having an eigenvalue that equals unity) at the *one particular* point in parameter space at which it was computed. This is why we need to compute T_α many times, for various selections of α, in our search for eigenstates of the system.

Normally one would vary only E, in which case unit eigenvalues of T_E mark eigen*energies* of the system and the usual energy spectrum is produced. However, it should be clear that it is also possible to fix E and vary some other parameter of the problem. One can even vary several of the parameters simultaneously.

In fact, if one varies several parameters simultaneously, while at the same time keeping them in a carefully chosen relationship to one another, one can arrange that despite the change the classical trajectories are left unchanged (or maybe trivially rescaled). *Scalable potentials* (such as billiards) show a particularly simple version of this effect—the classical trajectories scale trivially as the energy itself is changed. If we find such a scaling combination of parameters, we will only need to compute a mesh of classical trajectories once, then reuse them as necessary to calculate T for many parameter values. Thus we would be able to find *many eigenstates* (albeit not members of a single energy spectrum) from *a single set* of classical trajectories. Having to compute only a single set of trajectories, rather than a separate set for each eigenstate to be found, significantly reduces the work necessary to verify Bogomolny's method.

Treating Planck's constant as the variable parameter has the desired effect. (Any reluctance to vary one of nature's fundamental constants can be circumvented by noting that this operation is equivalent to varying other parameters of the problem in synchrony. Details are given in Appendix B.) Clearly Planck's constant has no effect on the classical trajectories; one set of them can be calculated and then used to calculate T for any value of $\hbar$.

In fact it is useful to think of $1/\hbar$ as the problem's *classicity*. Increasing the classicity at constant energy shortens the particle's de Broglie wavelength; this in turn allows more "nodes" to fit on the energy shell, so that more highly excited, more "classical" eigenstates result. In the sense that states of higher classicity (everything

else held constant) have higher excitation numbers, classicity is analogous to energy, and it helps to think of it as a kind of pseudoenergy—though beware that the analogy is not exact (for example, eigenstates of classicity at fixed energy are not orthogonal to one another).

In our numerical experiment outlined in Chapter 4, we use this trick. We search for eigenstates of *fixed energy and variable classicity*, producing an eigen*classicity* spectrum for the system. In effect we are able to enjoy the computational leverage which is usually associated with scalable potentials, but without having to limit ourselves to a (non-generic) scalable potential. Moreover, this trick allows us to change independently the two parameters which are expected to affect the performance of the semiclassical algorithm: E (which sets the degree of chaos) and $1/\hbar$ (which sets how close we are to the semiclassical limit).

Chapter 3

Computing Exact Eigenclassicities

To evaluate the efficacy of Bogomolny's method for calculating approximate eigenclassicities, it was necessary to compute the exact eigenclassicities of our system for reference. In this chapter, we describe

- the quantum mechanical eigenclassicity problem which needs to be solved,
- a brief review of harmonic oscillator wavefunctions, including notation that we will use later,
- some comments about using 1-D harmonic oscillator wavefunctions as basis states for the 1-D harmonic oscillator eigenclassicity problem,
- an improved basis of "bent" 2-D harmonic oscillator wavefunctions to be used for the Nelson_2 potential, and
- the scale lengths and basis truncation used, and the empirical method by which they were chosen.

3.1 The eigenclassicity problem

Solving the quantum eigenclassicity problem is a bit more complicated (or at least more unfamiliar) than solving a quantum eigenenergy problem. The latter is given

by the following familiar equation:

$$H\,|\Psi_i\rangle = E_i\,|\Psi_i\rangle\,. \tag{3.1}$$

$|\Psi\rangle$ represents a full, quantum mechanical wavefunction, and is to be distinguished from $|\psi\rangle$, which represents a surface of section wavefunction like the ones operated on by the T operator. After some complete set of basis states $\{|n\rangle\}$ is chosen, and the matrix elements $\langle n|\,H\,|n'\rangle$ are computed, the problem reduces to an eigenvalue (matrix diagonalization) problem,

$$\sum_{n'} \langle n|\,H\,|n'\rangle\,\langle n'|\,\Psi_i\rangle = E_i\,\langle n|\,\Psi_i\rangle\,.$$

On the other hand, the eigenclassicity problem, even for a Hamiltonian which is equal to kinetic energy plus potential energy, takes a different form. One must rearrange equation (3.1) to isolate $1/\hbar$. To do this, we must "look inside" H:

$$\begin{aligned} H &= \sum_i \frac{p_i^2}{2} + V(\vec{q}) \\ &= \sum_i \hbar^2 \frac{k_i^2}{2} + V(\vec{q}) \\ &= \hbar^2 K + V \end{aligned}$$

where k_i are the wave numbers $p_i/\hbar$ associated with the momenta, and the last line defines K, a reduced kinetic energy in terms of wave numbers with Planck's constant taken out. In terms of those quantities, the eigenclassicity equation is

$$K\,|\Psi_i\rangle = \left(\frac{1}{\hbar_i}\right)^2 (E - V)\,|\Psi_i\rangle\,. \tag{3.2}$$

Here E is taken to be constant, and we look for the discrete values of the classicity $1/\hbar_i$, and non-zero eigenvectors $|\Psi_i\rangle$, for which the equation holds. Since the wavevectors on both the left and the right sides of the equality are multiplied by operators, this system is called a "generalized eigenvalue problem." In terms of matrices in some

basis, the problem that needs to be solved is

$$\sum_{n'} \langle n| K |n'\rangle \langle n'| \Psi_i\rangle = \left(\frac{1}{\hbar_i}\right)^2 \sum_{n'} \langle n| (E-V) |n'\rangle \langle n'| \Psi_i\rangle . \tag{3.3}$$

The eigenvectors corresponding to different eigenclassicities are not orthogonal in the usual way; instead of satisfying $\langle \Psi_i| \Psi_j\rangle = 0$, they satisfy

$$\langle \Psi_i| K |\Psi_j\rangle = 0$$

and

$$\langle \Psi_i| (E-V) |\Psi_j\rangle = 0.$$

Also note that the operator $(E-V)$ is not positive-definite, and in fact $(1/\hbar)^2$ can possess negative solutions (though of course only the positive solutions are physically meaningful).

3.2 1-D harmonic oscillator wavefunctions

Although this subject is well-worn, we will present a brief overview of the topic for convenience, to present our notation, and as a foundation for later sections.

The whole infrastructure of 1-D simple harmonic oscillator (SHO) eigenstates follows from the following definitions of the operators a and $a^\dagger$:

$$a \equiv \frac{1}{\sqrt{2}}\left(\alpha q + i\frac{k}{\alpha}\right)$$

$$a^\dagger \equiv \frac{1}{\sqrt{2}}\left(\alpha q - i\frac{k}{\alpha}\right)$$

$$q = \frac{1}{\alpha\sqrt{2}}(a + a^\dagger)$$

$$k = \frac{p}{\hbar} = -i\frac{\alpha}{\sqrt{2}}(a - a^\dagger)$$

α is an arbitrary real number and will momentarily be left indeterminate. The fol-

lowing commutators hold for any α:

$$[q, k] = i$$

$$[a, a^\dagger] = 1.$$

"Number states" are defined, for integer n and some choice of α, to be

$$|n, \alpha\rangle \equiv \frac{1}{\sqrt{n!}}(a^\dagger)^n |0\rangle$$

and depend on α through the definition of $a^\dagger$. (We will sometimes abbreviate the notation to $|n\rangle$ by not explicitly specifying α.) From these definitions follow (after a few simple steps) the effects of applying the raising and lowering operators to the number states:

$$a |n\rangle = \sqrt{n}\, |n-1\rangle$$

$$a^\dagger |n\rangle = \sqrt{n+1}\, |n+1\rangle$$

From $a |0\rangle = 0$ and the definition above, it is possible to show that in a position basis,

$$\langle q|\, n, \alpha\rangle = \sqrt{\frac{\alpha}{2^n n!}}\, \pi^{-1/4} \exp\left(-\frac{\alpha^2 q^2}{2}\right) H_n(\alpha q), \tag{3.4}$$

where H_n is the n^{th} Hermite polynomial. From this expression it is seen that α is only a scale parameter, with units of inverse length. The number states are eigenvectors of the number operator $N \equiv a^\dagger a$, with

$$a^\dagger a |n\rangle = n |n\rangle .$$

The simple harmonic oscillator is given by the following Hamiltonian:

$$H = \frac{\hbar^2 k^2}{2m} + \tfrac{1}{2} m\omega^2 q^2.$$

If we substitute for q and k the expressions involving a and $a^\dagger$, the Hamiltonian is

transformed into

$$\begin{aligned} H &= \left(-\frac{\hbar^2\alpha^2}{4m} + \frac{m\omega^2}{4\alpha^2}\right)\left(a^2 + a^{\dagger 2}\right) \\ &\quad + \left(\frac{\hbar^2\alpha^2}{4m} + \frac{m\omega^2}{4\alpha^2}\right)\left(aa^\dagger + a^\dagger a\right). \end{aligned}$$

Normally one takes this opportunity to kill the first term by choosing

$$\alpha^2 = \frac{m\omega}{\hbar} \tag{3.5}$$

and, after rewriting the second term, the Hamiltonian becomes

$$H = \hbar\omega(a^\dagger a + \tfrac{1}{2})$$

so that the number states are eigenstates of the Hamiltonian with

$$H\left|n, \alpha = \sqrt{m\omega/\hbar}\right\rangle = \hbar\omega(n + \tfrac{1}{2})\left|n, \alpha = \sqrt{m\omega/\hbar}\right\rangle.$$

Therefore, by making the particular choice for α specified by equation (3.5), it is possible analytically to find exact eigenfunctions and eigenvalues for the SHO, for either the eigenenergy problem:

$$E_n = \hbar\omega(n + \tfrac{1}{2})$$

or the eigenclassicity problem:

$$1/\hbar_n = (\omega/E)(n + \tfrac{1}{2}).$$

3.3 Using SHO number states as basis states

It must be strongly emphasized that although the choice of α given in equation (3.5) is the most convenient one to use when solving for harmonic oscillator eigenstates, with

any choice of α is associated a complete and orthonormal set of functions $\{|n,\alpha\rangle, n = 0\ldots\infty\}$ suitable for service as a basis set. One could even solve for harmonic oscillator energy eigenstates using a number state basis scaled by some "wrong" value of α. But then, instead of obtaining a diagonal Hamiltonian matrix, one would obtain a Hamiltonian matrix with non-zero off-diagonal elements; such matrices typically have to be diagonalized explicitly, presumably with a computer. The larger the off-diagonal elements, the worse the convergence, and the larger the matrix that needs to be used in order to obtain a given number of accurate eigenvalues.

The situation for a general (anharmonic) potential is even worse—harmonic oscillator wavefunctions can still be used as basis functions, but now there will always be off-diagonal matrix elements for *any choice* of α. The best one can then do is try to adjust α to minimize the magnitude of the off-diagonal matrix elements; this will optimize the numerical convergence of diagonalization algorithms, and allow reasonable-sized matrices to suffice.

It is now that we point out a hidden twist in the SHO eigenclassicity problem in the previous section: since the optimal α depends on $1/\hbar$, different classicity eigenstates for a single energy have different optimal values for α—conversely, a set of basis states with a fixed choice for α contains at most one exact eigenvector of the eigenclassicity problem, and all other solutions would need to be found numerically.

The situation is illustrated in figure 3-1. Wavefunctions of constant classicity and variable energy (Fig. 3-1(a)) become wider with increasing excitation number, because at higher energies the classical turning points move further from the origin. At fixed energy and increasing classicity, on the other hand, the classical turning points are fixed, and the spatial extent of wavefunctions actually *decreases* with increasing excitation number because tunnelling is more inhibited for states of higher classicity (smaller $\hbar$). Thus when using harmonic oscillator wavefunctions as a basis set for solving an eigenclassicity problem, one needs to choose a compromise α—to produce a basis set which, in position coordinates, has members that are wide enough to model the highly tunnelling, low excitation classicity eigenvectors, and simultaneously contains members with high enough spatial frequencies to represent the compact, high

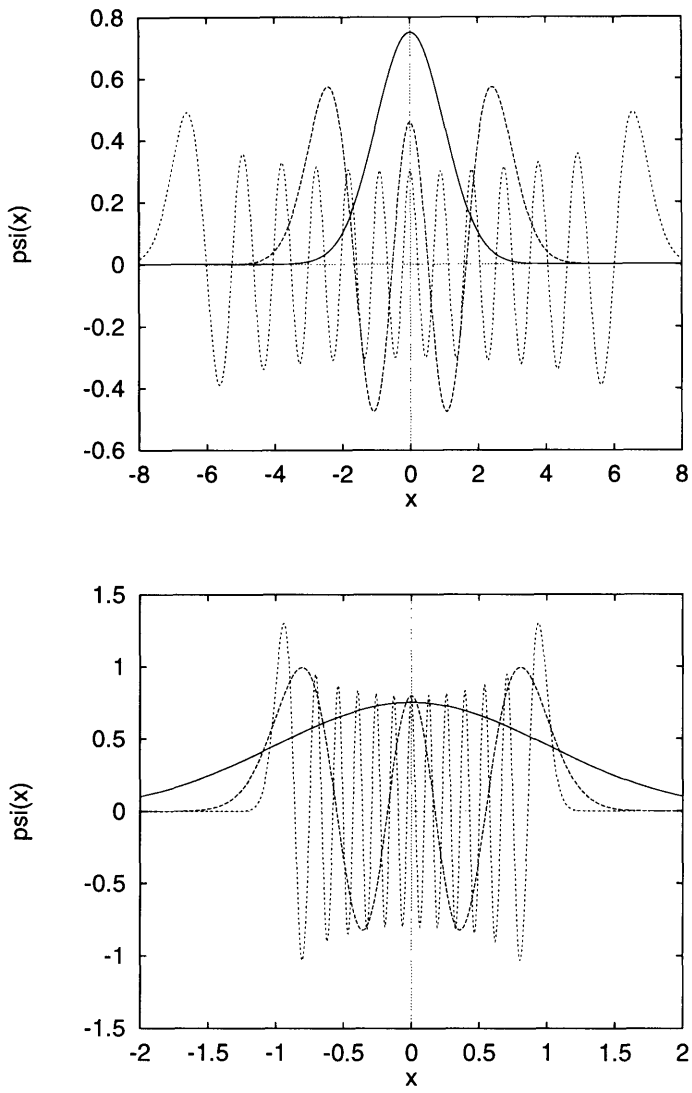

Figure 3-1: Energy eigenfunctions vs. classicity eigenfunctions for the 1-D simple harmonic oscillator. Each plot show states $n = 0$, 4, and 24. (a) Energy eigenfunctions (calculated at fixed $\hbar = 1$) get wider as the number of excitations increases, because the energetically allowed region grows. (b) Classicity eigenfunctions (calculated at constant $E = \frac{1}{2}$), on the other hand, all have the same classical turning points, and states of *lower* excitation number turn out, with their smaller $1/\hbar$, to be able to tunnel further into the classically forbidden region. Note also that the spatial frequencies of the wavefunctions increase faster with increasing excitation number than they do in the eigenenergy case.

excitation classicity eigenvectors. It is these two contradictory demands which are chiefly responsible for the fact that the eigenclassicity problem is harder than the eigenenergy problem.

3.4 Deforming the basis states for better convergence

We could continue by writing expressions for the Nelson$_2$ potential eigenclassicity equation (3.3) in terms of $a_{x,y}$ and $a^\dagger_{x,y}$ and diagonalize it in a basis of 2-D number states

$$|n_x, n_y\rangle \equiv |n_x\rangle \otimes |n_y\rangle \,.$$

In fact we *did* do that, and found that for the higher energy chaotic regime $E = 0.2$, convergence was not good enough to compute the desired number of eigenstates with the available computer resources. Instead, we transformed the basis functions by offsetting them vertically to follow the parabola $y = \frac{1}{2}x^2$ around which the Nelson$_2$ potential is centered. (This approach is not original; see [13].) In other words, we used $|n_1, n_2\rangle$ given by

$$\langle x, y|\, n_1, n_2\rangle = \left\langle x, y - \tfrac{1}{2}x^2 \right|\, n_x = n_1, n_y = n_2 \Big\rangle$$

This basis matches the problem more closely, and the diagonalization converges more readily in this basis than in the non-offset basis.

We formalize the relationship between the two bases by writing

$$|n_1, n_2\rangle = U\, |n_x = n_1, n_y = n_2\rangle$$

where the unitary operator U is defined by its effect on position eigenstates:

$$U\, |q_x, q_y\rangle = \left|q_x, q_y + \tfrac{1}{2}q_x^2\right\rangle$$

We now show that U can be written as

$$U = \exp\left\{-i\hat{k_y} \cdot \tfrac{1}{2}\hat{q_x}^2\right\},$$

(which looks somewhat like a translation operator). Starting with the definition of U, we get

$$\begin{aligned}
U &= \int dq_x \int dq_y \left|q_x, q_y + \tfrac{1}{2}q_x^2\right\rangle \left\langle q_x, q_y\right| \\
&= \int dq_x \int dq_y \int dk_y \left|k_y\right\rangle \left\langle k_y\right| \left|q_x, q_y + \tfrac{1}{2}q_x^2\right\rangle \left\langle q_x, q_y\right| \\
&= \int dq_x \int dq_y \int dk_y \left|q_x\right\rangle \otimes \left|k_y\right\rangle \tfrac{1}{\sqrt{2\pi}} \exp\left\{-ik_y \cdot (q_y + \tfrac{1}{2}q_x^2)\right\} \left\langle q_x, q_y\right| \\
&= \int dq_x \int dq_y \int dk_y \exp\left\{-ik_y \tfrac{1}{2}q_x^2\right\} \left|q_x\right\rangle \otimes \left|k_y\right\rangle \tfrac{1}{\sqrt{2\pi}} \exp\left\{-ik_y q_y\right\} \left\langle q_x, q_y\right| \\
&= \int dq_x \int dq_y \int dk_y \exp\left\{-i\hat{k_y} \tfrac{1}{2}\hat{q_x}^2\right\} \left|q_x\right\rangle \otimes \left|k_y\right\rangle \left\langle k_y\right| \left.q_y\right\rangle \left\langle q_x, q_y\right| \\
&= \exp\left\{-i\hat{k_y} \tfrac{1}{2}\hat{q_x}^2\right\} \int dq_x \int dq_y \left|q_x, q_y\right\rangle \left\langle q_x, q_y\right| \\
U &= \exp\left\{-i\hat{k_y} \tfrac{1}{2}\hat{q_x}^2\right\}
\end{aligned}$$

From the expression for U its commutators in the $\{x, y\}$ basis can be worked out:

$$[U, q_x] = 0$$

$$[U, q_y] = -\tfrac{1}{2}U q_x^2$$

$$[U, k_x] = U q_x k_y$$

$$[U, k_y] = 0$$

(The first and last commutators are obvious; the second and third follow from the identity

$$[\exp G, A] = \left\{[G, A] + \tfrac{1}{2!}[G, [G, A]] + \cdots\right\} \exp G$$

.)

Now we would like to find expressions for the raising and lowering operators that are associated with the new basis. It can be seen by inspection that the following

operators have the desired effect:

$$a_{1,2} = U a_{x,y} U^\dagger$$

$$a^\dagger_{1,2} = U a^\dagger_{x,y} U^\dagger$$

From these raising and lowering operators can be defined position and momentum operators in the new basis, by using the expressions from the old basis:

$$\hat{q_1} \equiv U \hat{q_x} U^\dagger = \hat{q_x}$$

$$\hat{q_2} \equiv U \hat{q_y} U^\dagger = \hat{q_y} - \tfrac{1}{2}\hat{q_x}^2$$

$$\hat{k_1} = \hat{p_1}/\hbar \equiv U \hat{k_x} U^\dagger = \hat{k_x} + \hat{q_x}\hat{k_y}$$

$$\hat{k_2} = \hat{p_2}/\hbar \equiv U \hat{k_y} U^\dagger = \hat{k_y}$$

The above relations can also be inverted, giving

$$\hat{q_x} = \hat{q_1}$$

$$\hat{q_y} = \hat{q_2} + \tfrac{1}{2}\hat{q_1}^2$$

$$\hat{k_x} = \hat{k_1} - \hat{q_1}\hat{k_2}$$

$$\hat{k_y} = \hat{k_2}$$

Finally we can substitute these expressions into the Nelson$_2$Hamiltonian:

$$\begin{aligned} H &= \tfrac{1}{2}\hbar^2 k_x^2 + \tfrac{1}{2}\hbar^2 k_y^2 + \tfrac{1}{2}\omega^2 q_x^2 + \tfrac{1}{2}(q_y - \tfrac{1}{2}q_x^2)^2 \\ &= \tfrac{1}{2}\hbar^2 k_1^2 + \tfrac{1}{2}\hbar^2 k_2^2 + \tfrac{1}{2}\omega^2 q_1^2 + \tfrac{1}{2}q_2^2 + \tfrac{1}{2}\hbar^2 q_1^2 k_2^2 - \tfrac{1}{2}\hbar^2(q_1 k_1 + k_1 q_1)k_2 \\ &= \tfrac{1}{2}\hbar^2(k_1 - q_1 k_2)^2 + \tfrac{1}{2}\hbar^2 k_2^2 + \tfrac{1}{2}\omega^2 q_1^2 + \tfrac{1}{2}q_2^2 \end{aligned}$$

In the new basis the system is closer to a perturbed harmonic oscillator, though now the perturbation involves both position and momentum operators.

For equation (3.3) we need K and V independently, so we rewrite these parts of the Hamiltonian in terms of the raising and lowering operators to facilitate the calculation of their matrix elements in the $|n_1, n_2\rangle$ basis.

$$\begin{aligned}
K &= \tfrac{1}{2}(k_1 - q_1 k_2)^2 + \tfrac{1}{2}k_2^2 \\
&= \tfrac{1}{2}k_1^2 + \tfrac{1}{2}k_2^2 + \tfrac{1}{2}q_1^2 k_2^2 - \tfrac{1}{2}(q_1 k_1 + k_1 q_1)k_2 \\
&= \frac{1}{2}\left\{ -\frac{\alpha_1^2}{2}(a_1^2 - (2N_1 + 1) + a_1^{\dagger 2}) \right. \\
&\quad -\frac{\alpha_2^2}{2}(a_2^2 - (2N_2 + 1) + a_2^{\dagger 2}) \\
&\quad -\frac{\alpha_2^2}{4\alpha_1^2}(a_1^2 + (2N_1 + 1) + a_2^{\dagger 2})(a_2^2 - (2N_2 + 1) + a_2^{\dagger 2}) \\
&\quad \left. + \frac{\alpha_2}{\sqrt{2}}(a_1^2 - a_1^{\dagger 2})(a_2 - a_2^{\dagger}) \right\} \\
V &= \tfrac{1}{2}\omega^2 q_1^2 + \tfrac{1}{2}q_2^2 \\
&= \frac{1}{2}\left\{ \omega^2 \frac{1}{2\alpha_1^2}(a_1^2 + (2N_1 + 1) + a_1^{\dagger 2}) \right. \\
&\quad \left. + \frac{1}{2\alpha_2^2}(a_2^2 + (2N_2 + 1) + a_2^{\dagger 2}) \right\}
\end{aligned}$$

A handy, symmetric form for the raising and lowering operators is as follows:

$$a_i = \sum_{n_i} |n_i\rangle \sqrt{n_i + 1}\, \langle n_i + 1|$$

$$a_i^2 = \sum_{n_i} |n_i\rangle \sqrt{(n_i + 1)(n_i + 2)}\, \langle n_i + 2|$$

$$a_i^{\dagger} = \sum_{n_i} |n_i + 1\rangle \sqrt{n_i + 1}\, \langle n_i|$$

$$a_i^{\dagger 2} = \sum_{n_i} |n_i + 2\rangle \sqrt{(n_i + 1)(n_i + 2)}\, \langle n_i|$$

From this it is straightforward to make a table of the nonzero matrix elements of K and V:

$$\langle n_1, n_2|\, K\, |n_1, n_2\rangle = \frac{\alpha_1^2}{4}(2n_1 + 1) + \frac{\alpha_2^2}{4}(2n_2 + 1)$$

$$+\frac{\alpha_2^2}{8\alpha_1^2}(2n_1+1)(2n_2+1)$$

$$\langle n_1,n_2|\,K\,|n_1+2,n_2\rangle = \left\{-\frac{\alpha_1^2}{4}+\frac{\alpha_2^2}{8\alpha_1^2}(2n_2+1)\right\}\sqrt{(n_1+1)(n_1+2)}$$

$$\langle n_1,n_2|\,K\,|n_1+2,n_2+1\rangle = \frac{\alpha_2}{2\sqrt{2}}\sqrt{(n_1+1)(n_1+2)(n_2+1)}$$

$$\langle n_1,n_2|\,K\,|n_1,n_2+2\rangle = \left\{-\frac{\alpha_2^2}{8\alpha_1^2}(2n_1+1)-\frac{\alpha_2^2}{4}\right\}\sqrt{(n_2+1)(n_2+2)}$$

$$\langle n_1,n_2|\,K\,|n_1+2,n_2+2\rangle = -\frac{\alpha_2^2}{8\alpha_1^2}\sqrt{(n_1+1)(n_1+2)(n_2+1)(n_2+2)}$$

$$\langle n_1,n_2+1|\,K\,|n_1+2,n_2\rangle = -\frac{\alpha_2}{2\sqrt{2}}\sqrt{(n_1+1)(n_1+2)(n_2+1)}$$

$$\langle n_1,n_2+2|\,K\,|n_1+2,n_2\rangle = -\frac{\alpha_2^2}{8\alpha_1^2}\sqrt{(n_1+1)(n_1+2)(n_2+1)(n_2+2)}$$

$$\langle n_1,n_2|\,V\,|n_1,n_2\rangle = \frac{\omega^2}{4\alpha_1^2}(2n_1+1)+\frac{1}{4\alpha_2^2}(2n_2+1)$$

$$\langle n_1,n_2|\,V\,|n_1+2,n_2\rangle = \frac{\omega^2}{4\alpha_1^2}\sqrt{(n_1+1)(n_1+2)}$$

$$\langle n_1,n_2|\,V\,|n_1,n_2+2\rangle = \frac{1}{4\alpha_2^2}\sqrt{(n_2+1)(n_2+2)}$$

Of course the matrices are Hermitian (in fact real symmetric) so the redundant matrix elements are not listed. The two operators are quite sparse, coupling a state only to a few of its neighbors in the (n_1,n_2) plane. Because of symmetry, states with even n_1 do not couple to states with odd n_1, and vice versa. We emphasize that α_1 and α_2 are still free parameters, and can be chosen so as to optimize the convergence of the diagonalization, as outlined in the next section.

3.5 The basis truncation

Unless an exact solution to equation (3.2) is known, the matrix equation will have to be solved numerically on a computer. For this to be possible, the infinite matrix of

Eq. (3.2) needs to be truncated to finite size by limiting the number of basis states which are considered. This effectively restricts the search for solution vectors to a subspace of the full Hilbert space. Any solution vectors which lie fully within that subspace are found, along with their eigenvalues, exactly.

In our basis of deformed 2-D harmonic oscillator wavefunctions, choosing a basis truncation $\mathcal{B} = \{|n_1, n_2\rangle\}$ means choosing a set of lattice points (n_1, n_2) in the first quadrant of the (n_1, n_2) plane. We found that one good and simple set of indices to include in a basis is those which lie within an ellipse:

$$\mathcal{B}(n_{1\max}, n_{2\max}) \equiv \left\{ |n_1, n_2\rangle : \frac{n_1^2}{n_{1\max}^2} + \frac{n_2^2}{n_{2\max}^2} \leq 1 \right\}.$$

Since the potential is symmetric about the y-axis, states with even parity do not couple to states with odd parity, and the two subspaces are best separated beforehand by including basis states with either only even or only odd n_1 indices respectively in each subproblem.

It is still necessary to choose the basis semimajor axes $n_{1\max}$ and $n_{2\max}$, and the two scale parameters α_1 and α_2. We adjusted these four parameters semi-empirically, by doing a sample diagonalization for one reasonable choice of parameters, then examining how well the diagonalization succeeded. This is easily done by comparing the numerical spectral staircase function

$$N(\leq 1/\hbar) \equiv \sum_i \theta(1/\hbar - 1/\hbar_i)$$

to the Thomas-Fermi smoothed spectral staircase, given in equation (4.1). $\theta(x)$ is the Heaviside step function, which is 1 for $x > 0$ and 0 for $x < 0$. An example comparison (with non-optimal parameters) is plotted in figure 3-2, where it is seen that the numerical results reproduce the eigenclassicities up to about $(1/\hbar) \lesssim 55$.

If the above sample diagonalization fails to produce enough accurate eigenstates, it is necessary to adjust the four parameters so as to improve the results. Naturally one could take the brute-force approach of simply increasing $n_{1\max}$ and $n_{2\max}$ blindly—as these approach infinity, the eigenvalues are guaranteed to get better (and your

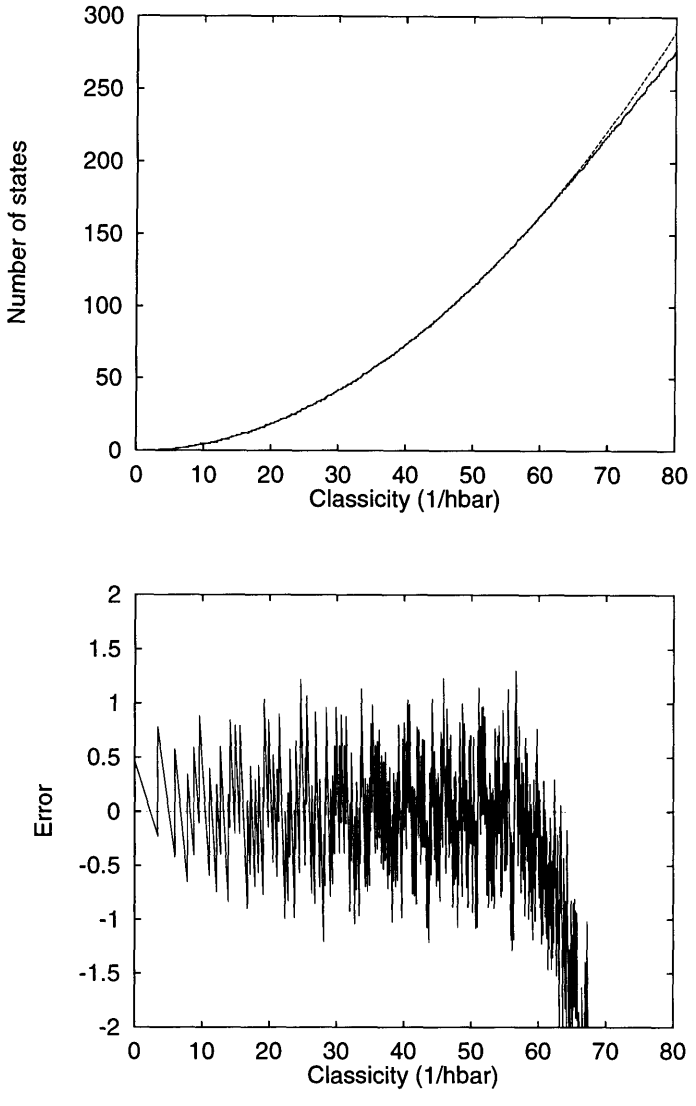

Figure 3-2: Example comparison of a numerical spectral staircase function to the smoothed Thomas-Fermi estimate, for a preliminary, poorly optimized diagonalization (the same one used for figure 3-3). The range of reliability of a diagonalization can be tested by plotting the associated spectral staircase next to the smoothed Thomas-Fermi estimate. (a) The two staircases side by side. (b) The difference between the two staircases. It can readily be seen that the diagonalization breaks down around $1/\hbar \sim 55$ (the 138th eigenclassicity), shortly before the diagonalization ceases to reproduce even the large scale features of the staircase.

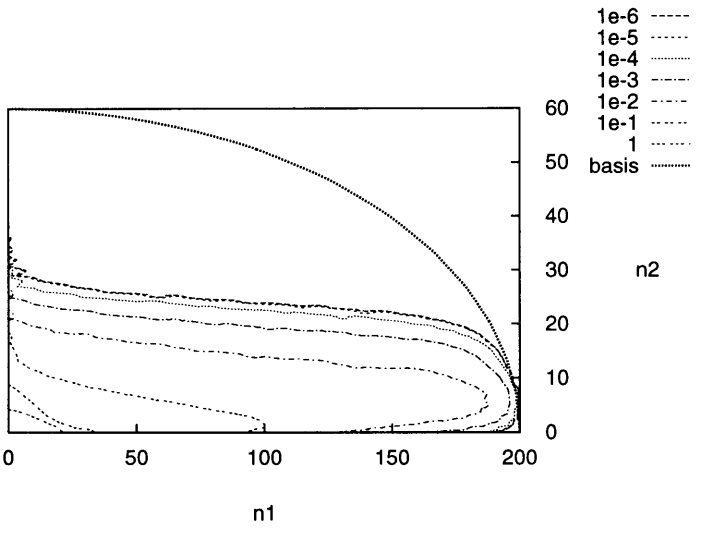

Figure 3-3: Example "basis usage function" plot (logarithmic scale). The function plotted measures to what extent each basis function $|n_1, n_2\rangle$ was needed to reproduce the first 200 eigenstates in the same poorly-optimized diagonalization used for figure 3-2. Only the states inside of the ellipse were included in the basis. It can be seen that only about half of the available range in the n_2 direction was actually needed, while the n_1 range is seen to be insufficient by the fact that the usage function is pushing up against the ellipse in that direction and would clearly "like" to expand further.

computer budget is guaranteed to quickly run out). Instead, we devised a simple and intuitive graphical way to tell us how to increase the basis set efficiently. We plotted, on the (n_1, n_2) plane, the "basis usage function"

$$u(n_1, n_2, i) \equiv \sum_{i'=0}^{i-1} |\langle n_1, n_2 | \Psi_{i'} \rangle|^2$$

which measures to what extent a particular basis function $|n_1, n_2\rangle$ was used in the representation of the first i eigenfunctions. Such a plot is shown in figure 3-3. The heavy ellipse shows the envelope of basis functions used; u is artificially zero outside of that curve because those functions were not available in the basis to *be* used. A good basis truncation will have u approaching zero of its own accord *inside* the envelope, but not too far inside because any basis states with $u = 0$ need not have been included in the basis in the first place. Fig. 3-3 show a basis truncation which is

Energy	0.004	0.2
α_1	20.53	4.46
α_2	43.42	6.14
$n_{1\max}$	190	250
$n_{2\max}$	82	40
# of basis states	6201	4007
Matrix band half-width	85	43
# even parity eigenstates reproduced accurately	360	290
Maximum eigenclassicity reproduced accurately	4500	80

Table 3.1: Parameters for quantum mechanical matrix diagonalizations. Parameters for the even-parity diagonalization are shown; odd-parity computations used similar parameters and achieved similar results. The matrices' banded structure was exploited (band halfwidths are listed), though not the fact that even within the band, most matrix elements are zero. We spent more effort optimizing the parameters for the more challenging chaotic case ($E = 0.2$); if the same effort had been invested in the regular regime ($E = 0.004$), those eigenstates could have been obtained from a significantly smaller matrix than was actually used.

not particularly good because, while only about half of the available range in the n_2 direction has been used, the n_1 range is already seen to be insufficient by the fact that u does not approach zero before it is forced to by hitting the limits of the basis. In this case it would be appropriate to increase $n_{1\max}$ and to decrease $n_{2\max}$ in the next attempt. In fact, the unexpected pattern of basis usages in the two directions was a hint that the basis scale lengths were not optimal, and better results were indeed obtained when α_1 was increased by 50%.

After a couple of iterations, we found parameters which enabled us to compute enough exact, quantum mechanical eigenclassicities to compare with the semiclassical results. See table 3.1 for the final selections and results. We will henceforth call the computed quantum mechanical values the "exact" values—not in reference to their numerical virtues, but rather because they are computed on the basis of an *exact* theory (as opposed to a semiclassical approximation).

Chapter 4

Numerical Experiment

4.1 The model system

We applied Bogomolny's method to the case of a particle moving in a smooth non-linear oscillator with Hamiltonian

$$H = \tfrac{1}{2}\left(p_x^2 + p_y^2\right) + \tfrac{1}{2}\omega^2 x^2 + \tfrac{1}{2}\left(y - \tfrac{1}{2}x^2\right)^2 .$$

Aside from a minor rescaling of variables discussed in Appendix B, this system is identical to the "Nelson" potential studied by Baranger and Davies [10] and Provost [13]; to eliminate confusion we will refer to our rescaled potential as "Nelson$_2$." We fixed the value of $\omega^2 = 0.05$ (the same value as used by those authors), and used the y-axis as our surface of section.

The system is an anisotropic harmonic oscillator elongated along the x-direction which has been bent up along the parabola $y = \frac{1}{2}x^2$; some contour lines of this potential are shown in figure 4-1. The system has a rich periodic orbit structure [10] and is bound at all energies. As energy is increased the particle explores more and more of the curved "horns" and the motion becomes increasingly chaotic. The Thomas-Fermi classical estimate of the number of even and odd states for our potential, including

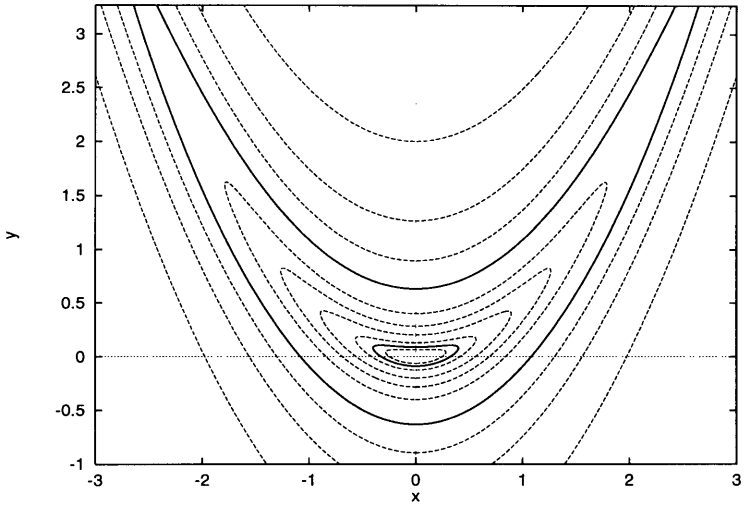

Figure 4-1: Some contours of the Nelson$_2$ potential. The two solid contour lines are for the energies $E = 0.004$ and $E = 0.2$, which were chosen for the numerical experiments; the former is mostly regular, while the latter is mostly chaotic. The surface of section used was the y-axis.

corrections up to $\mathcal{O}(\hbar^2)$, is given by [13]:

$$N(< E \text{ or } < (1/\hbar)) = \frac{E^2}{4\hbar^2\omega}\left\{1 \pm \frac{\hbar\omega}{E} - \frac{\hbar^2}{12}\left[\frac{\omega^2+1}{E^2} + \frac{1}{\omega^2 E}\right]\right\}; \qquad (4.1)$$

the plus and minus correspond to the expressions for even and odd parity states, respectively. To first order the number of states increases quadratically with both energy and classicity.

We computed eigenclassicity spectra for two different values of energy: $E = 0.004$, where the system is predominantly regular; and $E = 0.2$, where it is predominantly chaotic. Parameters of that computation are summarized in table 4.1. For the two energies we calculated all of the eigenclassicities, of both parities, in the ranges $0 \leq (1/\hbar) \leq 4000$ and $0 \leq (1/\hbar) \leq 60$, respectively; a total of 574 and 321 states fall in those ranges. Details are contained in the following sections.

Energy	0.004	0.2
Classicity range	0–4000	0–60
# states in range (even and odd parity)	574	321
# of classical trajectories used	243×243	729×729
# of basis states used	36	36
# of T diagonalizations done	1603	1998

Table 4.1: Parameters for semiclassical computations of eigenclassicities of the Nelson$_2$ potential. In order to reproduce the T operator eigenvalue curves accurately, more T diagonalizations were done than would be needed only to isolate the eigenclassicities.

4.2 The semiclassical eigenclassicity spectrum

In applying Bogomolny's method, we took advantage of the potential's mirror symmetry about the y-axis by using the T operator associated with half-Poincaré mapping trajectories, as discussed in Section 2.3. Thus eigenstates of the system are expected to occur at values of $1/\hbar$ for which T has an eigenvalue of ± 1. The set of half-trajectories that we used were started on a rectangular mesh of initial conditions in the allowed (y, θ) plane, with 243×243 trajectories for $E = 0.004$, and 729×729 trajectories for $E = 0.2$.

We calculated T as a matrix in a basis composed of simple harmonic oscillator eigenfunctions on the y-axis (remember the basis need only be complete on the surface of section). The length scale of the basis functions was chosen such that they would be solutions to the Schrödinger equation that would apply to motion on the y-axis:

$$\left(-\frac{\hbar^2}{2}\frac{d^2}{dy^2} + \frac{1}{2}y^2\right)\phi_n(y) = \hbar\left(n + \tfrac{1}{2}\right)\phi_n(y),$$

with $\hbar$ chosen to correspond to the classicity used in that particular T calculation; thus, the basis states vary smoothly with classicity. The number of basis states used throughout was 36.

To create the curves of eigenvalues of T as a function of $(1/\hbar)$ which will be shown below, we wrote a driver program which was able to interpolate from the eigenvalues at one value of classicity to the corresponding ones at another nearby classicity, or, when the correspondence was ambiguous, to fill the gap by calculating a set of eigenvalues at an additional classicity between the first two. Thus the curves below are reconstructed and plotted faithfully, in full detail.

4.3 T operator eigenvalues—qualitative observations

Much of the discussion of our numerical results concentrates on the properties and behavior of the eigenvalues of the T operator as a function of classicity $(1/\hbar)$. Recall that T and its eigenvalues can be computed for any value of classicity, so the eigenvalues trace out continuous curves in the complex plane as the classicity is varied. Figure 4-2 shows examples of such curves in the complex plane, for each of the two energies. Figure 4-3 shows the magnitudes of each of the T-matrix eigenvalues as a function of classicity; in order to also indicate the complex phase angle of the eigenvalues, a symbol is plotted whenever an eigenvalue has a phase of 0 or π. The horizontal axes of figures 4-3(a) and 4-3(b) are scaled relative to one another in such a way that the Thomas-Fermi densities of states are comparable (so for example, to get the same number of eigenstates in the chaotic regime as are shown in the regular regime, we would have has to continue the computation to $1/\hbar = 80$).

4.3.1 T eigenvalue magnitudes; the dimension of T

We immediately see the extent to which the semiclassical T matrix satisfies Bogomolny's prediction of unitarity. The dimension of T is supposed to follow Eq. (2.3), which, evaluated for our potential, gives

$$\dim T = E \cdot (1/\hbar). \tag{4.2}$$

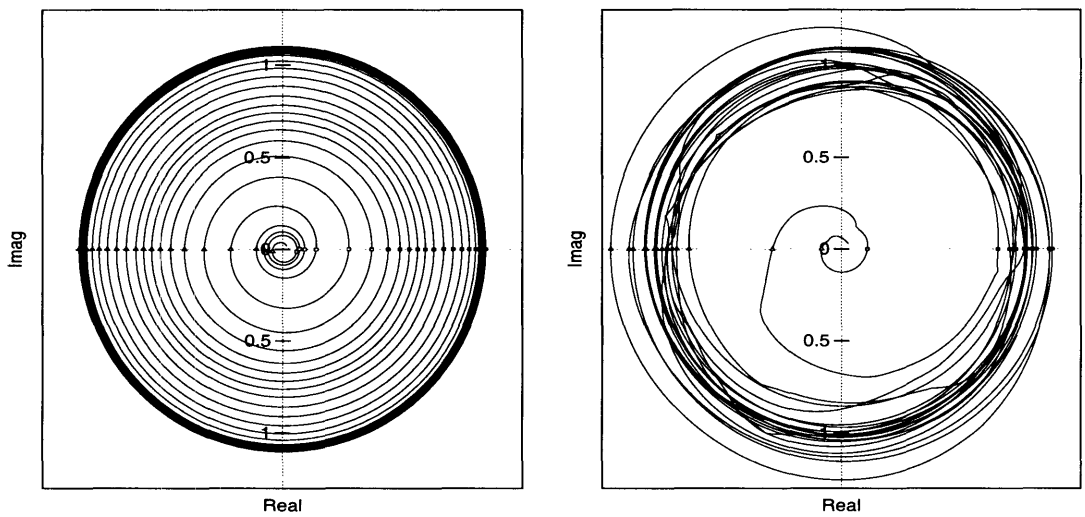

Figure 4-2: Typical eigenvalue curves in the complex plane. Plotted are the curves that two typical eigenvalues follow as the classicity $(1/\hbar)$ is scanned. The eigenvalues remain near the origin until the classicity reaches a certain threshold (which is different for different eigenvalues of T), at which time they begin to spiral out to the unit circle. After that point, each time that they cross the positive or negative real axis, Bogomolny's theory predicts that the quantum system should have an even or odd parity eigenstate, respectively. Energies are: (a) $E = 0.004$; (b) $E = 0.2$. In each case, the fourth T-operator eigenvalue to move from the origin to the unit circle is plotted.

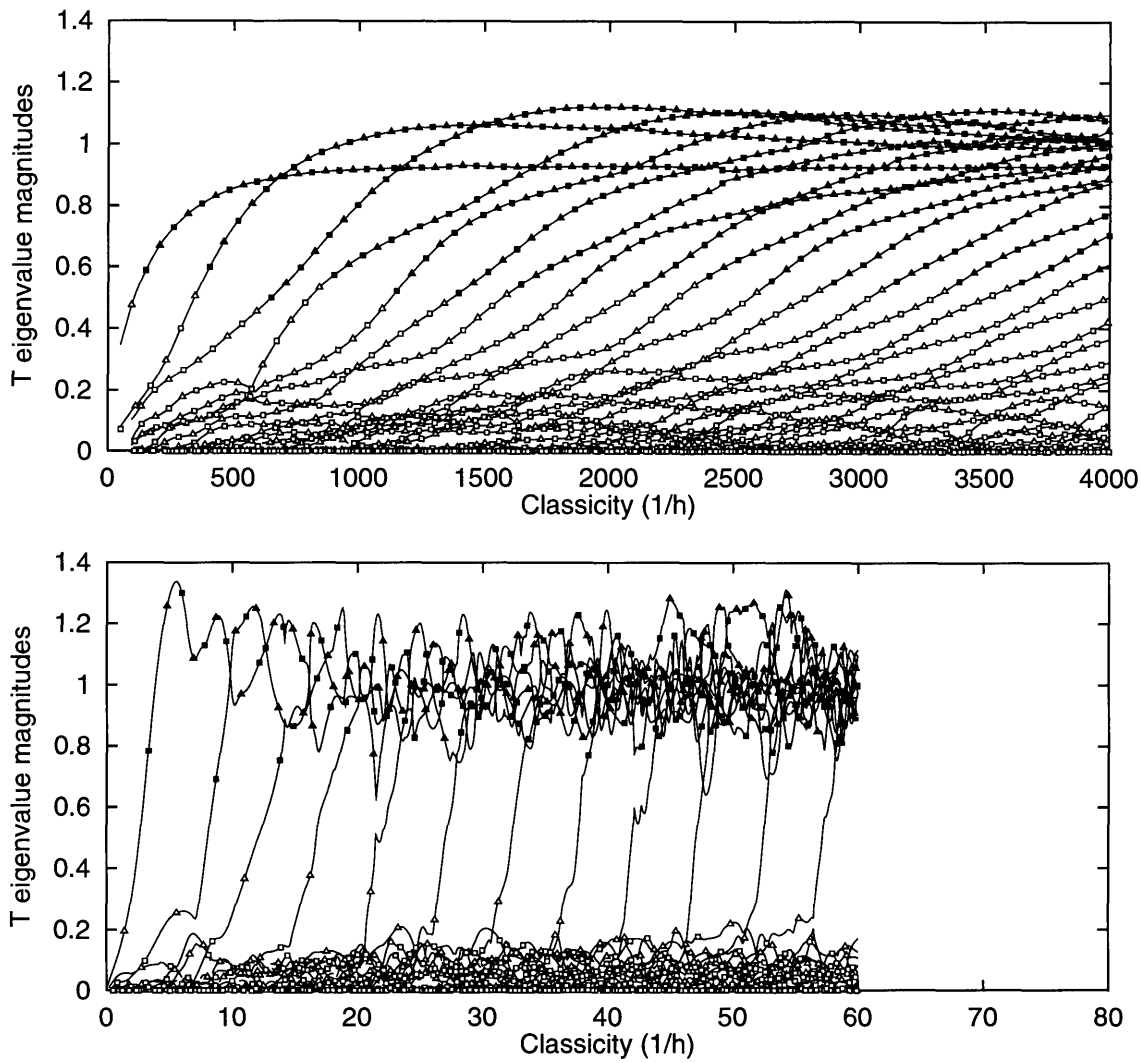

Figure 4-3: Magnitudes of the T-matrix eigenvalues as a function of $1/\hbar$. As the classicity is increased, eigenvalues move, one by one, from the origin towards unit magnitude. Squares are plotted at those points where the eigenvalues have phases of 0 (candidates to be even parity eigenstates), triangles at phase π (odd eigenstates). The symbols are plotted solid for those candidates which turn out to be associated with true eigenstates of the quantum system ("Class 1" eigenvalues), and open for all others ("Class 0" eigenstates). (a) $E = 0.004$, which is in the classically regular regime. (b) $E = 0.2$, which is in the classically chaotic regime. The horizontal axes are scaled such that the densities of states in the horizontal directions are equal for the two energies. The plots predict the first 574 and 321 eigenstates, respectively, of the full quantum mechanical system.

In contrast to a true unitary matrix, whose eigenvalues all lie on the unit circle, T has two classes of eigenvalues. A finite number of them (the number given roughly by Eq. (4.2)) lie in an annulus near the unit circle and are associated with true quantum eigenstates—these we call "Class 1 eigenvalues." The rest of T's eigenvalues (an infinite number of them, limited in numerical experiments by the size of the basis used) are located in a cloud near the origin and are not associated with true quantum eigenstates—these we call "Class 0 eigenvalues." As the classicity is increased, so does the dimension of T: one by one, Class 0 eigenvalues spiral out from the origin to the unit circle and join Class 1. This phenomenon can be seen in figures 4-2 and 4-3. These figures also reveal that the motion of an eigenvalue from Class 0 to Class 1 occurs much more rapidly in the chaotic regime than in the classical regime; in the latter case it is more difficult to define exactly when the transition occurs—a fact which causes some trouble in reconstructing the spectrum, as we shall see. The fact that the eigenvalue curves are vastly smoother in the regular regime than in the chaotic regime will be explained below in Section 4.3.3.

To test Eq. (4.2) quantitatively, we need a proxy for the dimension of T that can be applied to computed T matrices—hopefully one which reflects the fact that the dimension varies continuously with classicity. (We cannot just use the size of the matrix, because that is imposed externally by our choice of basis truncation.) We use

$$\dim T \equiv \mathrm{Tr}\ TT^{\dagger}, \tag{4.3}$$

which we plot in Fig. 4-4 alongside Bogomolny's prediction (Eq. (4.2)). As can be seen, the agreement is quite good, even at the finite classicity range shown. It is also noteworthy that the dimension varies even more smoothly than do the curves of the individual eigenvalue magnitudes (Fig. 4-3); this is because variations in the magnitude of one eigenvalue tend to be negatively correlated with variations in those of another.

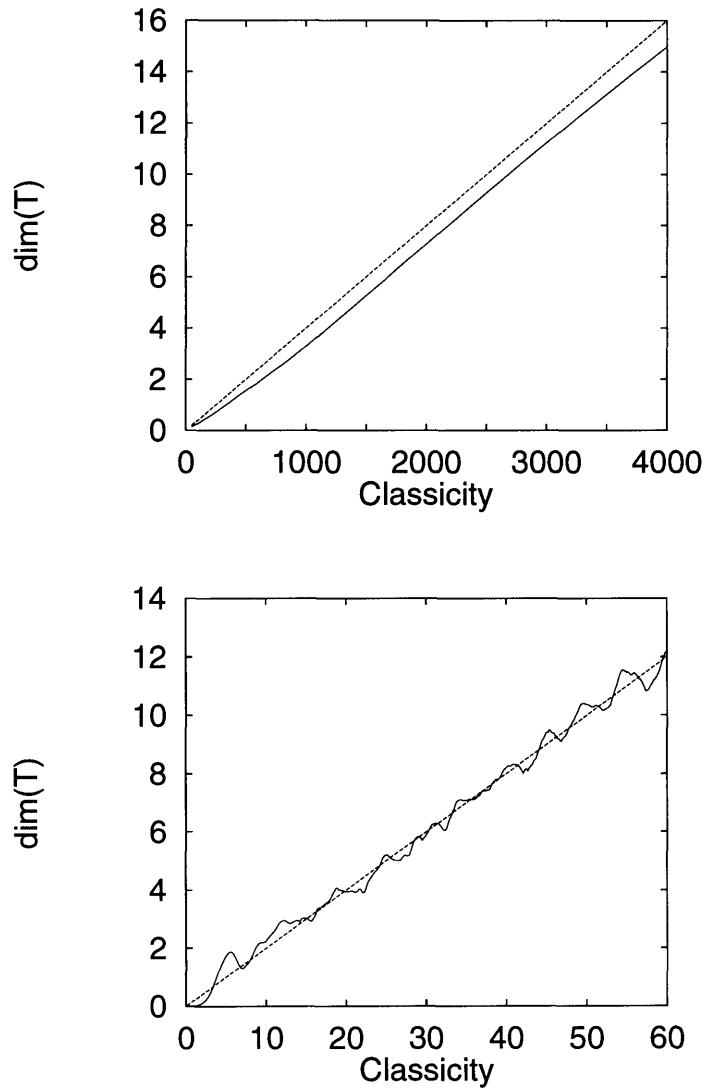

Figure 4-4: The dimension of the desymmetrized T operator as a function of classicity, for (a) $E = 0.004$, (b) $E = 0.2$. The dashed curves show Bogomolny's theoretical prediction (Eq. (4.2)); the solid curves, the results of our numerical experiment (Eq. (4.3)). In addition to the good agreement, it is interesting that these curves are considerably smoother than are the individual curves in Fig. 4-3; the excursions of those curves tend to cancel one another out. The reason for the shift in (a) is unknown.

4.3.2 T eigenvalue phases; looking for eigenstates

Recall that the criterion for an even eigenstate of the system is that T have an eigenvalue equal to 1 (for brevity we temporarily ignore the odd-parity eigenstates which occur at eigenvalues of -1). Of course Bogomolny's method is a semiclassical approximation, which always entails the use of a stationary phase approximation to the exact Feynman path integrals. Thus we shouldn't be surprised that although the eigenvalues approach a band around the unit circle, they never equal 1 exactly. Therefore a more robust criterion is needed than "equality to 1."

What is clear is that quantum eigenstates should only be associated with Class 1 eigenvalues—the eigenvalues which have magnitudes of approximately unity. As the classicity is increased, these eigenvalues rotate counterclockwise along the unit circle. On each rotation they pass close to 1 and "generate" an eigenstate; we need to decide at exactly which point the eigenstate is likely to occur. At least three possible criteria suggest themselves:

1. the point at which $\det(1 - T) = 0$ is most nearly fulfilled

2. the point where an eigenvalue closest approaches 1

3. the point where an eigenvalue crosses the positive real axis (has a phase of 0)

Although criterion 1 is the one emphasized by Bogomolny, we reject it because the determinant mixes together information about all of the eigenvalues of T, whereas eigenstates are each associated with a single eigenvalue of T. Criteria 2 and 3 produce results which differ only very slightly from one another. Criterion 3 is more robust than 2 and, we believe, more appropriate; therefore in our search for even parity eigenstates, we concentrate on those points where the T operator has a Class 1 eigenvalue with $phase = 0$. (Odd eigenstates are similarly found where a Class 1 eigenvalue has $phase = \pi$.) Accordingly, in figure 4-3 we have placed symbols on the curves whenever the eigenvalue crosses the real axis: squares and triangles mark the points where the eigenvalues have phases of 0 or π, and which are thus candidates to be even or odd eigenstates, respectively.

It is important to emphasize that there is *no ambiguity at all* in the recipe for finding places where an eigenvalue crosses the real axis. Through the course of our numerical explorations, we found that the eigenvalues' phases increase monotonically as the classicity was increased, except for a very few, brief exceptions. Since T can be computed and diagonalized at any value of classicity, this means that any simple scheme suitable for finding a bracketed zero of a function suffices to pinpoint the classicity at which a T operator eigenvalue crosses the real axis of the complex plane.

The next task in a purely semiclassical calculation would be to determine which of the phase = 0 points correspond to quantum states at all (or equivalently, which of the phase = 0 points occur for Class 1 eigenvalues, and which for Class 0). We had it easy—since we had the exact quantum results, we knew where eigenclassicities were supposed to be; if there was still some ambiguity, we could look at the surface of section wavefunctions (which will be discussed below) and match them up that way. But we would like to use our experience to describe how Class 1 eigenvalues could be distinguished from Class 0 eigenvalues in a purely semiclassical calculation, *without* the benefit of knowing the exact answers.

In the semiclassical limit, Class 1 eigenvalues are supposed to all have magnitude 1, and Class 0 eigenvalues, magnitude 0. Figure 4-5 summarizes the extent to which this prediction was met at finite classicity in our system. While it is true that the eigenvalues tend to cluster around either the origin or the unit circle, the bands are pretty wide. Does the width of the bands cause practical problems?

In the regular regime, it sometimes does: there is a range of magnitudes, around 0.475–0.55, in which both Class 1 and Class 0 eigenvalues occur. In this overlap area, magnitude information is not sufficient to classify the eigenvalues. Fortunately, only a few percent of the eigenvalues fall into this uncertain range; the rest are predicted unambiguously by Bogomolny's method. Even *in* this range, it is likely that in many cases one could tell which of the ambiguous eigenvalues need to be included in Class 1 by looking for deficits in the semiclassical staircase as compared to the Thomas-Fermi smoothed spectral staircase function.

In the chaotic regime, the width of the bands causes no problem: it is still easy

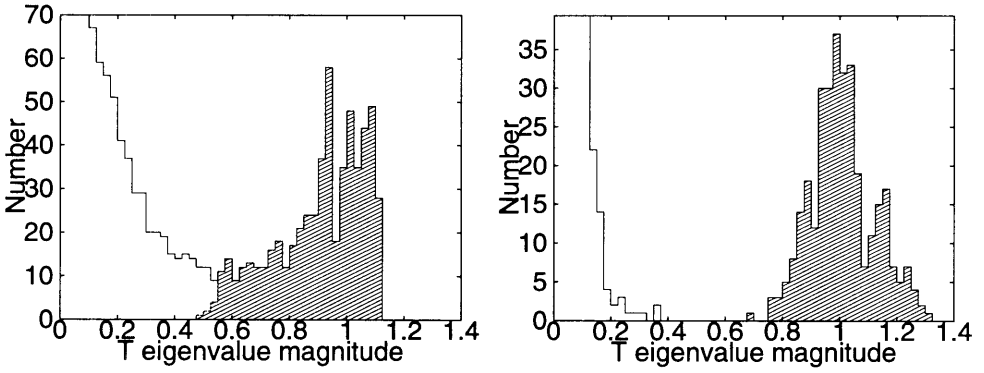

Figure 4-5: The separation of eigenvalues into Class 0 and Class 1. Plotted is the distribution of magnitudes of T operator eigenvalues which cross the (positive or negative) real axis. The part of the histogram which is shaded contains Class 1 crossings, which are associated with true quantum eigenstates; the unshaded part, Class 0 crossings. (a) $E = 0.004$. In this (regular) regime, there is a transition region around magnitude 0.5, in which Class 0 and Class 1 eigenstates are both present and thus difficult to distinguish by magnitude alone. (b) $E = 0.2$. In this (chaotic) regime, the two classes are well separated and Class 1 eigenvalues can easily be identified by their larger magnitudes. Note that in both cases, there are an infinite number of Class 0 crossings near zero magnitude.

to distinguish Class 1 from Class 0 eigenvalues, because of the large gap separating them. In our experiment in the chaotic regime, no Class 0 eigenvalues had magnitudes above 0.4, and no Class 1 eigenvalues had magnitudes below 0.65. This fortuitous circumstance is not only the result of the eigenvalues' spiraling quickly from the origin to the unit circle; as seen in figure 4-6, they all spiral out along a relatively narrow band in the lower complex half plane, and the entire journey is completed in less than the time it takes for half a rotation around the origin. As a result, there is *no ambiguity whatsoever* about the semiclassical method's predictions for the location of eigenclassicities in the chaotic regime (later we will discuss how accurate those unambiguous predictions are). This reliability is in contrast to that of other semiclassical methods, which frequently fail to resolve adjacent eigenstates and thereby leave doubt about the number of eigenstates in a spectrum.

Altogether, the first 574 eigenstates in the regular regime, and the first 321 eigenstates in the chaotic regime (in each case, some even, some odd parity) are reproduced

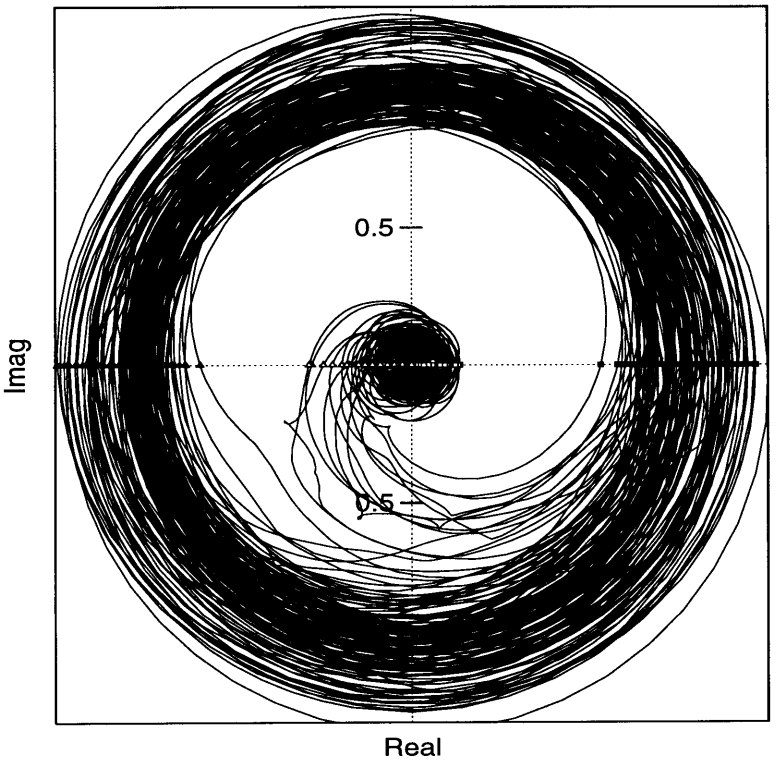

Figure 4-6: T-matrix eigenvalues in the complex plane, for $E = 0.2$. This figure is similar to figure 4-2, except that all of the eigenvalues of T are shown on the same plot. The striking feature revealed is that all of the eigenvalues spiral from the origin to the unit circle along a single band in the lower half of the complex plane. Within that rotation of π radians, they manage to make it all the way from Class 0 to Class 1; during their brief transition, they are away from the real axis and so do not produce crossings of uncertain class.

by the data. The *accuracy* of the semiclassical eigenstates will be discussed in Section 4.4, after a few more qualitative observations.

4.3.3 Quantum numbers from the semiclassical data

Each Class 1 eigenvalue of the T operator produces many eigenstates, one each time it rotates through the real axis. Consequently it is possible to separate the eigenstates into groups, based on which T operator eigenvalue each one is associated with. In figure 4-3, eigenstates in a group all lie on the same eigenvalue curve, like beads on a string. Although the groups are well defined in both regimes, they are truly significant only in the regular regime.

For the mostly regular energy $E = 0.004$, the system is nearly an anisotropic harmonic oscillator, so it is nearly separable into x- and y-motions. Eigenstates of the system can therefore be labeled by two "almost good" quantum numbers, n'_x and n'_y, which count the number of excitations along and perpendicular to the surface of section, respectively. The near separability is the reason that the eigenvalue curves in the regular regime are so smooth and unkinked; and the quantum numbers can be read off the picture as well. All of the eigenstates on the first eigenvalue curve have $n'_y = 0$—that is, they have no excitations in the vertical direction; those on the second curve have $n'_y = 1$; on the third curve, $n'_y = 2$; etc. Meanwhile n'_x can be read off the diagram too: the first eigenstate on a particular curve has $n'_x = 0$; the second, $n'_x = 1$; etc.

For the mostly chaotic energy $E = 0.2$, however, the system is far from separable, and it has no set of good quantum numbers. The eigenstates still lie on continuous curves, but now the curves are kinked and bent whenever two eigenvalues approach each other in the complex plane. We see evidence that each interaction of two curves is accompanied by an intermixing of the eigenstates' properties in the same manner as happens at "avoided crossings" of energy levels, seen when a quantum mechanical system's external parameter is scanned adiabatically. So although the eigenstates are still connected by eigenvalue curves, the eigenstates lying on a single curve do not necessarily have similar properties, and the grouping by curves is not helpful.

4.4 Accuracy of eigenclassicity spectrum

We have now outlined all of the steps necessary to compute the eigenclassicity spectrum predicted by Bogomolny's quantum surface of section method. In order to check its accuracy, it was necessary to decide, for each of the semiclassically computed eigenclassicities, which of the exact eigenclassicities it was "trying to predict." This we did manually by comparing the two spectra; usually the eigenstates lined up so well that the correlation was obvious. When two states were very close to one another, the further step was taken of comparing the exact and semiclassical surface of section wavefunctions; this almost always made it obvious how to match up the numbers.

Figure 4-7 shows the errors of the semiclassical approximation as a function of classicity, for the two energy values. Figures 4-7(a) and 4-7(b) are scaled so as to be directly comparable to one another, in the sense that the vertical and horizontal axes are scaled in proportion to the respective Thomas-Fermi densities of state for the two energies. Each symbol on these plots represents an eigenclassicity predicted by Bogomolny's method; its vertical position shows the amount by which the semiclassical prediction differed from the exact value. In figure 4-7(a), line segments connect eigenstates which are associated with the same T-matrix eigenvalue; this was not done in figure 4-7(b) for the reason mentioned at the end of the previous section (for that same reason, connecting them would not result in smooth curves but rather in a tangled jumble anyway).

We have already discussed some differences between the regular and the chaotic regimes—that when the system is classically chaotic it is somewhat more effort to calculate T, but somewhat less difficult to distinguish Class 1 from Class 0 eigenvalues—now we ask: how accurately does Bogomolny's method predict eigenclassicities in the two regimes? From our numerical experiment it appears that the semiclassical does not care about the degree of classical chaos; at least in this experiment, *eigenstate positions are approximated by Bogomolny's scheme just as well in the classically chaotic regime as in the classically regular regime.*

Note also that the worst errors seem to be roughly constant at all classicities—

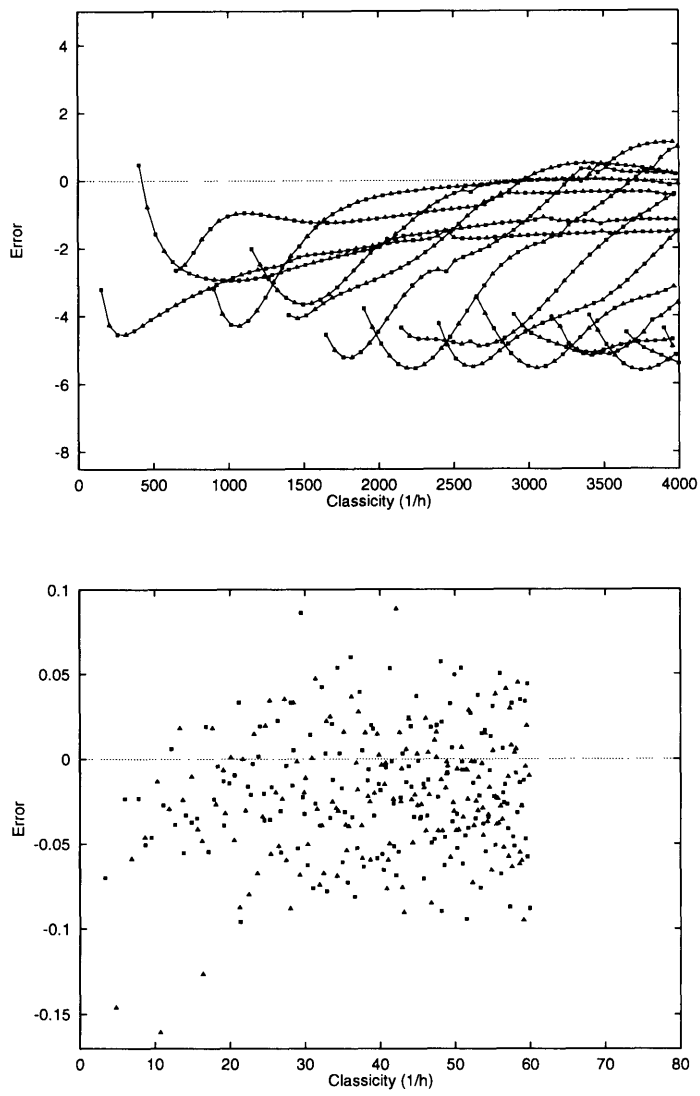

Figure 4-7: Errors in the semiclassical eigenclassicity spectra. The discrepancy between the semiclassically predicted eigenclassicities and the exact values (obtained by diagonalizing the Hamiltonian), for (a) $E = 0.004$ and (b) $E = 0.2$. Squares represent even parity states; triangles, odd. In (a), lines connect eigenstates which are associated by being on the same curves in Fig. 4-3 and which thus have in common the approximate quantum number n'_y. Corresponding connections are not made in (b) because in this chaotic regime, associations of eigenstates do not form anything resembling continuous curves. Note that the average errors seem to be roughly constant or even slowly decreasing as the system becomes more classical.

high excitation states' positions are approximated just as well as low excitation states'. Moreover, when one follows individual curves in figure 4-7(a) (the nearly separable regime), one sees that individually, the errors along any one curve seem to be decreasing towards zero. Remembering from Section 4.3.3 that the eigenstates along a given curve share the same n_y quantum number and have increasing n_x quantum numbers, it seems that, at least in the regular regime, *the semiclassical predictions are better for states which have more excitations transverse to the surface of section, but roughly constant regardless of the number of excitations along the SOS.*

Why might this be? While we do not fully understand this result, we offer the following possible explanation: In the 2-D eigenclassicity problem, states with a constant number of vertical excitations have a smaller and smaller *fraction* of their energy in the vertical direction as the classicity is increased. They thus shrink in the vertical direction, moving ever farther from the classically forbidden region where tunnelling is important. But since tunnelling trajectories are not included in the semiclassical method, the result might be to cause the observed improvement in the approximation.

One can argue that efforts to find an analogous correlation (between errors and excitations along or perpendicular to the SOS) in the classically chaotic regime are doomed to failure because of the lack of even approximate quantum numbers. Not entirely satisfied by that argument, we tried anyway, but so far without success.

The above comments refer to the absolute errors of Bogomolny's method in approximating the eigenclassicities of a quantum system. Figure 4-8 shows to what extent the method is able to meet a more exacting standard—the ability to resolve individual eigenstates. There are theoretical reasons to believe that no semiclassical approximation which is correct only to first order in $\hbar$ will be able to resolve highly-excited eigenstates of a system with more than one degree of freedom: the density of states increases more quickly than the semiclassical approximation can hope to converge. The ability of a method to resolve individual eigenstates is measured by dividing its errors by the system's *mean level spacing.* When this quantity approaches 1, nearby features of a spectrum can no longer be separated reliably.

Figure 4-8 shows this ratio for our system. The mean level spacing decreases

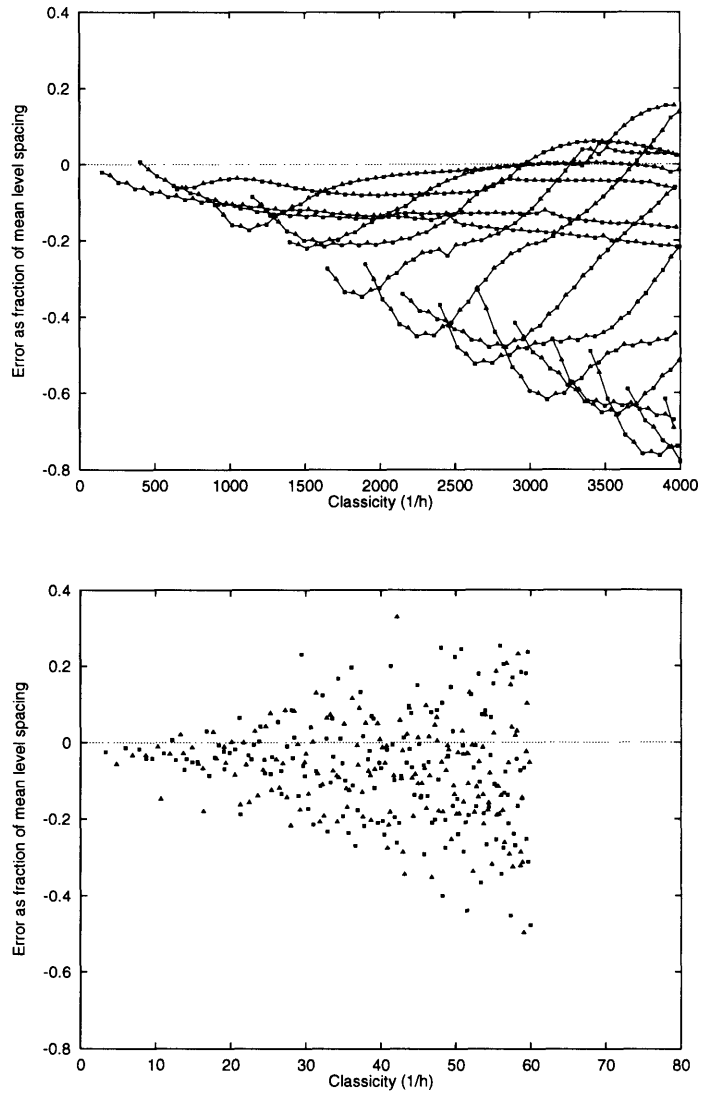

Figure 4-8: Semiclassical errors in units of the mean level spacing. (a) $E = 0.004$; (b) $E = 0.2$. Alas, the rough constancy the the absolute errors demonstrated in Fig. 4-7 means that due to the increasing density of states of the quantum system, the semiclassical errors *as a fraction of the mean level spacing*, shown here, increase with increasing classicity, eventually preventing the resolution of individual eigenstates semiclassically. Nevertheless, after predicting (in the case of (a)) 574 eigenstates, the worst semiclassical errors have yet to quite reach one mean level spacing.

like the reciprocal of the classicity, thereby "raising the standard" against which the approximations are judged. It is seen that Bogomolny's method is a victim of the usual disease: the ratio of error to desymmetrized level spacing increases as the classicity is increased, so it will never be able to single out spectral features at very high excitation number. Still, its strain of the ailment is relatively nonvirulent—the worst error ratios are just creeping up towards 1 after hundreds of eigenstates have been predicted accurately.

4.5 Calculating surface of section wavefunctions

The eigenstates of the T operator are the values of the quantum mechanical wavefunction on the surface of section. That is, if

$$\Psi(x,y) \equiv \langle x,y|\,\Psi\rangle$$

is the 2-D quantum wavefunction, then to within a normalization,

$$\begin{aligned}\psi(y) &\equiv \langle y|\,\psi\rangle \\ &\propto \Psi(0,y).\end{aligned}$$

Odd parity surface of section eigenstates (which are zero on the SOS) can be found too—intuitively, by moving the surface of section an infinitesmal distance δx from the y-axis:

$$\begin{aligned}\psi_{\rm odd}(y) &\propto \Psi(\delta x,y) \\ &\propto \left.\frac{\partial\Psi(x,y)}{\partial x}\right|_{x=0}\end{aligned}$$

As usual, the eigenvalue problem only gives us the semiclassical wavefunctions to within a complex prefactor. Naturally we choose the magnitude of this prefactor to normalize the vector to 1, but there is still a complex phase that needs to be determined.

Since ideally, a phase could be chosen to make the SOS wavefunction pure real, it is sensible to choose the phase so as to minimize the imaginary part. Specifically, we try to minimize

$$I \equiv \int dy \, [\text{Im } \langle y | \psi \rangle]^2.$$

Conveniently, this integral need never be done. Assuming that $|n\rangle$ is an orthogonal complete basis, and that $|y\rangle\, n$ is always real, the required prefactor phase is simply

$$e^{i\phi} = \pm \sqrt{\frac{\sum_n \langle n | \psi \rangle^2}{\left| \sum_n \langle n | \psi \rangle^2 \right|}} \tag{4.4}$$

Since we store the SOS eigenfunctions in such a basis, only the sums appearing in (4.4) need to be done and no integrals. It turns out that after this best phase is chosen, the SOS wavefunctions indeed turn out to have only small imaginary parts.

A sequence of surface of section wavefunctions is plotted in the picture gallery in Appendix A, along with the exact quantum mechanical SOS wavefunctions. It can be seen from those figures that the semiclassical SOS wavefunctions capture, in almost all cases, the qualitative features of their exact counterparts. The semiclassical prediction is often rather poor at predicting the relative heights of peaks in the probability. Moreover it can be seen that the semiclassical SOS wavefunctions are often too "sqeezed in" near the classical turning points, since it does not model tunnelling. However, in many cases the details are predicted with surprising fidelity.

Chapter 5

Action Spectra of Quantum Eigenstates

One of the significant advantages of using a semiclassical technique is the ability to get some intuitive feel for the classical behavior which is most closely analogous to a particular quantum eigenstate. For example, when we see an atomic energy state that has high azimuthal angular momentum, we reasonably expect that classical trajectories which have electrons swinging around the nucleus at large radius should participate strongly in the semiclassical calculation. Conversely, when stable, short-period periodic orbits are present in a classical dynamics of the system, we are not (any longer!) surprised to see quantum states "scarred" by those orbits. In this chapter, we show how it is possible, using Bogomolny's method, to find a "spectrum" of the actions of classical orbits which contribute to a particular, semiclassically determined, quantum eigenstate. This exercise by no means exhausts the possibilities, in the framework of Bogomolny's method, for exploring the correspondence between quantum states and classical trajectories; however, we hope that this section will give the reader a taste for the possibilities available.

5.1 The action spectrum of the classical system

Our approach is quite simple, really: in the method of the quantum surface of section, eigenstates of a quantum system are associated with SOS wavefunctions which are invariant under the action of the transfer operator:

$$T\,|\psi\rangle = |\psi\rangle\,.$$

We obtain $|\psi\rangle$ by diagonalizing the T operator in matrix form.

All classical trajectories of the correct energy contribute to the T operator, but they do not contribute equally. According to equation (2.5), we see that the trajectory which starts at (y,θ), for example, is weighted by the *purely classical* factor

$$|p_x|^{1/2}\left|\frac{\partial Y'(y,\theta,E)}{\partial\theta}\right|^{1/2}_{yE\Sigma} \tag{5.1}$$

even before it is inserted into the semiclassical integral. To see the range of classical trajectories which are present at all, a first step is to plot a histogram of all of the actions appearing in the integral, weighted by the above factor. Specifically, we plot

$$h_0(S') \equiv \int dy \int d\theta\ |p_x|^{1/2}\left|\frac{\partial Y'}{\partial\theta}\right|^{1/2} \delta\left(S' - S(y,\theta,E)\right)$$

The result, which is the simplest of a series of "action spectra" that we shall plot, is shown in figure 5-1. The spectrum is characteristic of the classical system—depending on the shape of the potential, the choice of SOS, and the choice of energy only—and does not involve $\hbar$ at all.

Spikes in the action spectra occur near trajectories where the action is stationary with respect to initial conditions. We can work out the criteria; we require that

$$\left.\frac{\partial S}{\partial y}\right|_\theta = \left.\frac{\partial S}{\partial\theta}\right|_y = 0$$

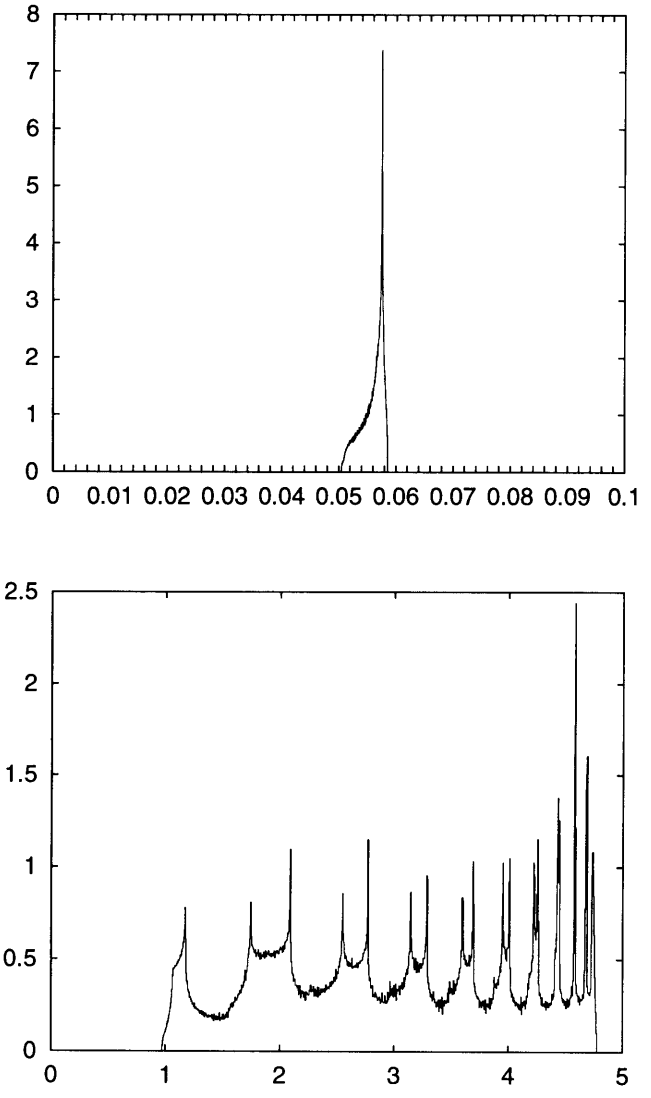

Figure 5-1: Classical action spectra for the Nelson_2 potential. Plotted is a spectrum of the actions of all of the trajectories of one Poincaré mapping, weighted by the purely classical factor shown in Eq. (5.1). The spikes are caused by caustics, at trajectories where the action is stationary with respect to a small change in initial conditions. (a) $E = 0.004$; (b) $E = 0.2$.

Writing $S = S(y, y'(y, \theta))$, and making use of the identities

$$\left.\frac{\partial S}{\partial y}\right|_{y'} = -p_y$$

$$\left.\frac{\partial S}{\partial y'}\right|_{y} = p'_y,$$

the two criteria are equivalent to

$$p'_y \left.\frac{\partial y'}{\partial \theta}\right|_{y} = 0 \text{ and } p'_y \left.\frac{\partial y'}{\partial y}\right|_{\theta} = p_y.$$

All of the quantities are finite, so there are two cases.

The first case for which a spike occurs in the action spectrum is

$$p_y = p'_y = 0$$

and corresponds to trajectories which intersect the SOS perpendicularly at both start and end. These trajectories are often half of symmetric periodic orbits, if the SOS is a symmetry axis of the potential.

The second case occurs when

$$\left.\frac{\partial y'}{\partial \theta}\right|_{y} = 0 \text{ and } p'_y \left.\frac{\partial y'}{\partial y}\right|_{\theta} = p_y$$

The first equality demands that the trajectories return to the surface of section focused, but the second condition does not seem to have any simple physical interpretation.

5.2 The action spectrum of a quantum eigenstate

But we have more information, which we can use to augment the previous plot. Namely, after we diagonalize T and find an SOS eigenfunction which satisfies Bogomolny's condition, we can find the spectrum of actions which contribute to that

particular quantum state. This we do by re-examining equation (2.5). The eigenvalue of an SOS wavefunction $|\psi\rangle$ is given by $\langle\psi|\,T\,|\psi\rangle$, so the contribution due to the single orbit starting at (y,θ) to this eigenvalue is given by

$$\begin{aligned}\Delta\langle\psi|\,T\,|\psi\rangle &= \frac{1}{(2\pi i\hbar)^{1/2}}\,|p_x|^{1/2}\left|\frac{\partial Y'}{\partial\theta}\right|^{1/2}_{yE\Sigma} \\ &\quad\times\exp\left(i\frac{S(y,\theta)}{\hbar}-i\frac{\pi}{2}\nu\right)\langle\psi|\,Y'(y,\theta,E)\rangle\,\langle y|\,\psi\rangle\,. \qquad (5.2)\end{aligned}$$

The notation used is such that $\langle\psi|\,T\,|\psi\rangle$ is equal to the integral of $\Delta\langle\psi|\,T\,|\psi\rangle$ over all initial conditions y and θ on the surface of section.

We will plot two slightly different types of action spectra for each SOS wavefunction. The first is a histogram of the actions weighted by the absolute value of expression (5.2), and therefore shows the total of the contributions from trajectories with action S, before destructive interference is taken into account. The second does take into account destructive interference, by summing, for each action, the expression (5.2) *including* the complex phases. Specifically, the two spectra are given by:

$$\begin{aligned}h_1(S') &\equiv \int dy\int d\theta\left|\Delta\langle\psi|\,T\,|\psi\rangle\right|\,\delta\left(S'-S(y,\theta,E)\right) \\ &= \frac{1}{(2\pi\hbar)^{1/2}}\int dy\int d\theta\;|p_x|^{1/2}\left|\frac{\partial Y'}{\partial\theta}\right|^{1/2} \\ &\quad\times\left|\langle\psi|\,Y'(y,\theta)\rangle\cdot\langle y|\,\psi\rangle\right|\,\delta\left(S'-S(y,\theta,E)\right) \\ h_2(S') &\equiv \int dy\int d\theta\;\Delta\langle\psi|\,T\,|\psi\rangle\;\delta\left(S'-S(y,\theta,E)\right).\end{aligned}$$

h_2 contains the most information, since

$$\int dS\,h_2(S)=\langle\psi|\,T\,|\psi\rangle\,.$$

h_2 is complex, so in the figures we plot its magnitude.

These spectra are plotted for a number of the eigenstates of the system, in both the chaotic and the regular regimes, in the picture gallery in Appendix A. It can be

seen that many of the peaks contained in figure 5-1 are missing or diminished in a typical h_1 spectrum; this indicates that the orbits represented in the peak intersect the surface of section in a region where the SOS wavefunction is small, so they do not couple to the wavefunction. There are also many instances where peaks visible in the h_1 spectrum are absent in the h_2 spectrum. This happens when two or more groups of trajectories have similar actions, but different phases or Maslov indices and therefore destructively interfere.

Chapter 6

Conclusions

What is the point of a semiclassical theory? Historically, semiclassical theory came before, and inspired, matrix mechanics. However, in the intervening years, as the quantum method revealed its power and wide applicability, semiclassical methods barely inched forward. But finally in the late 1960's and early 1970's, two things happened. One was the (re-)discovery of chaos, and the realization that a big fraction of classical systems had been left unexplored and misunderstood, unknowingly assumed nonexistent by scientists whose training was virtually limited to ballistic trajectories, harmonic oscillators, and two-body Kepler problems. The second thing that happened was Gutzwiller's discovery of his periodic orbit theory for semiclassical quantization. For the first time, semiclassical mechanics was liberated from the torus and allowed to wander free. The fashionable blending of these two developments, dubbed *quantum chaos*, is at its core nothing more than an attempt to understand semiclassical mechanics off the torus.

Gutzwiller's trace formula is a beautiful edifice, so elegant that physicists have the gut feeling that it *must* be right. This makes it all the more frustrating that it is so hard to use. Periodic orbits are wonderful, canonically invariant objects that are easy to picture and describe. Unfortunately, very long period orbits in a typical chaotic potential are also furiously difficult to calculate. A speck of initial conditions, in a moderately to highly chaotic system, stretches into a gossamer hairball after only a few oscillations, and finding periodic orbits means finding places where the

hairball and speck coincide—for all possible specks of initial conditions. A few such heroic computations have been done, and they are indeed able to reproduce the gross features of the quantum spectrum, and even individual low-lying states. However, as a practical method the trace formula has a long way to go.

It is not necessary to discard periodic orbit theory, but maybe it *is* time to expand our toolbox. It has been noted with admiration that periodic orbits, of longer and longer period, eventually densely explore every part of the phase space. Thus, it is argued, when we go to long enough orbits, the periodic orbits will "know" all there is to be known about the system's classical mechanics. But this is vast overkill. We don't need to limit ourselves to periodic orbits if we want to explore all of phase space. Any set of trajectories—if sprinkled finely enough—does the job very nicely.

Bogomolny's quantum surface of section method does just this. It democratically solicits the contributions of any and every trajectory. When the vote is over, periodic orbits still have disproportionate influence. But their influence comes incidentally, only because periodic orbits come with an entourage of similar behavior, non-periodic trajectories.

This thesis presented an exploration of Bogomolny's method. We explained how to apply this technique to an arbitrary potential in a practical way, and estimated just how efficient the method is when applied to systems of different dimension and different degrees of chaos. We suggested a practical and general way, by solving for eigenclassicities rather than eigenenergies, of testing this and other semiclassical theories with reduced effort. Then we used Bogomolny's method to perform a semiclassical analysis of a generic, non-scalable, nonlinear oscillator, giving practical advice and techniques that will be useful to future users of the method. Our computation yielded hundreds of eigenvalue predictions in both the classically regular and the classically chaotic regimes, all accurate to less than a mean level spacing. We also computed the surface of section wavefunctions predicted by the method and found that they also agree quite well with their exact counterparts. We explored some of the properties of the T operator, especially its dimension and the nature of its unitarity. Finally, we showed how it was possible to extract information about the classical trajectories

associated with a single, particular, quantum wavefunction through the use of the "action spectrum."

The hybrid nature of Bogomolny's transfer operator—produced by summing classical trajectories, but then diagonalized using matrix methods—makes it something of a *semi*-semiclassical method. As such, it does not fulfill Michael Berry's requirements for the yet-unattained "Holy Grail" of a *purely semiclassical method* which is able to *resolve arbitrarily highly excited eigenenergies* (indeed, it falls short on both counts). What this method *is*, however, is a practical method of semiclassically approximating information about quantum systems; a method which, though somewhat intricate to implement the first time, can function as a self-contained "black-box" which inputs Hamiltonians and outputs approximate quantum-mechanical spectra.

Appendix A

Picture Gallery—SOS Wavefunctions and Action Spectra

This appendix contains a sample of the surface of section wavefunctions predicted by Bogomolny's method, and their corresponding action spectra. In each energy regime, 20 such pairs are presented, at equivalent parts of each spectrum. The eigenstates were not specially selected, and are typical of other eigenstates that we looked at.

The upper figure on each page gives the probability density along the surface of section,

$$\psi(y) \equiv \Psi(x = 0, y)$$

as explained in section 4.5. The wavefunctions are all normalized to unit probability, and the complex phase of the semiclassical wavefunctions is chosen so as to minimize $\int dy \, \mathrm{Im}\, [\psi(y)]^2$. The three curves are: (1) the exact $\psi(y)^2$, which is necessarily real; (2) the semiclassically predicted $|\psi(y)|^2$; and (3) the square of the residual imaginary part of the semiclassically predicted wavefunction, $[\mathrm{Im}\ \psi(y)]^2$ (which ideally should be zero). None of the SOS wavefunctions are wildly wrong, though often the peaks' relative heights are not predicted well. It is also noticable that the semiclassical wavefunctions are often "pushed in" near the classical turning points, since they are not able to tunnel like the exact wavefunctions can. Most of the predictions, however, match the exact SOS wavefunctions quite well.

The lower figure on each page shows two types of action spectrum for the same eigenstate. In each figure, the solid line represents $h_1(S)$ and the dashed line, $h_2(S)$; these two functions are explained in Chapter 5. Even in the regular regime ($E = 0.004$), there is a marked difference in the extent to which different trajectories contribute to T. However, it is in the chaotic regime where the signatures of individual eigenfunctions are most distinct from one another. In some instances, the T operator is dominated by contributions from only a few classical trajectories—in those cases we would expect that the full quantum mechanical wavefunctions would be visibly scarred by those orbits. Unfortunately, further investigation of this subject requires information about classical orbits and full quantum eigenstates which has not been collected, and so will have to wait for the future.

A.1 Regular regime: $E = 0.004$

The figures in this section are for energy 0.004, which is in the mostly regular regime. The eigenstates covered are the 20 in the classicity range $2500 \leq 1/\hbar \leq 2617$.

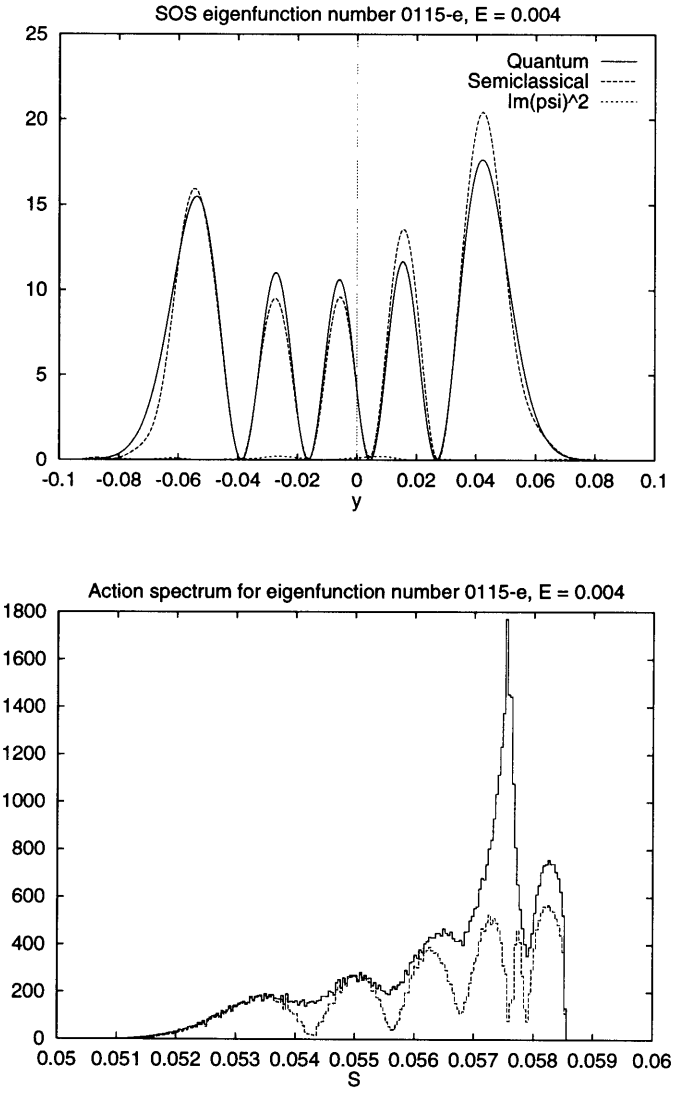

Figure A-1: SOS eigenfunction and action spectrum, 115th even eigenstate. Exact $1/\hbar = 2506.08$; $\Delta(1/\hbar) = -0.39$; magnitude of T eigenvalue $|t_i| = 1.048$.

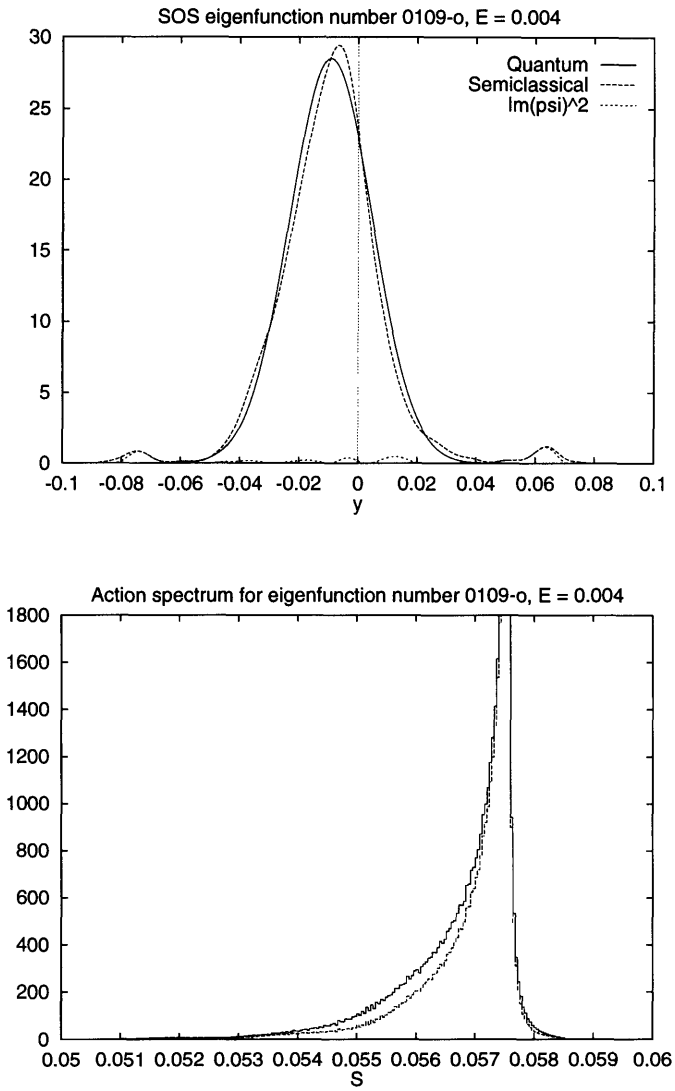

Figure A-2: SOS eigenfunction and action spectrum, 109th odd eigenstate. Exact $1/\hbar = 2508.20$; $\Delta(1/\hbar) = -1.69$; magnitude of T eigenvalue $|t_i| = 0.917$.

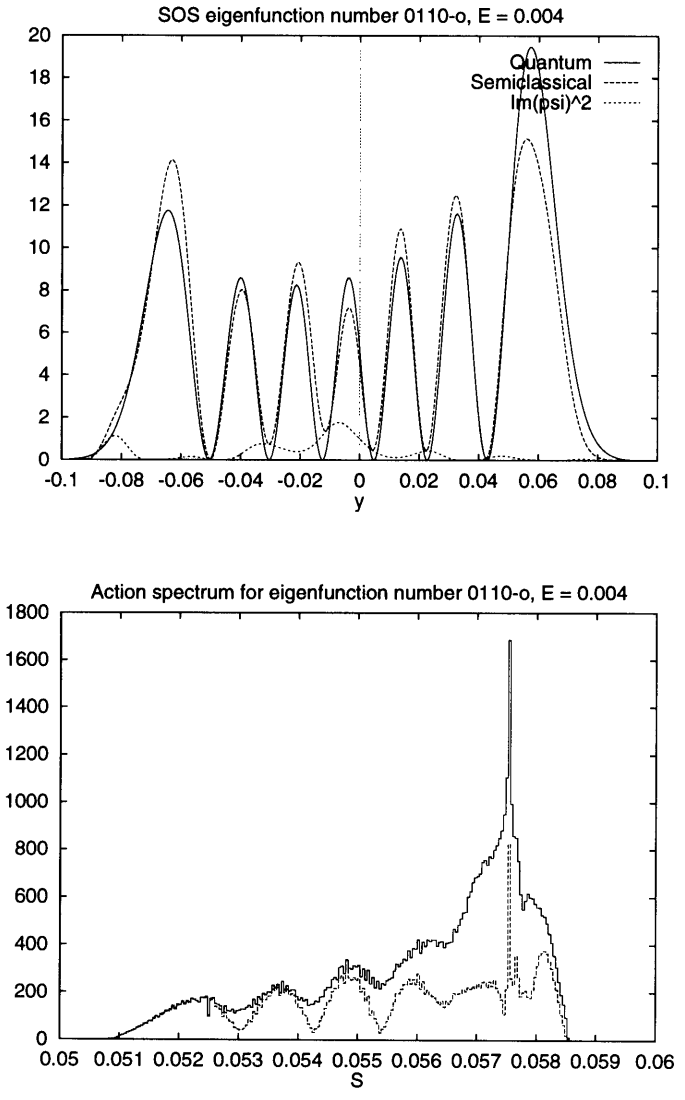

Figure A-3: SOS eigenfunction and action spectrum, 110th odd eigenstate. Exact $1/\hbar = 2511.33$; $\Delta(1/\hbar) = -2.38$; magnitude of T eigenvalue $|t_i| = 0.892$.

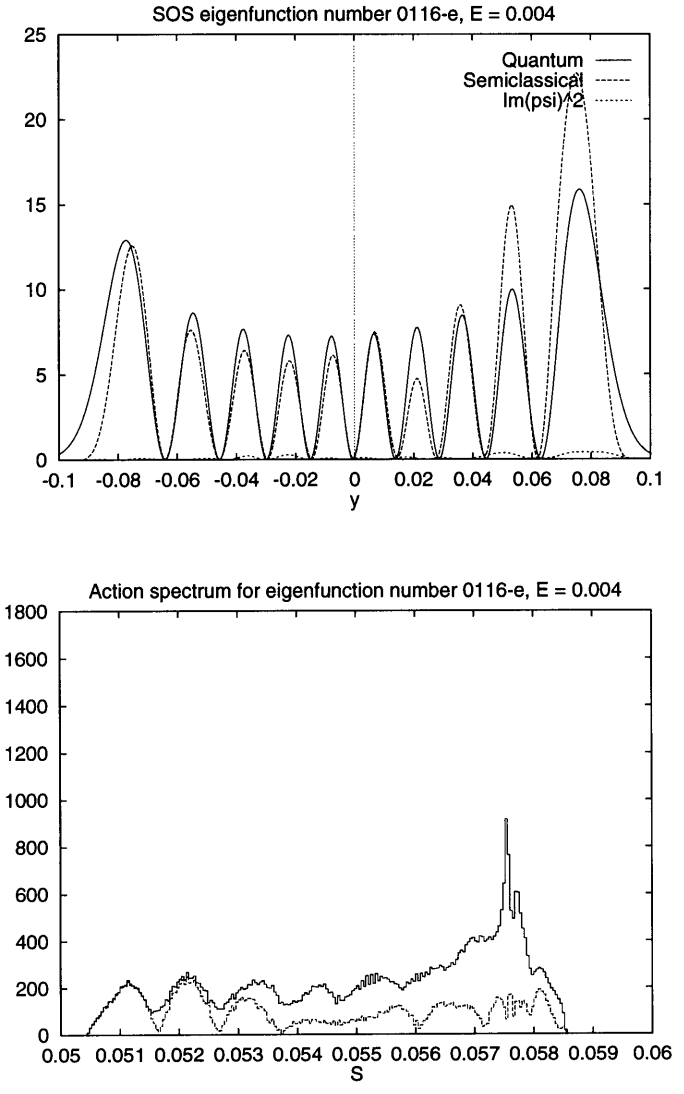

Figure A-4: SOS eigenfunction and action spectrum, 116th even eigenstate. Exact $1/\hbar = 2521.05$; $\Delta(1/\hbar) = -5.26$; magnitude of T eigenvalue $|t_i| = 0.623$.

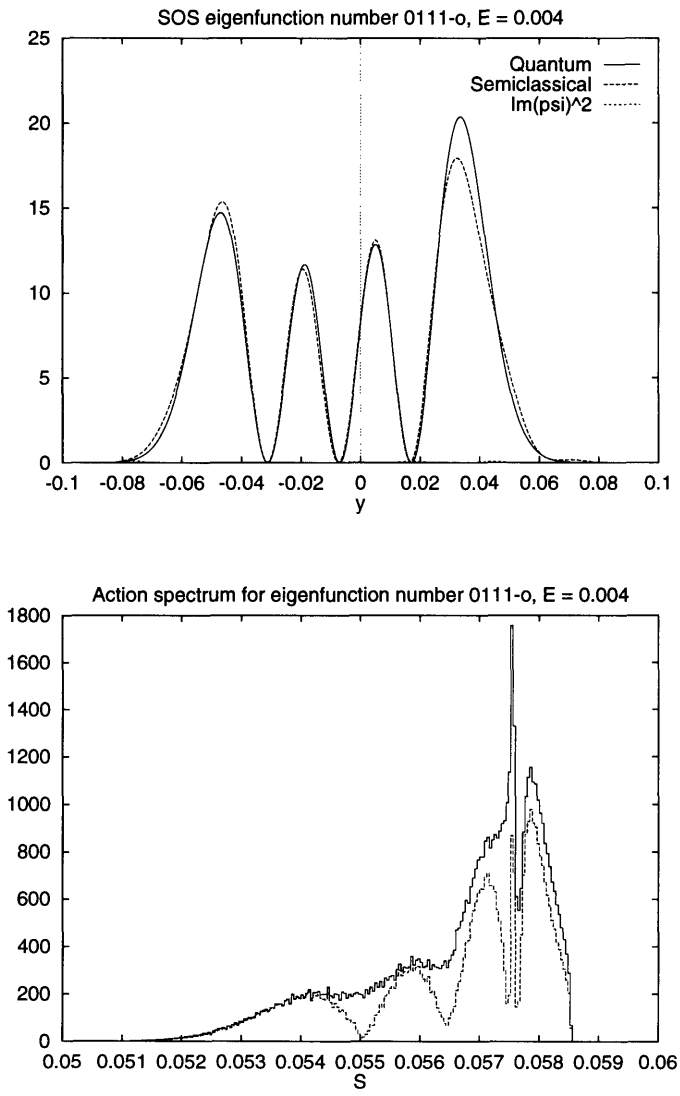

Figure A-5: SOS eigenfunction and action spectrum, 111th odd eigenstate. Exact $1/\hbar = 2525.75$; $\Delta(1/\hbar) = -0.18$; magnitude of T eigenvalue $|t_i| = 1.103$.

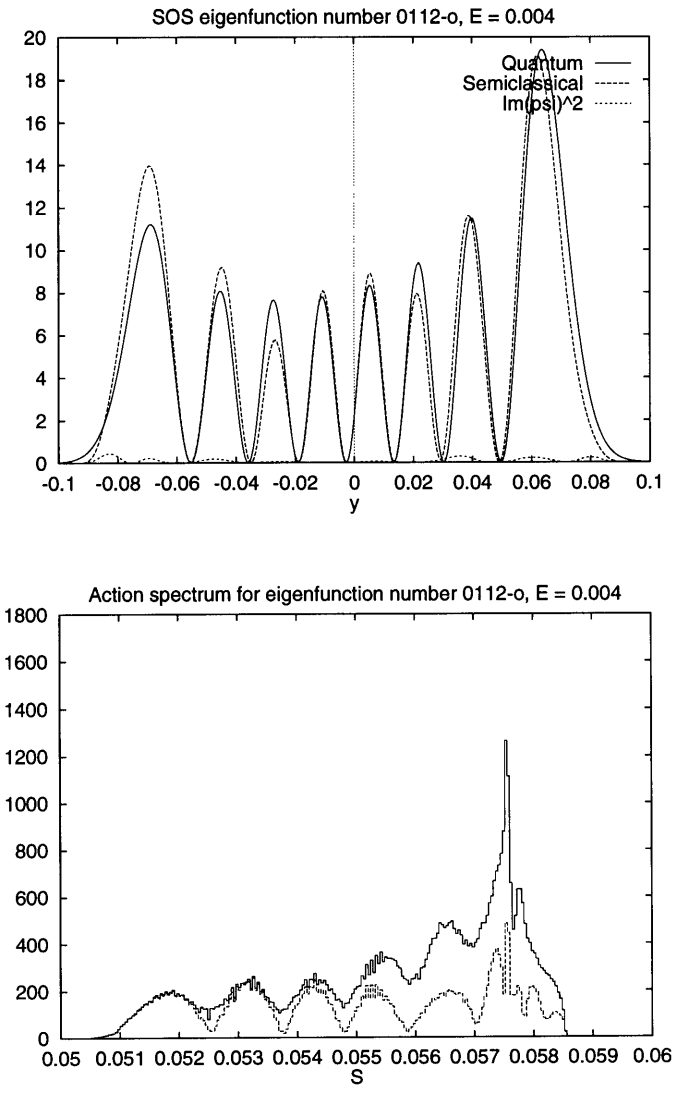

Figure A-6: SOS eigenfunction and action spectrum, 112th odd eigenstate. Exact $1/\hbar = 2537.00$; $\Delta(1/\hbar) = -4.25$; magnitude of T eigenvalue $|t_i| = 0.780$.

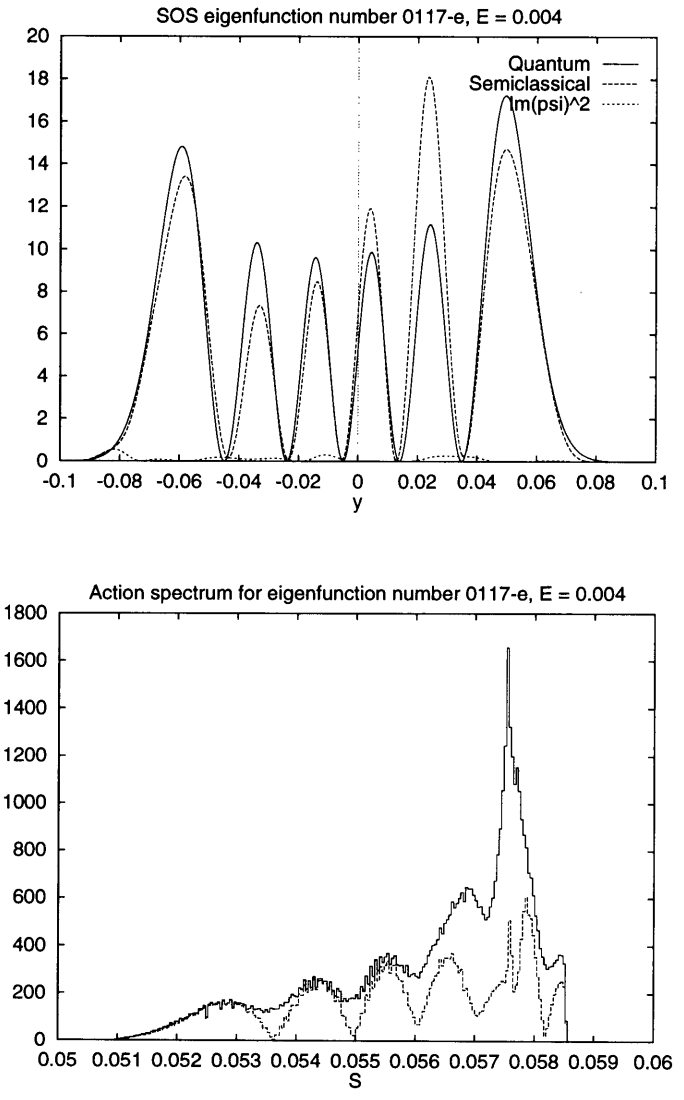

Figure A-7: SOS eigenfunction and action spectrum, 117th even eigenstate. Exact $1/\hbar = 2538.35$; $\Delta(1/\hbar) = -1.30$; magnitude of T eigenvalue $|t_i| = 0.957$.

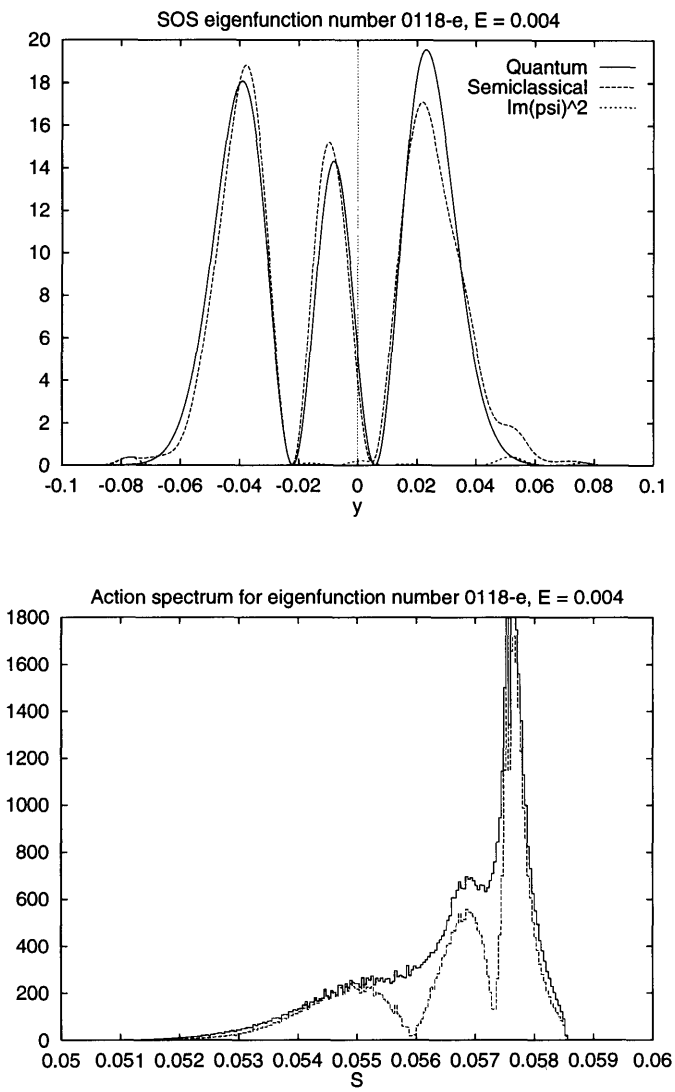

Figure A-8: SOS eigenfunction and action spectrum, 118th even eigenstate. Exact $1/\hbar = 2541.71$; $\Delta(1/\hbar) = -0.82$; magnitude of T eigenvalue $|t_i| = 1.096$.

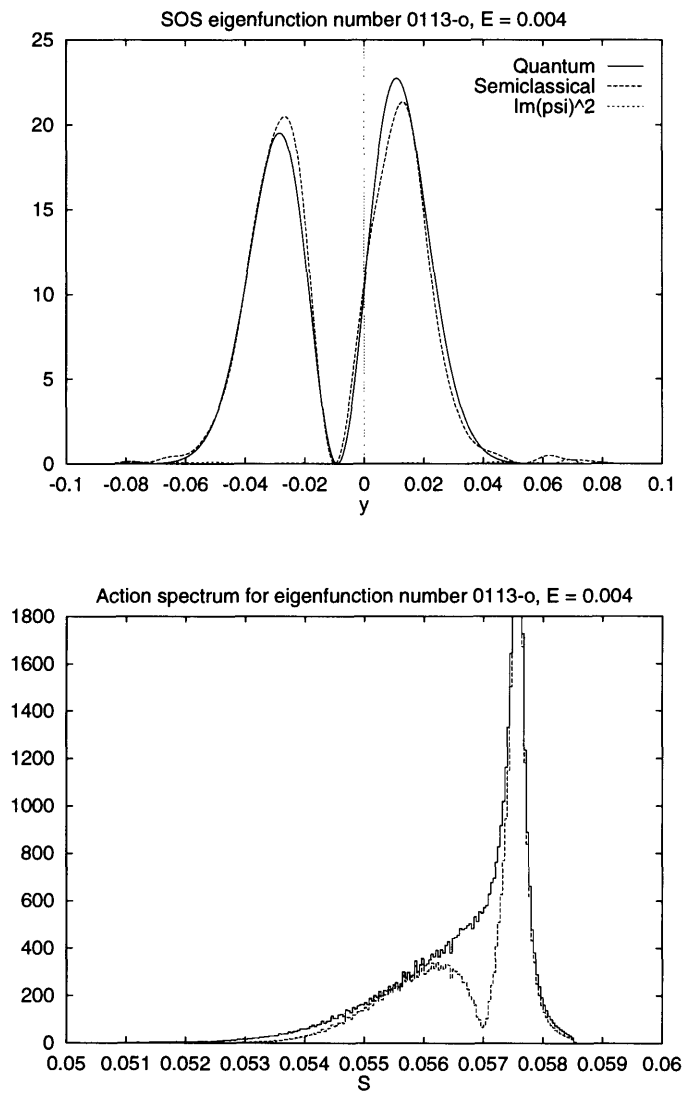

Figure A-9: SOS eigenfunction and action spectrum, 113th odd eigenstate. Exact $1/\hbar = 2554.04$; $\Delta(1/\hbar) = -1.42$; magnitude of T eigenvalue $|t_i| = 1.024$.

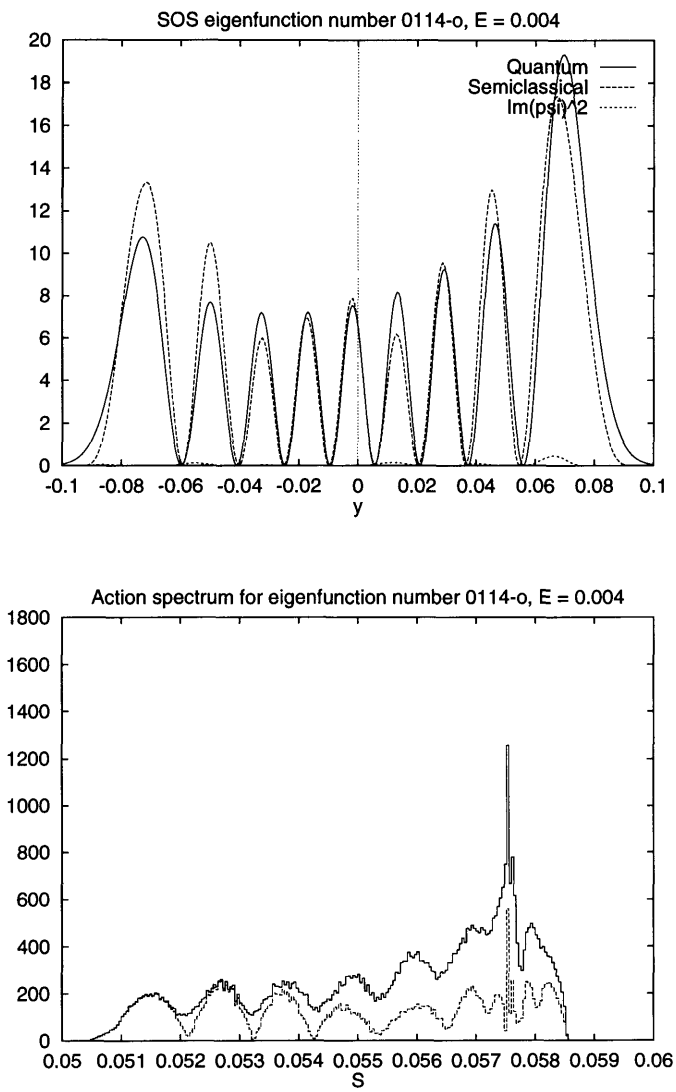

Figure A-10: SOS eigenfunction and action spectrum, 114th odd eigenstate. Exact $1/\hbar = 2559.62$; $\Delta(1/\hbar) = -4.84$; magnitude of T eigenvalue $|t_i| = 0.761$.

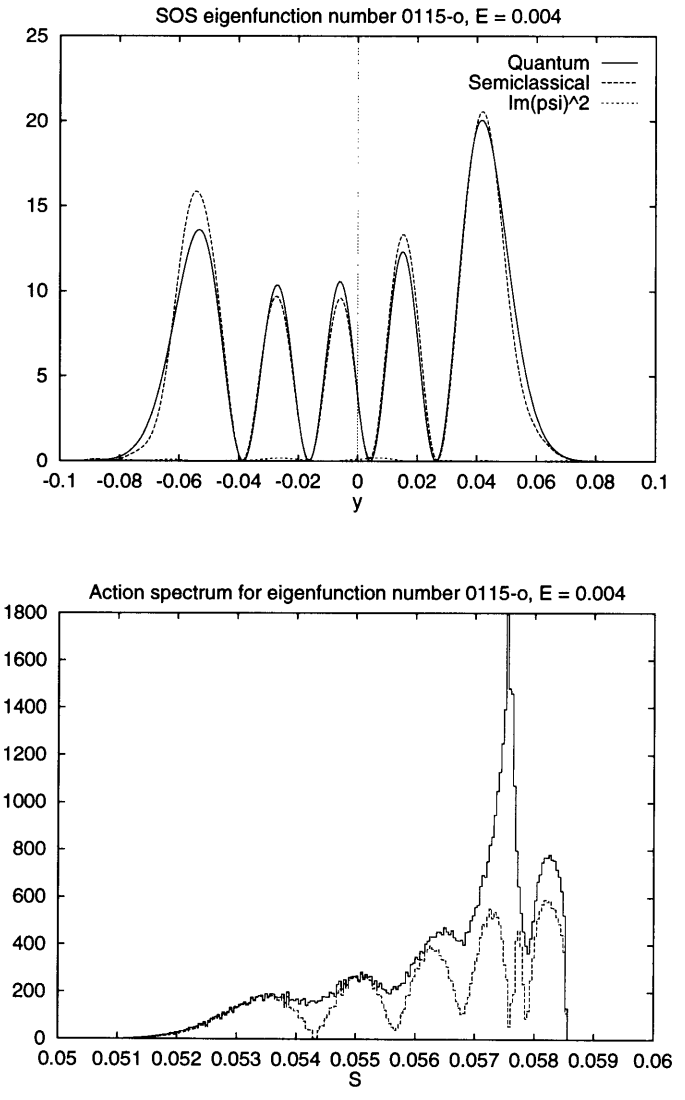

Figure A-11: SOS eigenfunction and action spectrum, 115th odd eigenstate. Exact $1/\hbar = 2561.45$; $\Delta(1/\hbar) = -0.30$; magnitude of T eigenvalue $|t_i| = 1.059$.

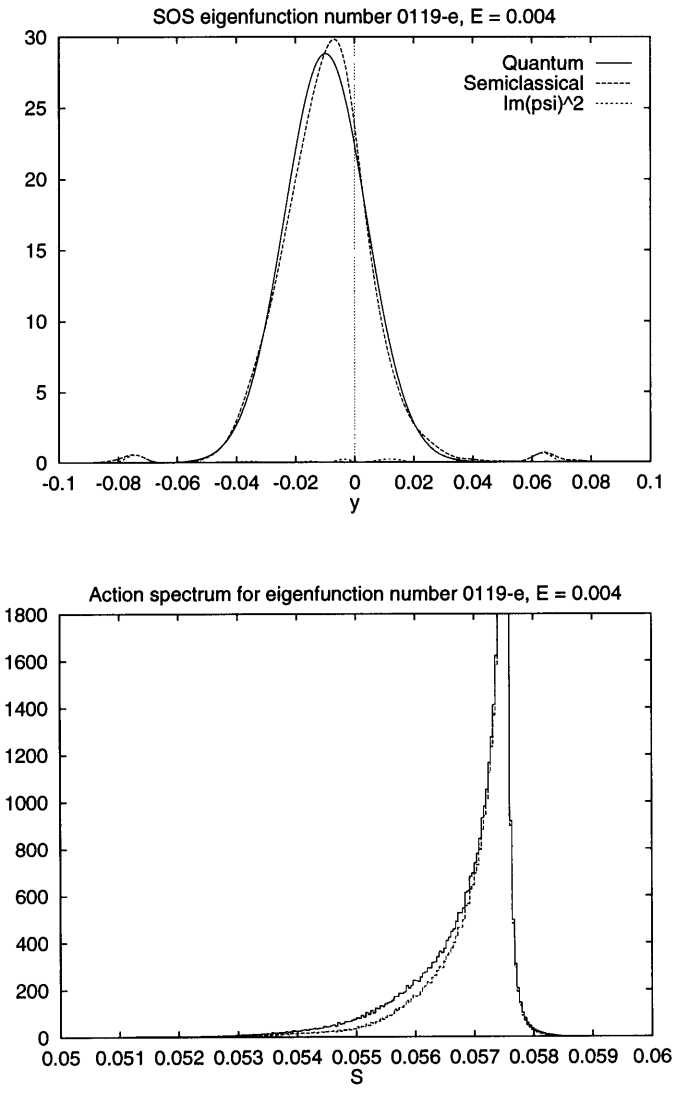

Figure A-12: SOS eigenfunction and action spectrum, 119th even eigenstate. Exact $1/\hbar = 2562.81$; $\Delta(1/\hbar) = -1.72$; magnitude of T eigenvalue $|t_i| = 0.920$.

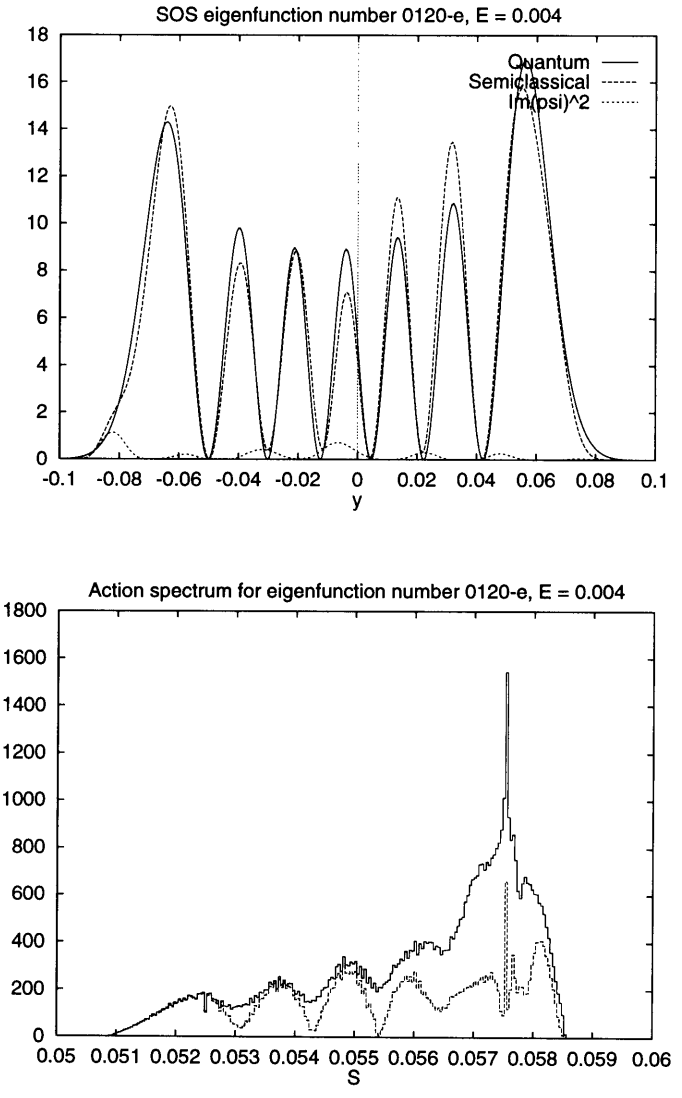

Figure A-13: SOS eigenfunction and action spectrum, 120th even eigenstate. Exact $1/\hbar = 2567.54$; $\Delta(1/\hbar) = -2.26$; magnitude of T eigenvalue $|t_i| = 0.903$.

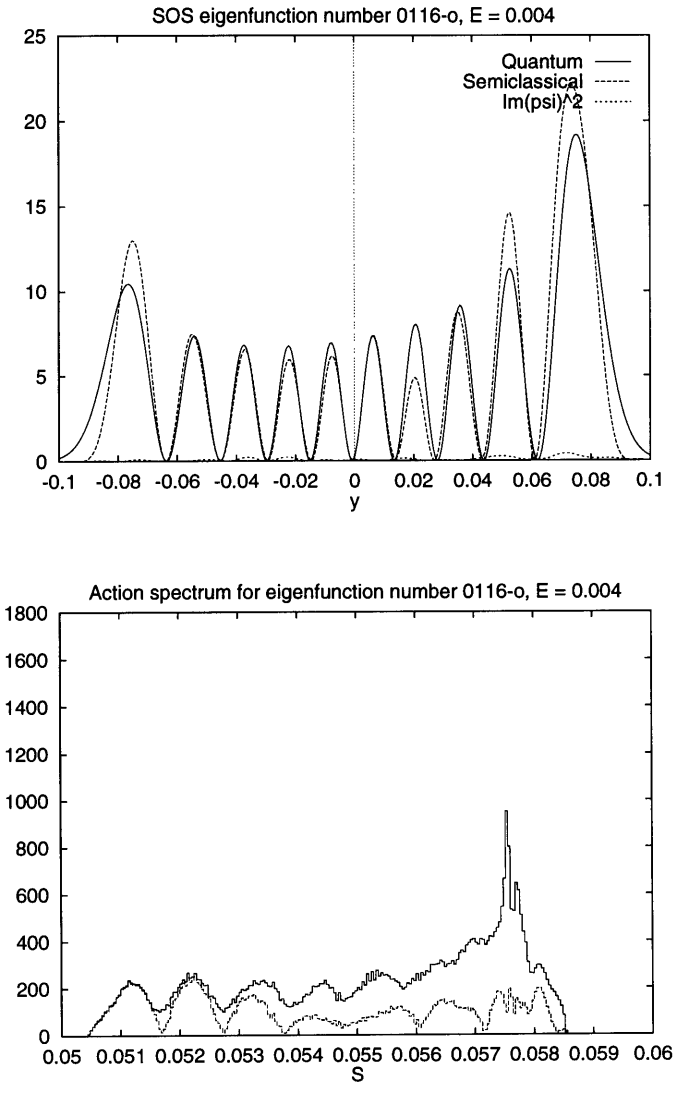

Figure A-14: SOS eigenfunction and action spectrum, 116th odd eigenstate. Exact $1/\hbar = 2579.16$; $\Delta(1/\hbar) = -5.46$; magnitude of T eigenvalue $|t_i| = 0.646$.

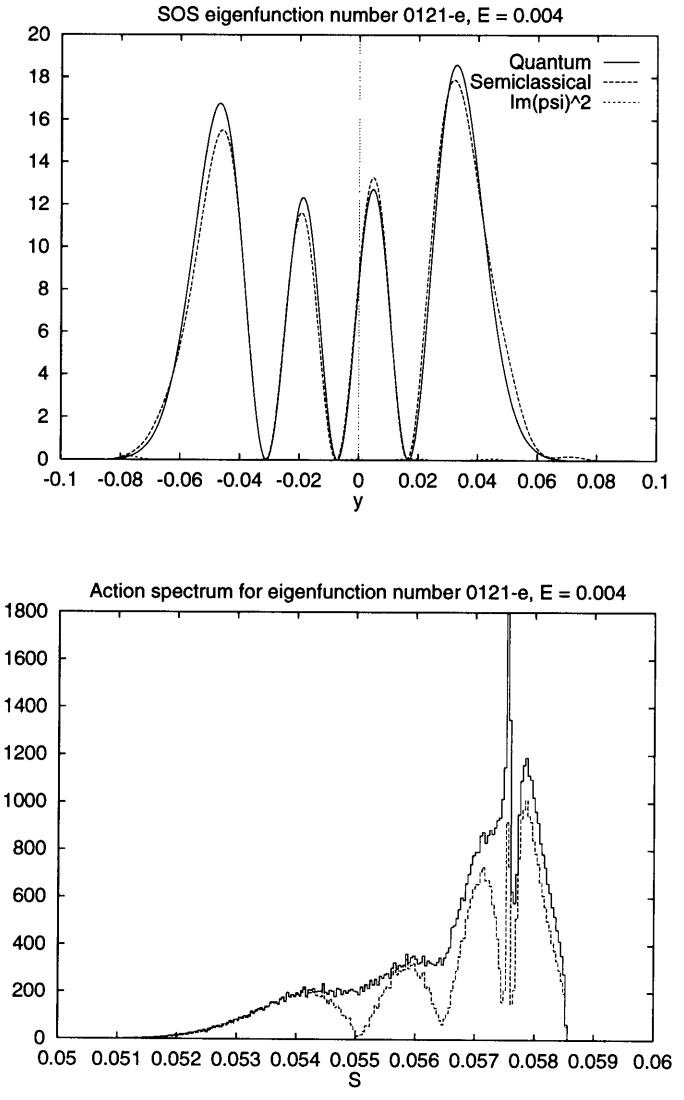

Figure A-15: SOS eigenfunction and action spectrum, 121st even eigenstate. Exact $1/\hbar = 2580.81$; $\Delta(1/\hbar) = -0.16$; magnitude of T eigenvalue $|t_i| = 1.103$.

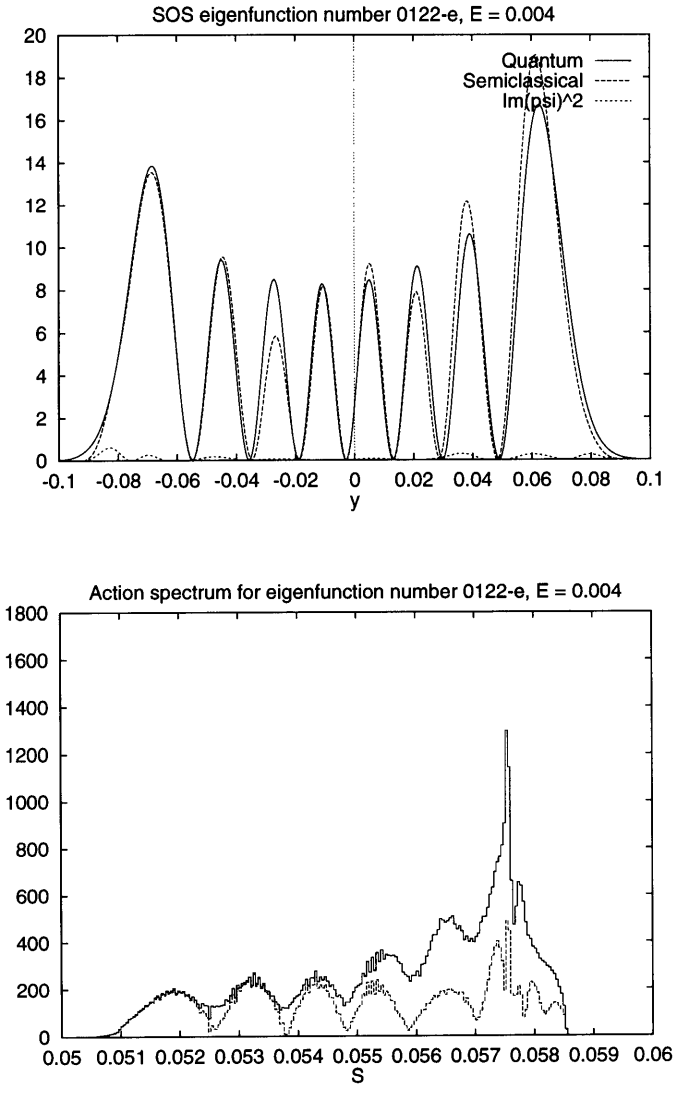

Figure A-16: SOS eigenfunction and action spectrum, 122nd even eigenstate. Exact $1/\hbar = 2593.72$; $\Delta(1/\hbar) = -3.85$; magnitude of T eigenvalue $|t_i| = 0.792$.

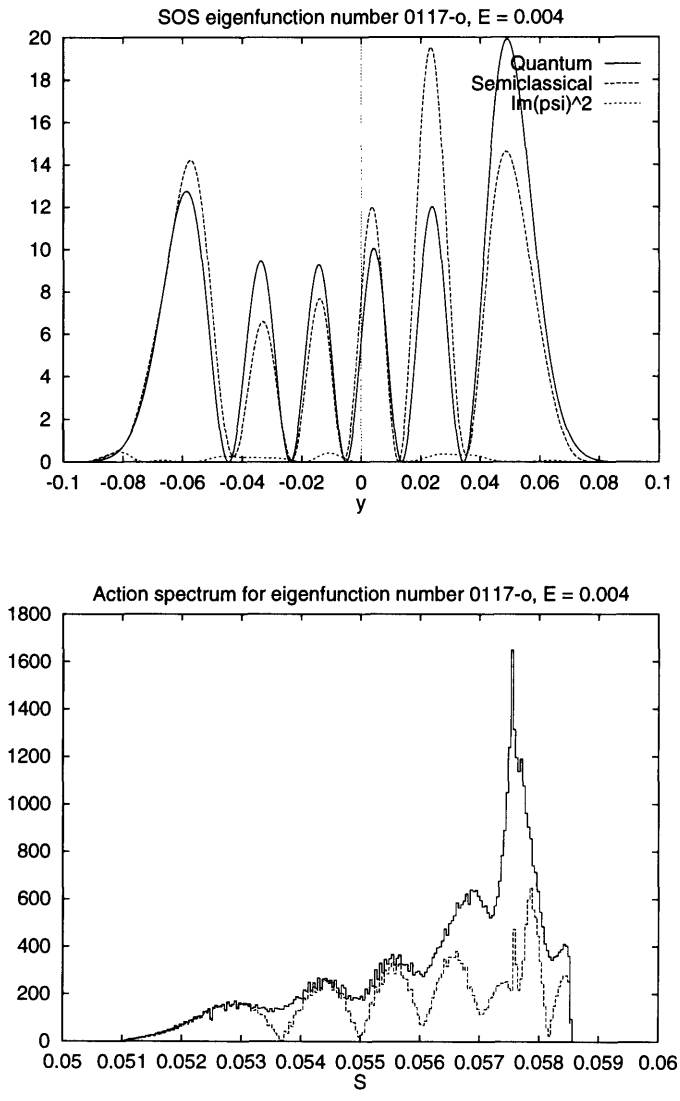

Figure A-17: SOS eigenfunction and action spectrum, 117th odd eigenstate. Exact $1/\hbar = 2594.07$; $\Delta(1/\hbar) = -1.06$; magnitude of T eigenvalue $|t_i| = 0.968$.

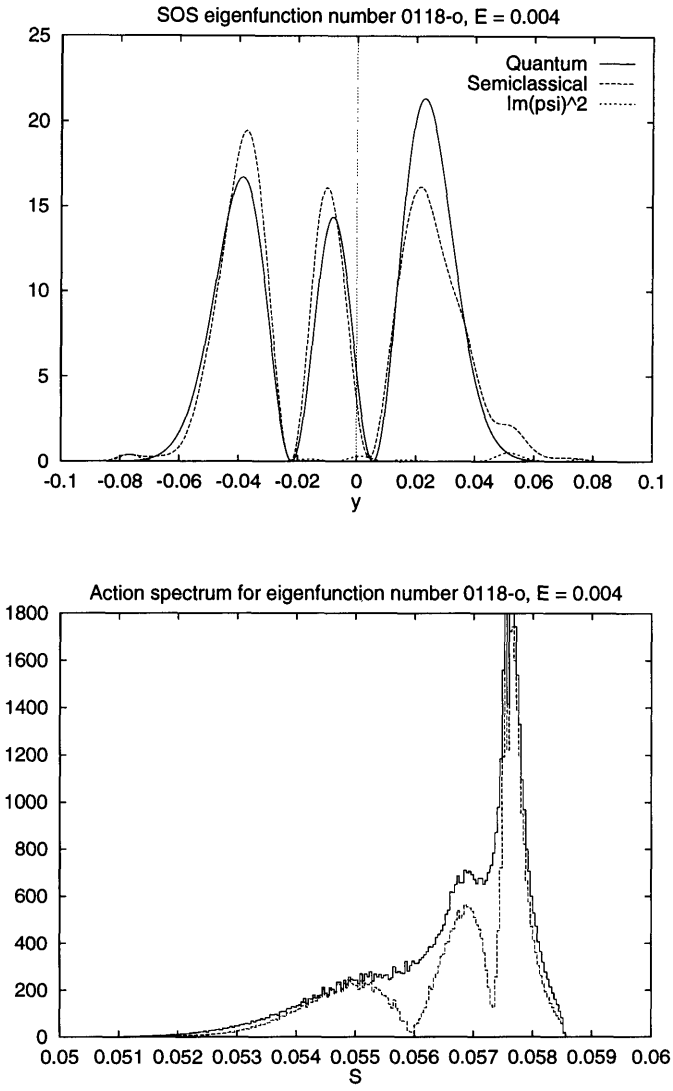

Figure A-18: SOS eigenfunction and action spectrum, 118th odd eigenstate. Exact $1/\hbar = 2596.53$; $\Delta(1/\hbar) = -0.80$; magnitude of T eigenvalue $|t_i| = 1.093$.

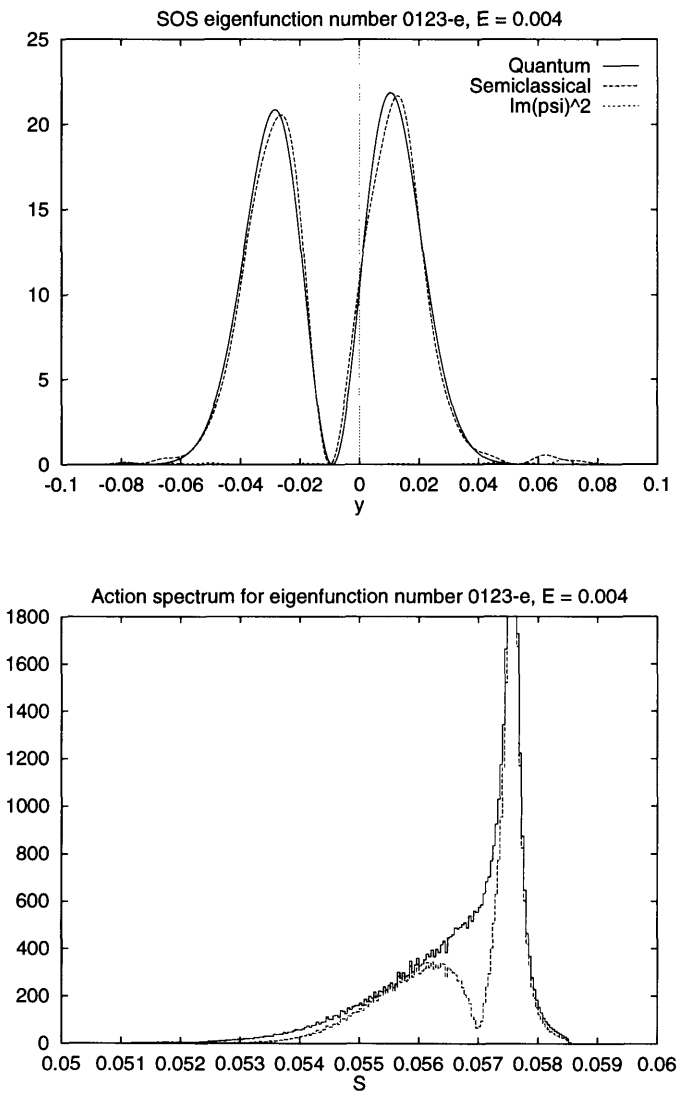

Figure A-19: SOS eigenfunction and action spectrum, 123rd even eigenstate. Exact $1/\hbar = 2608.72$; $\Delta(1/\hbar) = -1.38$; magnitude of T eigenvalue $|t_i| = 1.021$.

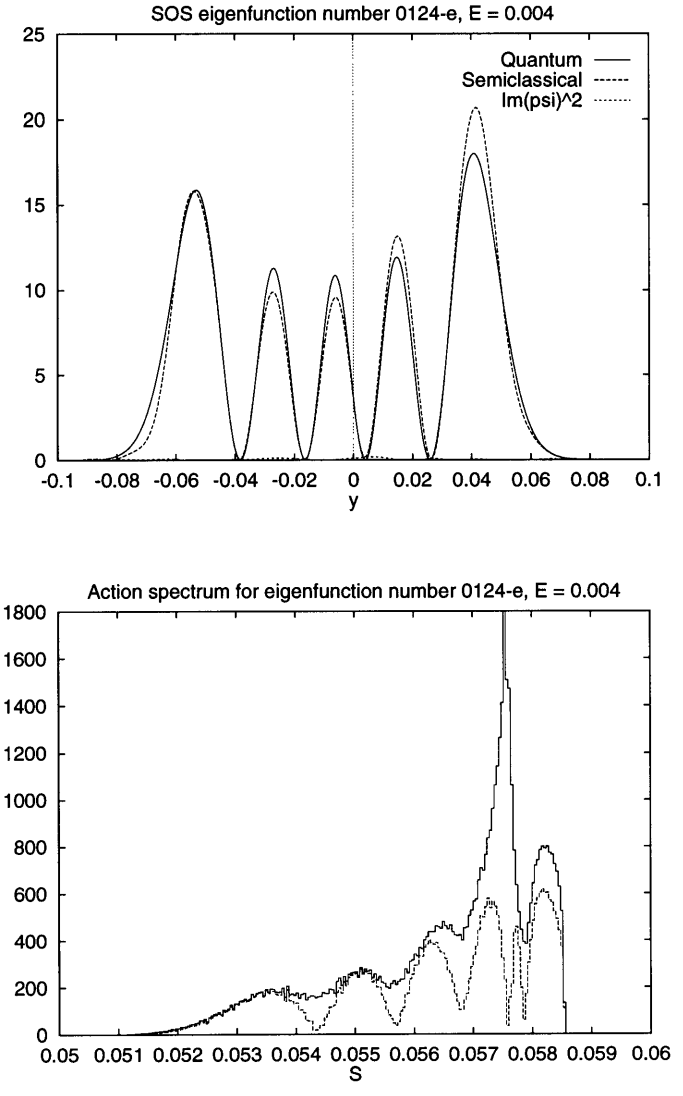

Figure A-20: SOS eigenfunction and action spectrum, 124th even eigenstate. Exact $1/\hbar = 2616.79$; $\Delta(1/\hbar) = -4.75$; magnitude of T eigenvalue $|t_i| = 0.784$.

A.2 Chaotic regime: $E = 0.2$

The figures in this section are for energy 0.2, which is in the mostly chaotic regime. The eigenstates covered are the 20 in the classicity range $50 \leq 1/\hbar \leq 52.2$.

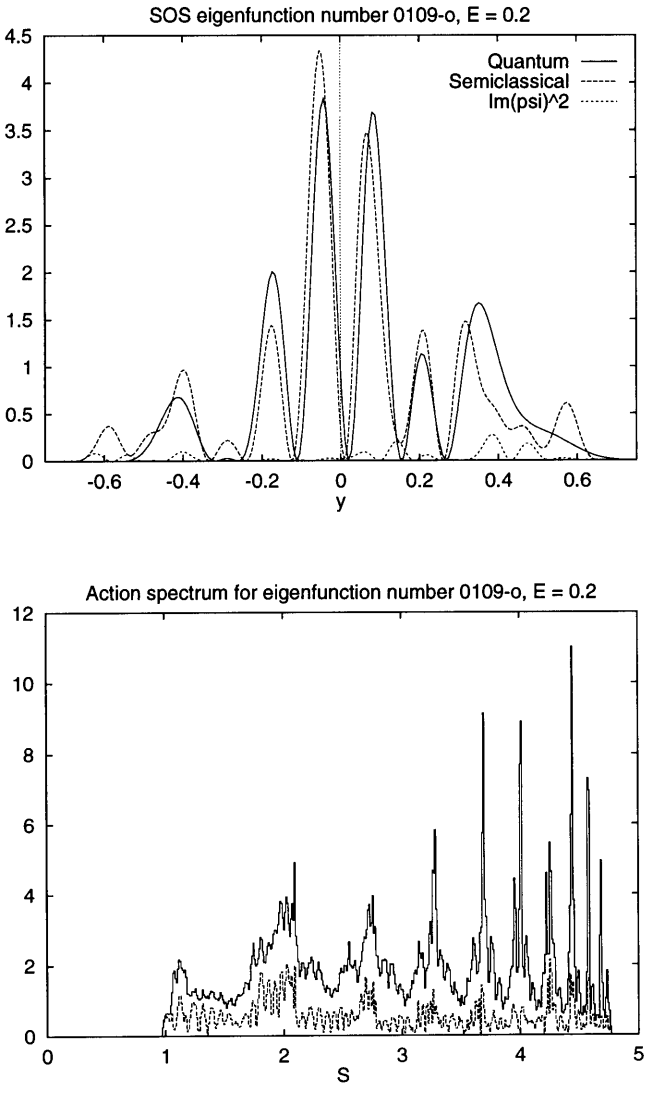

Figure A-21: SOS eigenfunction and action spectrum, 109th odd eigenstate. Exact $1/\hbar = 50.1654$; $\Delta(1/\hbar) = -0.0421$; magnitude of T eigenvalue $|t_i| = 0.973$.

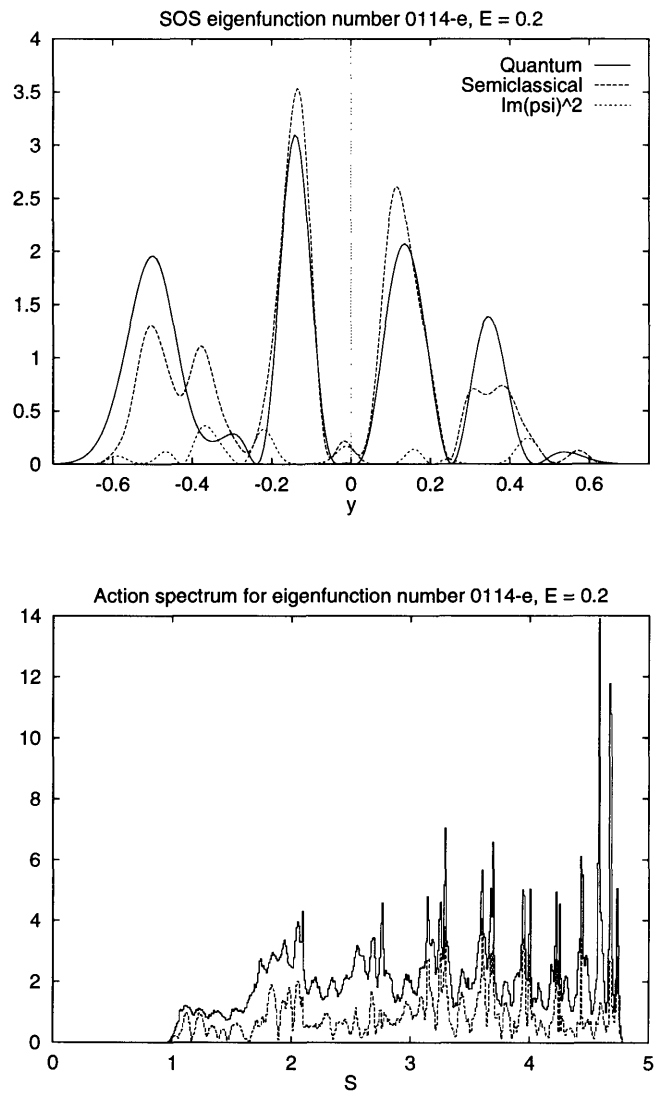

Figure A-22: SOS eigenfunction and action spectrum, 114th even eigenstate. Exact $1/\hbar = 50.2430$; $\Delta(1/\hbar) = -0.0325$; magnitude of T eigenvalue $|t_i| = 1.019$.

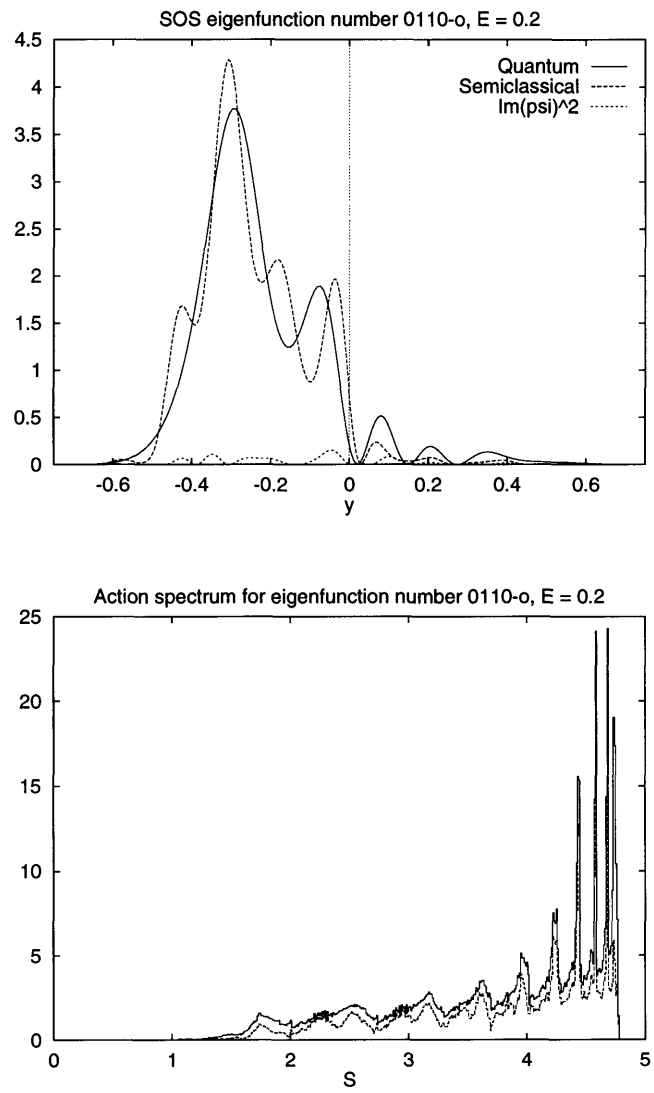

Figure A-23: SOS eigenfunction and action spectrum, 110th odd eigenstate. Exact $1/\hbar = 50.2787$; $\Delta(1/\hbar) = -0.0060$; magnitude of T eigenvalue $|t_i| = 1.248$.

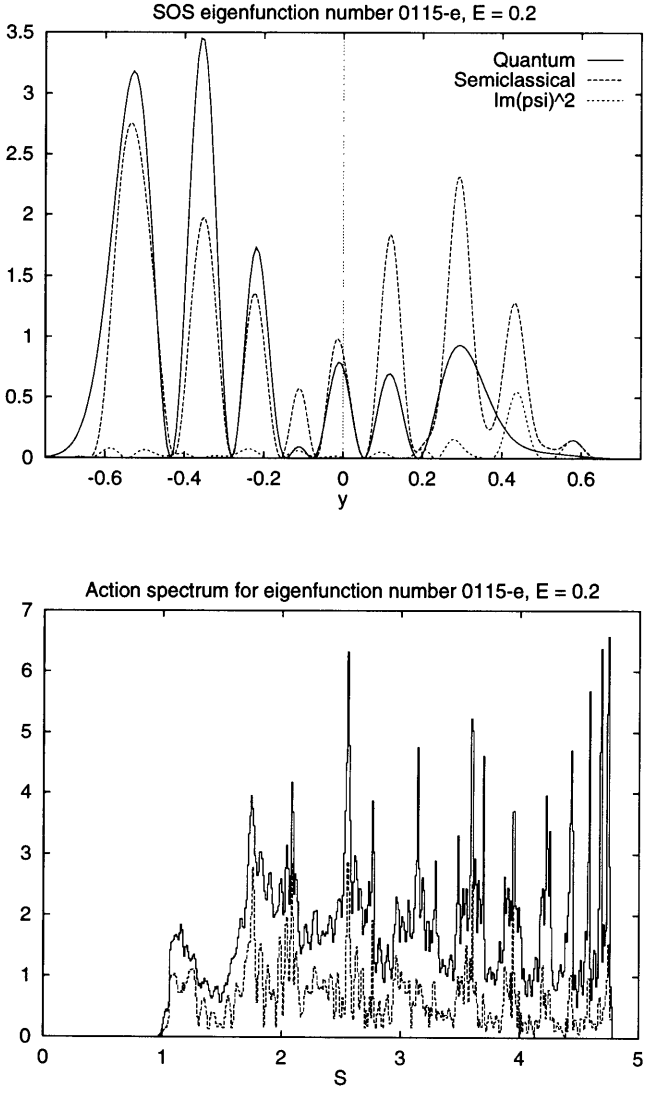

Figure A-24: SOS eigenfunction and action spectrum, 115th even eigenstate. Exact $1/\hbar = 50.3252$; $\Delta(1/\hbar) = -0.0526$; magnitude of T eigenvalue $|t_i| = 0.994$.

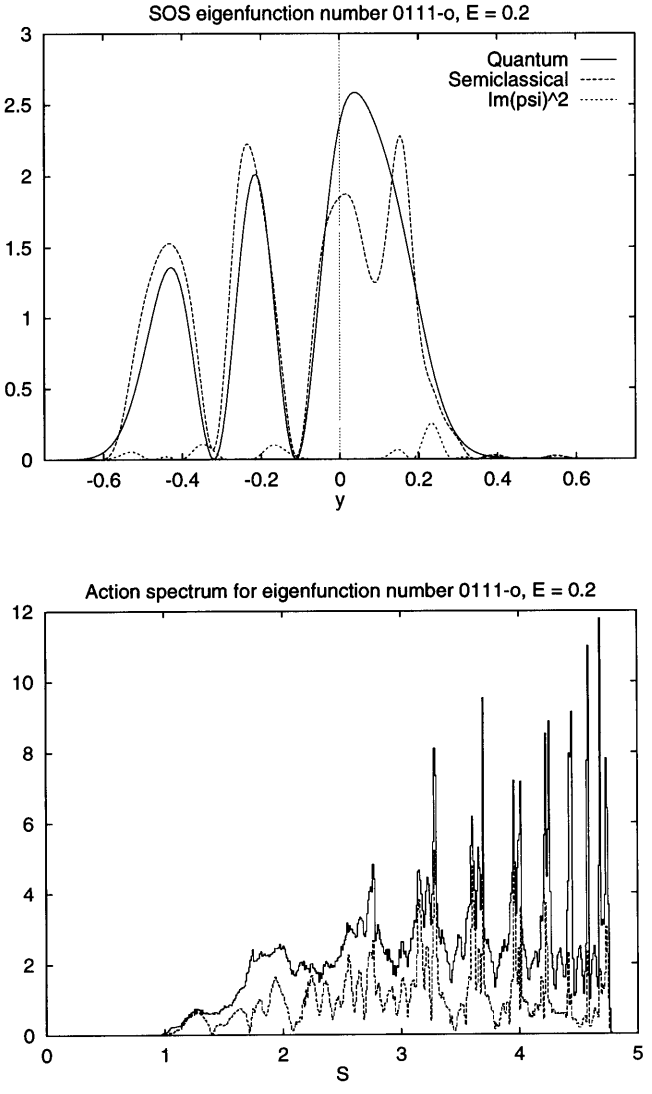

Figure A-25: SOS eigenfunction and action spectrum, 111th odd eigenstate. Exact $1/\hbar = 50.5255$; $\Delta(1/\hbar) = -0.0418$; magnitude of T eigenvalue $|t_i| = 1.064$.

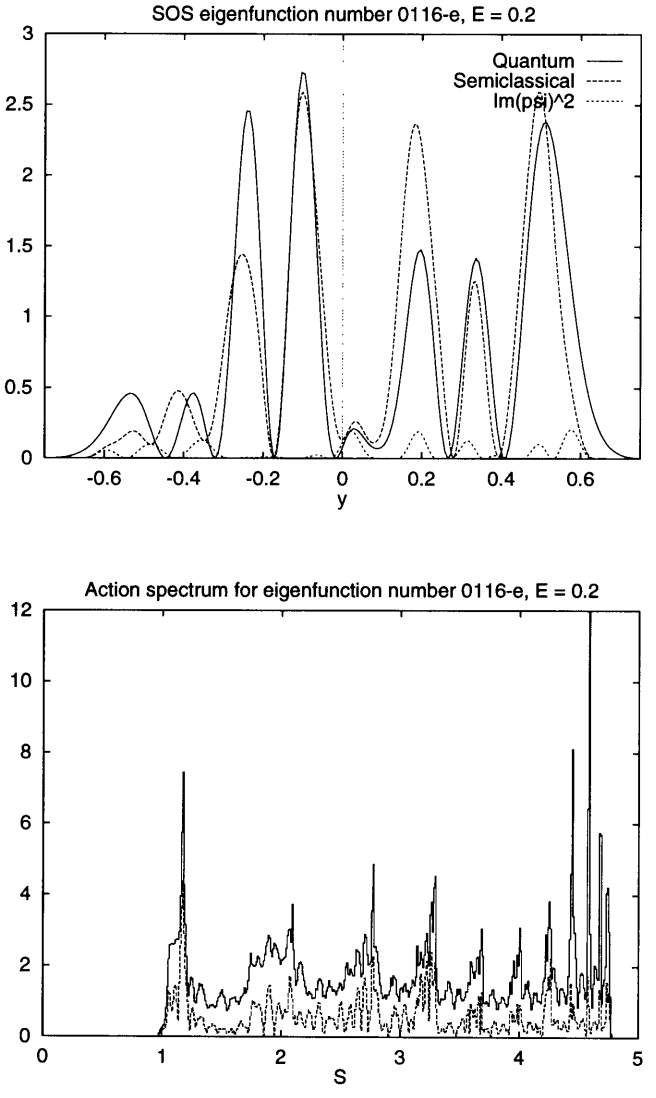

Figure A-26: SOS eigenfunction and action spectrum, 116th even eigenstate. Exact $1/\hbar = 50.7136$; $\Delta(1/\hbar) = 0.0534$; magnitude of T eigenvalue $|t_i| = 0.927$.

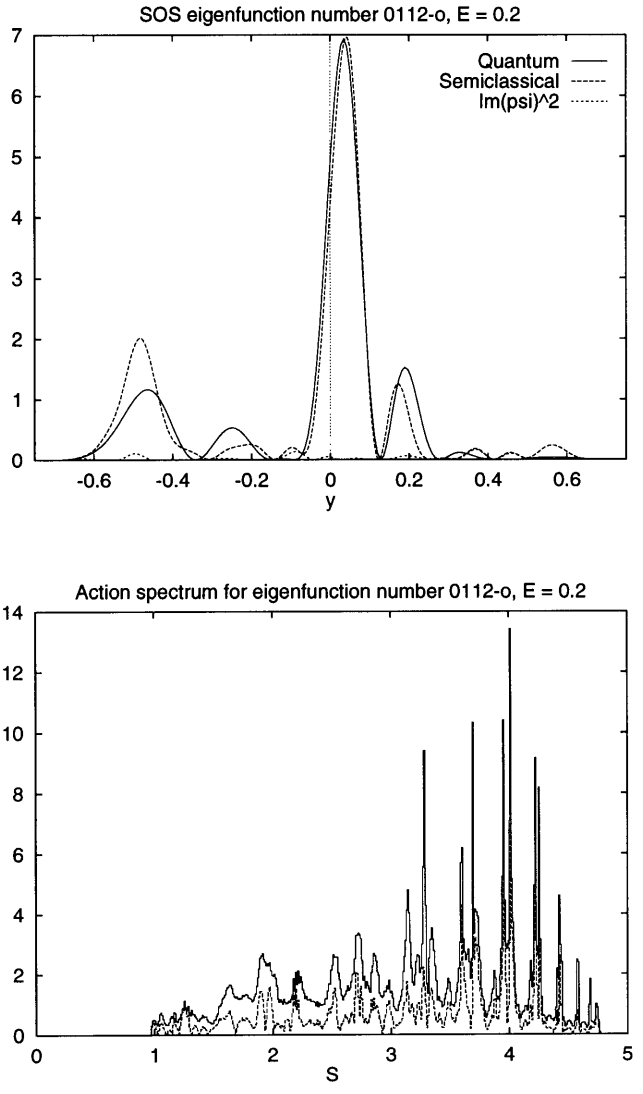

Figure A-27: SOS eigenfunction and action spectrum, 112th odd eigenstate. Exact $1/\hbar = 50.8336$; $\Delta(1/\hbar) = 0.0066$; magnitude of T eigenvalue $|t_i| = 1.026$.

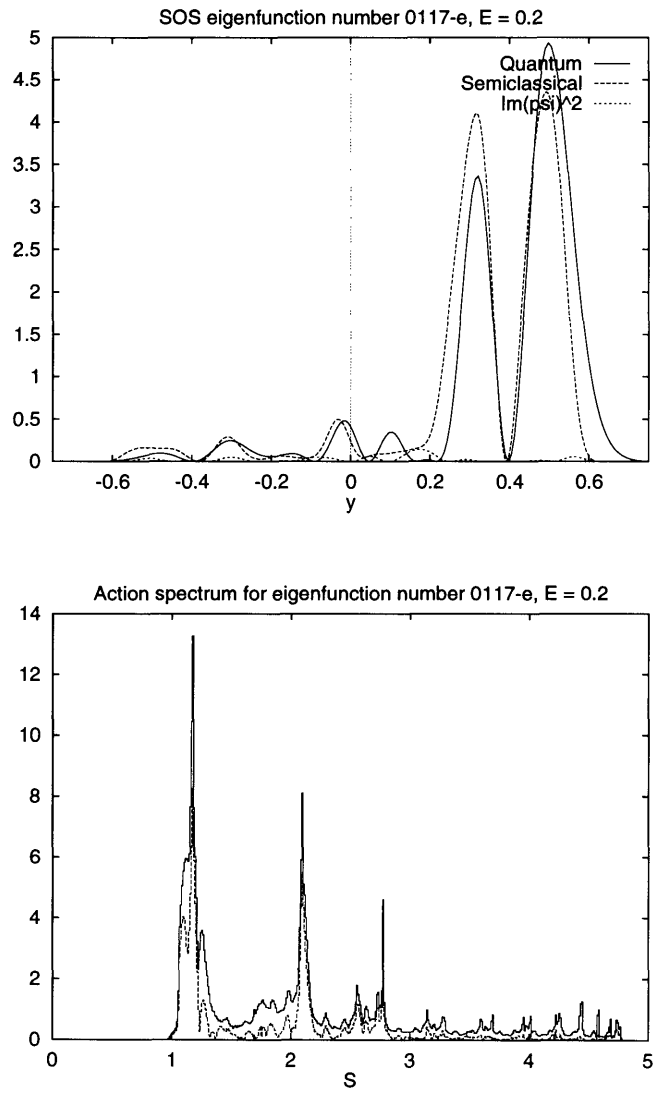

Figure A-28: SOS eigenfunction and action spectrum, 117th even eigenstate. Exact $1/\hbar = 50.9286$; $\Delta(1/\hbar) = -0.0016$; magnitude of T eigenvalue $|t_i| = 1.042$.

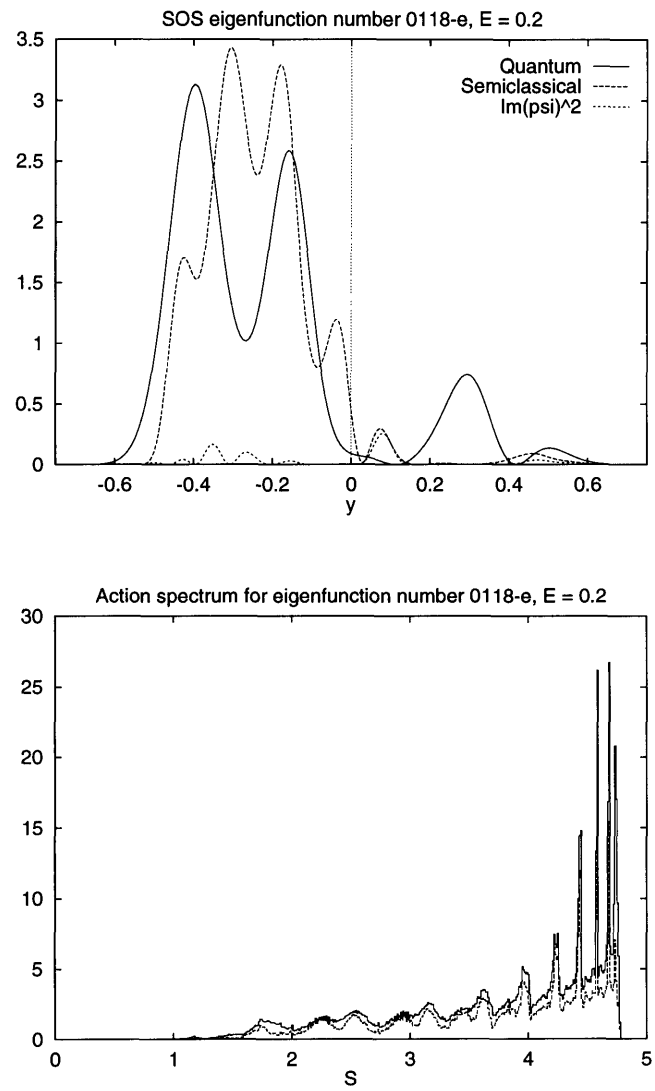

Figure A-29: SOS eigenfunction and action spectrum, 118th even eigenstate. Exact $1/\hbar = 50.9683$; $\Delta(1/\hbar) = -0.0065$; magnitude of T eigenvalue $|t_i| = 1.249$.

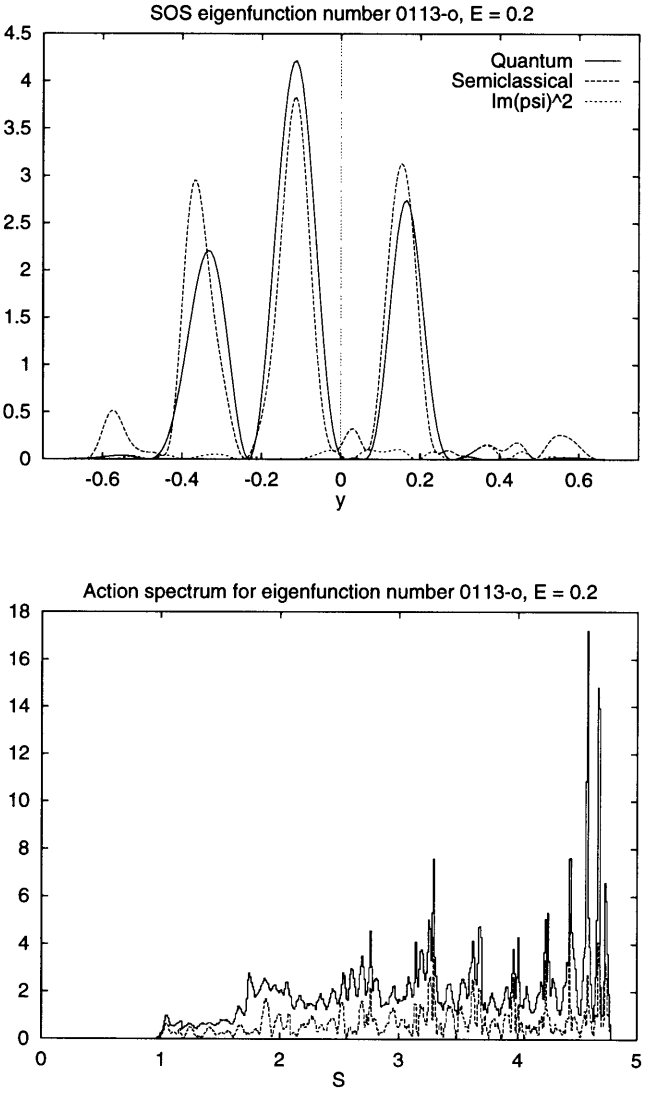

Figure A-30: SOS eigenfunction and action spectrum, 113th odd eigenstate. Exact $1/\hbar = 51.0808$; $\Delta(1/\hbar) = -0.0344$; magnitude of T eigenvalue $|t_i| = 0.973$.

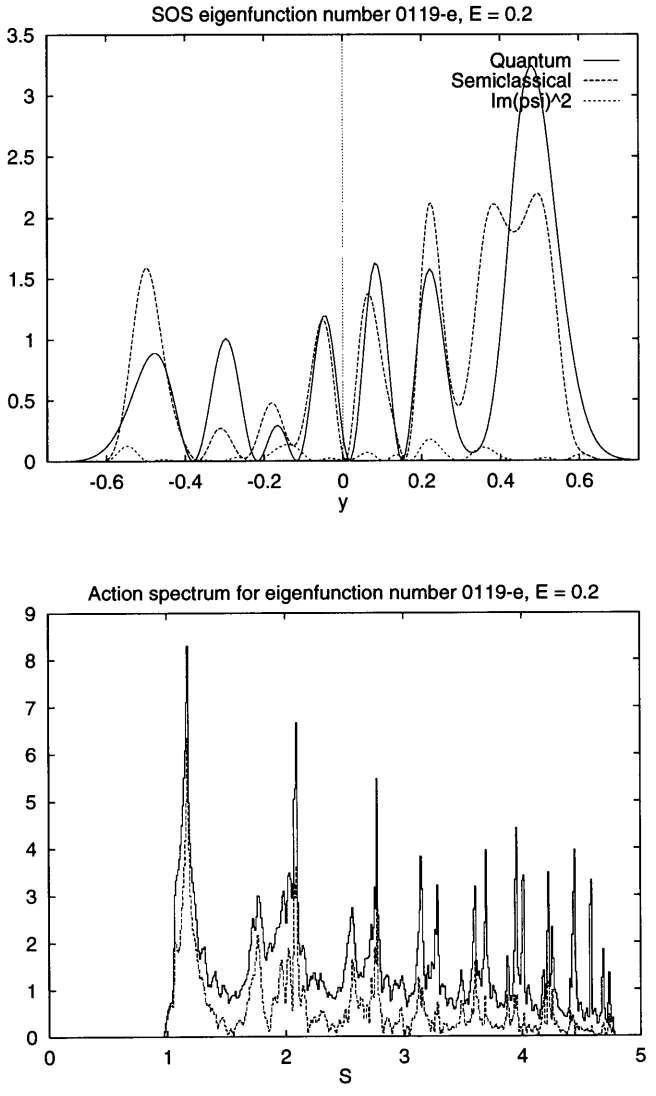

Figure A-31: SOS eigenfunction and action spectrum, 119th even eigenstate. Exact $1/\hbar = 51.0978$; $\Delta(1/\hbar) = -0.0617$; magnitude of T eigenvalue $|t_i| = 0.833$.

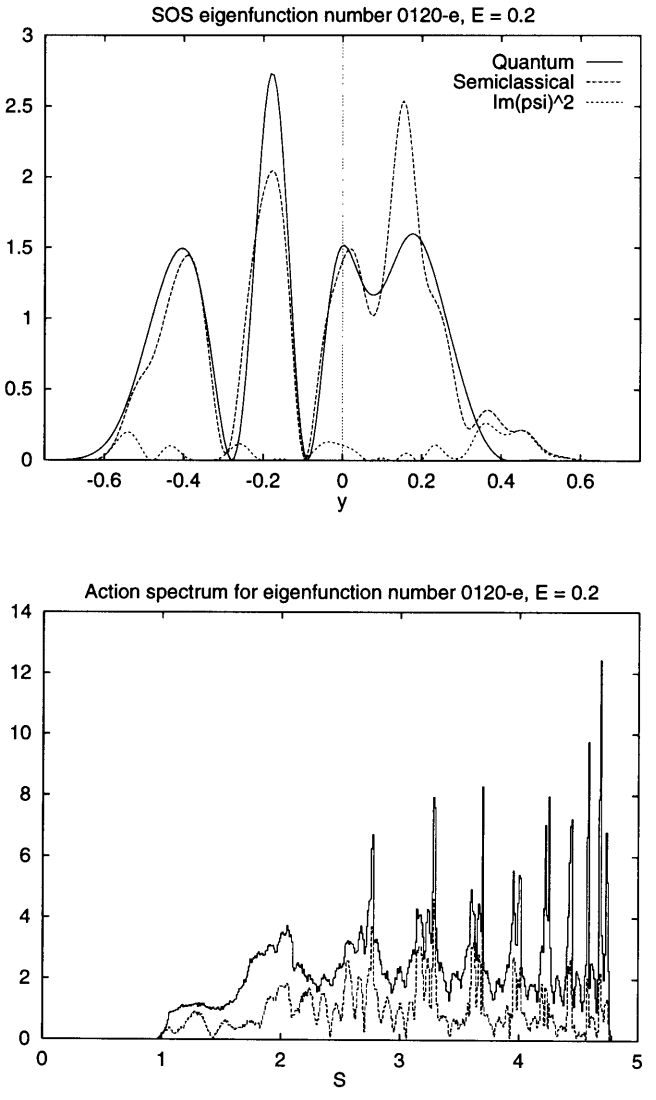

Figure A-32: SOS eigenfunction and action spectrum, 120th even eigenstate. Exact $1/\hbar = 51.3907$; $\Delta(1/\hbar) = -0.0451$; magnitude of T eigenvalue $|t_i| = 0.999$.

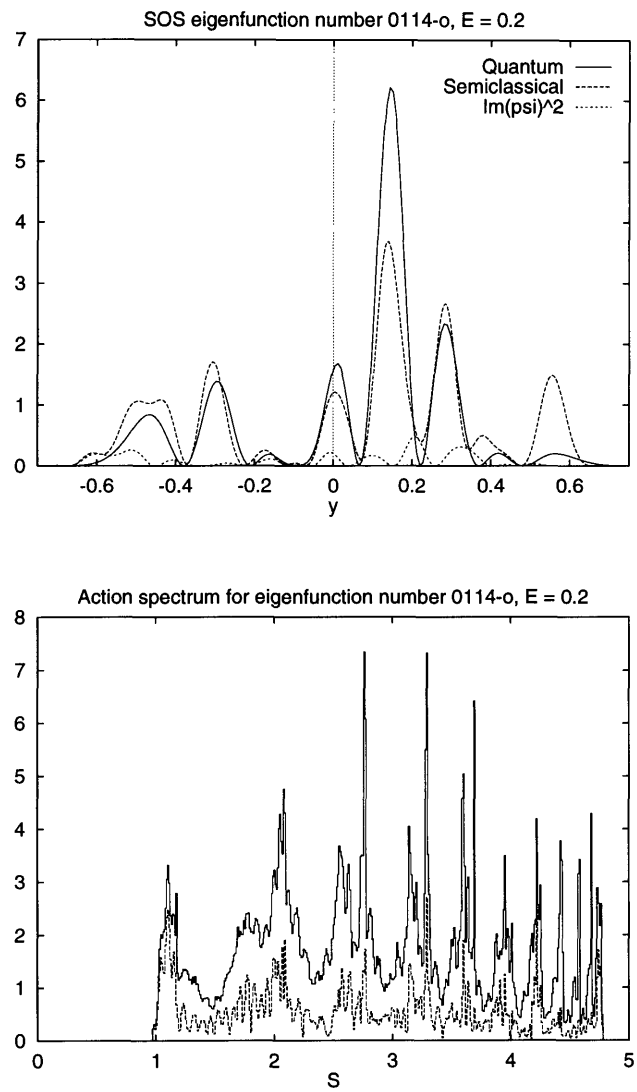

Figure A-33: SOS eigenfunction and action spectrum, 114th odd eigenstate. Exact $1/\hbar = 51.4824$; $\Delta(1/\hbar) = -0.0064$; magnitude of T eigenvalue $|t_i| = 0.890$.

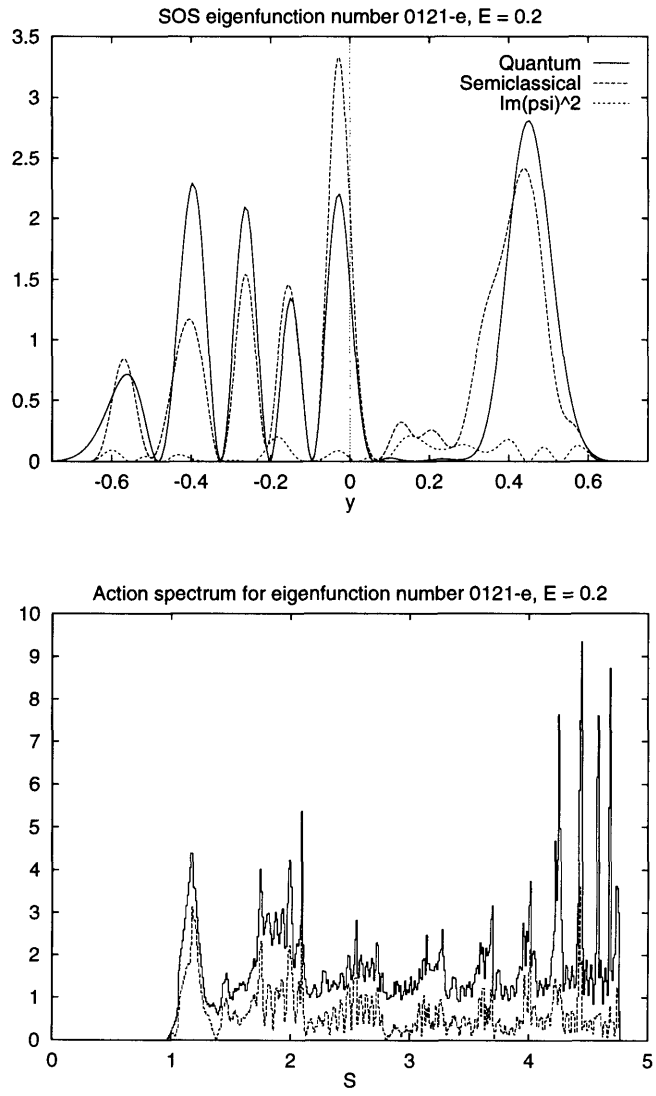

Figure A-34: SOS eigenfunction and action spectrum, 121st even eigenstate. Exact $1/\hbar = 51.5683$; $\Delta(1/\hbar) = -0.0942$; magnitude of T eigenvalue $|t_i| = 0.940$.

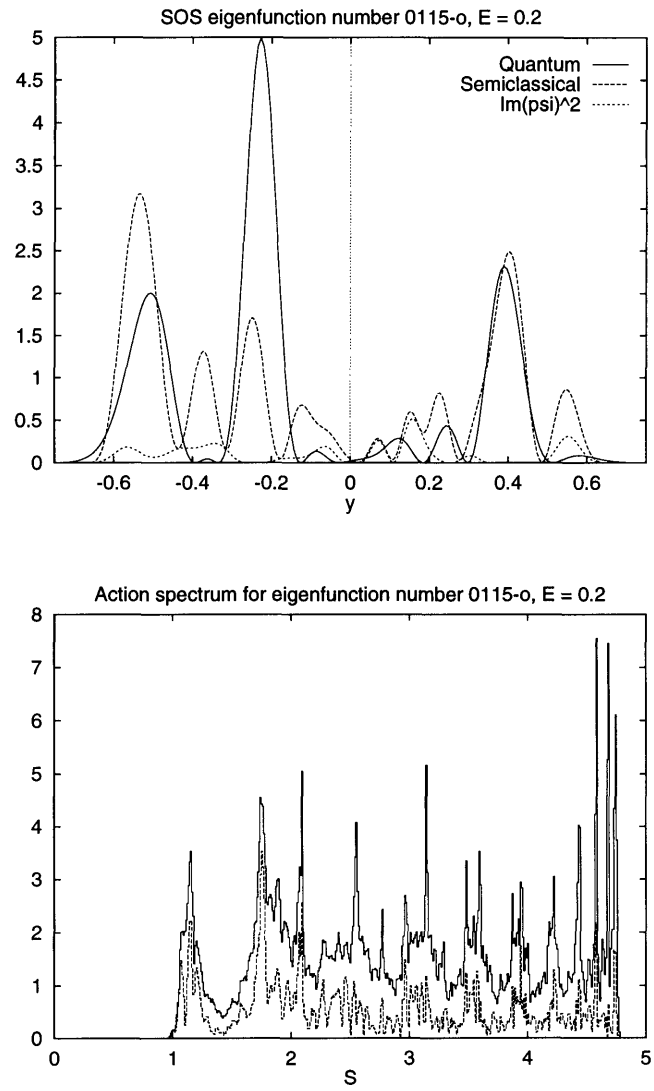

Figure A-35: SOS eigenfunction and action spectrum, 115th odd eigenstate. Exact $1/\hbar = 51.6258$; $\Delta(1/\hbar) = -0.0067$; magnitude of T eigenvalue $|t_i| = 0.998$.

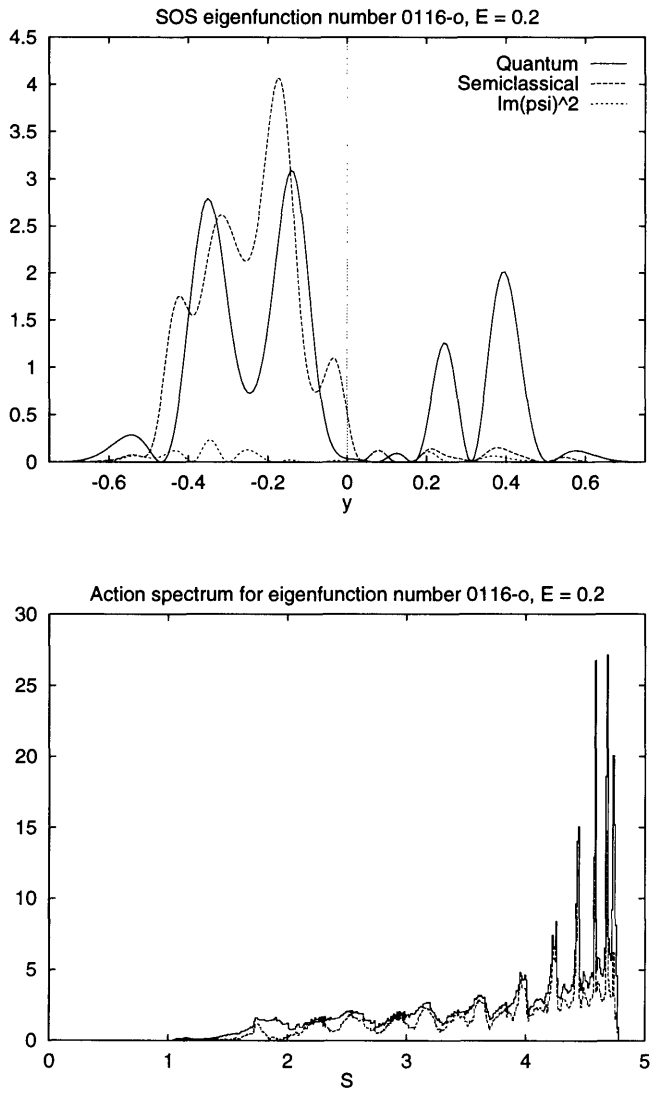

Figure A-36: SOS eigenfunction and action spectrum, 116th odd eigenstate. Exact $1/\hbar = 51.6768$; $\Delta(1/\hbar) = -0.0237$; magnitude of T eigenvalue $|t_i| = 1.267$.

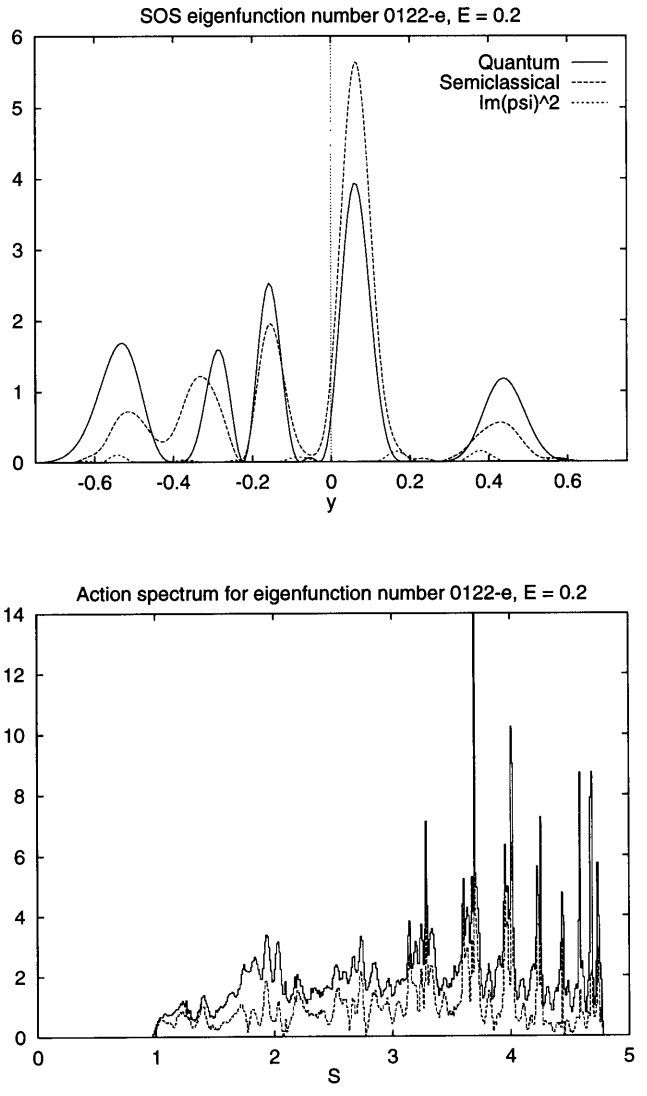

Figure A-37: SOS eigenfunction and action spectrum, 122nd even eigenstate. Exact $1/\hbar = 51.7800$; $\Delta(1/\hbar) = -0.0407$; magnitude of T eigenvalue $|t_i| = 1.026$.

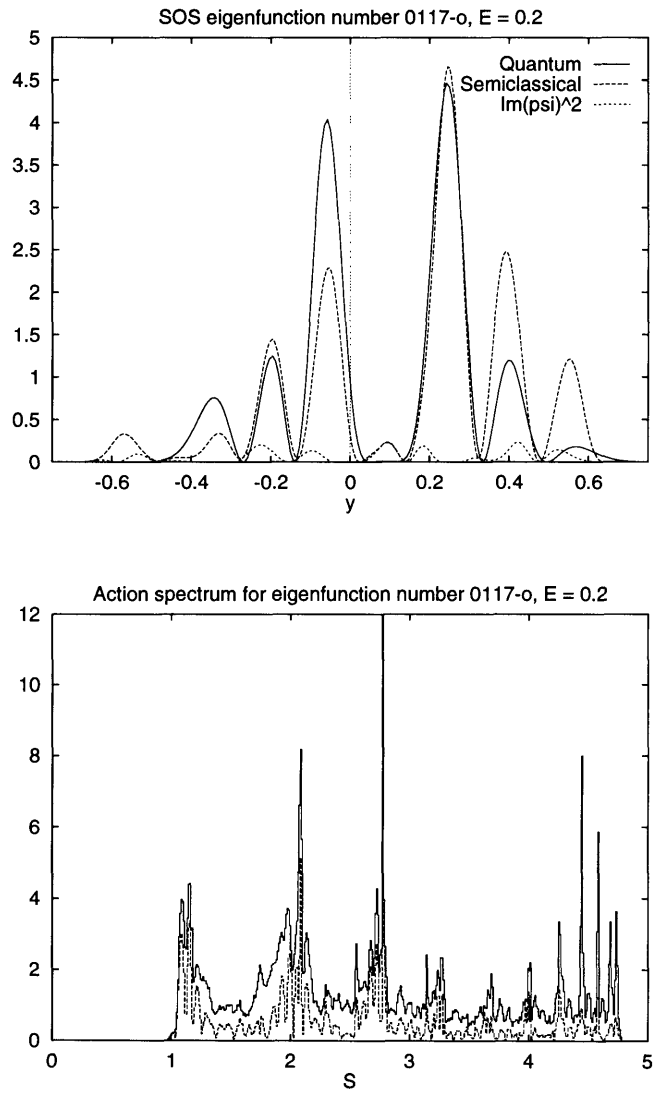

Figure A-38: SOS eigenfunction and action spectrum, 117th odd eigenstate. Exact $1/\hbar = 51.8046$; $\Delta(1/\hbar) = 0.0285$; magnitude of T eigenvalue $|t_i| = 1.000$.

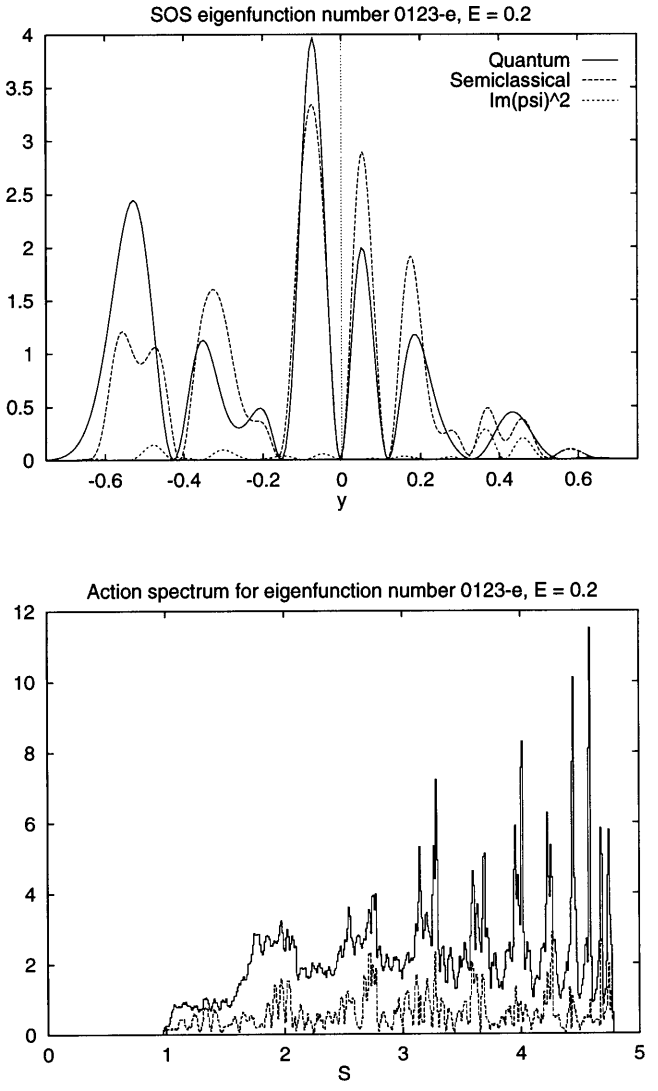

Figure A-39: SOS eigenfunction and action spectrum, 123rd even eigenstate. Exact $1/\hbar = 52.0133$; $\Delta(1/\hbar) = 0.0268$; magnitude of T eigenvalue $|t_i| = 0.980$.

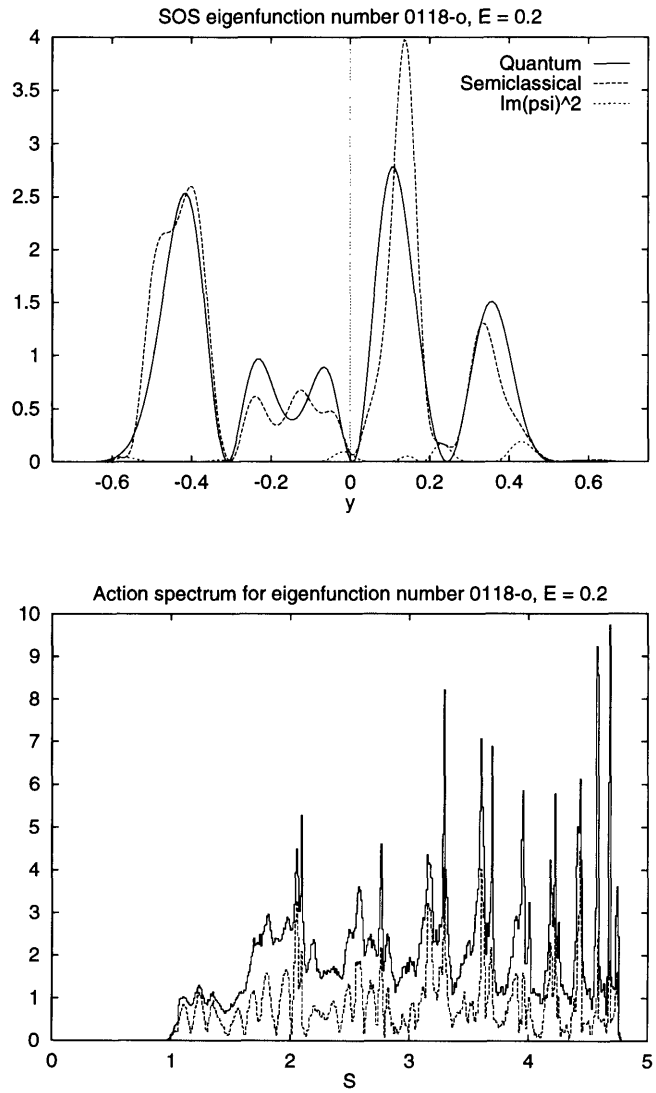

Figure A-40: SOS eigenfunction and action spectrum, 118th odd eigenstate. Exact $1/\hbar = 52.1647$; $\Delta(1/\hbar) = -0.0017$; magnitude of T eigenvalue $|t_i| = 0.924$.

Appendix B

Rescaling the Nelson$_2$ Potential

In this appendix, we discuss the rescaling of the "Nelson$_2$" potential that we use in the text, and its connection to the scaling for the true Nelson potential used by other authors (for example, [10]). We also discuss a different way of viewing the act of varying Planck's constant (as was done in the main text in the form of the classicity): by adding an additional parameter and rescaling the dynamical variables, the same effect can be obtained while using a constant value for $\hbar$.

B.1 Connection to the "Nelson" potential

The system which has been given the name "Nelson" is defined by

$$\bar{H} = \tfrac{1}{2}\bar{p}_x^2 + \tfrac{1}{2}\bar{p}_y^2 + \tfrac{1}{2}\bar{\mu}\bar{x}^2 + \left(\bar{y} - \tfrac{1}{2}\bar{x}^2\right)^2 \tag{B.1}$$

$$[\bar{q}_{x,y}, \bar{p}_{x,y}] = i\bar{\hbar} \tag{B.2}$$

$$\frac{d\bar{q}_{x,y}}{d\bar{t}} = \frac{\partial \bar{H}}{\partial \bar{p}_{x,y}} \tag{B.3}$$

$$\frac{d\bar{p}_{x,y}}{d\bar{t}} = -\frac{\partial \bar{H}}{\partial \bar{q}_{x,y}} \tag{B.4}$$

Here, overbars are used to distinguish the variables in this scheme from our variables, and we sometimes use the notation q_x for x, etc.

For Nelson$_2$, the analogous equations are as follows:

$$H = \tfrac{1}{2}p_x^2 + \tfrac{1}{2}p_y^2 + \tfrac{1}{2}\omega^2 x^2 + \tfrac{1}{2}\left(y - \tfrac{1}{2}x^2\right)^2 \tag{B.5}$$

$$[q_{x,y}, p_{x,y}] = i\hbar \tag{B.6}$$

$$\frac{dq_{x,y}}{dt} = \frac{\partial H}{\partial p_{x,y}} \tag{B.7}$$

$$\frac{dp_{x,y}}{dt} = -\frac{\partial H}{\partial q_{x,y}} \tag{B.8}$$

The difference is the factor of $\frac{1}{2}$ preceding the nonlinear term in the new scaling, which is convenient because it makes the angular frequency in the vertical direction equal to 1 (rather than $\sqrt{2}$), thereby mildly simplifying many equations by eliminating factors of $\sqrt{2}$.

Clearly the two sets of dynamical variables are related to one another by a simple scaling. In our equations, we make the apparently nonsensical substitutions

$$x \rightarrow \bar{x}\,(x/\bar{x})$$

etc., in order to isolate the parenthesised ratio on the right, which is purely numerical (and we also make the temporary identification $\bar{\mu} \equiv \bar{\omega}^2$). The result is

$$\begin{aligned}\bar{H}\left(H/\bar{H}\right) \;=\; & \tfrac{1}{2}\bar{p_x}^2\,(p_x/\bar{p_x})^2 + \tfrac{1}{2}\bar{p_y}^2\,(p_y/\bar{p_y})^2 \\ & + \tfrac{1}{2}\bar{\mu}\,(\mu/\bar{\mu})\,\bar{x}^2\,(x/\bar{x})^2 + \tfrac{1}{2}\left(\bar{y}\,(y/\bar{y}) - \tfrac{1}{2}\bar{x}^2\,(x/\bar{x})^2\right)^2\end{aligned}$$

$$[\bar{q}_{x,y}, \bar{p}_{x,y}]\,(q_{x,y}/\bar{q}_{x,y})\,(p_{x,y}/\bar{p}_{x,y}) = i\bar{\hbar}\left(\hbar/\bar{\hbar}\right)$$

$$\frac{d\bar{q}_{x,y}}{d\bar{t}}\frac{(q_{x,y}/\bar{q}_{x,y})}{(t/\bar{t})} = \frac{\partial \bar{H}}{\partial \bar{p}_{x,y}}\frac{\left(H/\bar{H}\right)}{(p_{x,y}/\bar{p}_{x,y})}$$

$$\frac{d\bar{p}_{x,y}}{d\bar{t}}\frac{(p_{x,y}/\bar{p}_{x,y})}{(t/\bar{t})} = -\frac{\partial \bar{H}}{\partial \bar{q}_{x,y}}\frac{\left(H/\bar{H}\right)}{(q_{x,y}/\bar{q}_{x,y})}$$

If we now require that these equations be equivalent to Nelson's, we are left with

constraints on the dimensionless ratios. The independent constraints are:

$$(p_{x,y}/\bar{p}_{x,y})^2 = \left(H/\bar{H}\right)$$

$$(\mu/\bar{\mu})\,(x/\bar{x})^2 = \left(H/\bar{H}\right)$$

$$(y/\bar{y})^2 = 2\left(H/\bar{H}\right)$$

$$(x/\bar{x})^2 = (y/\bar{y})$$

$$(q_{x,y}/\bar{q}_{x,y})\,(p_{x,y}/\bar{p}_{x,y}) = \left(H/\bar{H}\right)(t/\bar{t}) = \left(\hbar/\bar{\hbar}\right)$$

These eight equations contain eight unknowns (namely the dimensionless ratios), and can be solved simply; take their logarithms, for example, and they become a coupled set of eight linear equations. Their solution gives the relationship between our variables and the (overbarred) variables of Nelson:

$$q_{x,y} = \bar{q}_{x,y}$$

$$p_{x,y} = \tfrac{1}{\sqrt{2}}\bar{p}_{x,y}$$

$$H = \tfrac{1}{2}\bar{H}$$

$$\omega^2 = \tfrac{1}{2}\bar{\mu}$$

$$t = \sqrt{2}\,\bar{t}$$

$$\hbar = \tfrac{1}{\sqrt{2}}\bar{\hbar}$$

$$S = \tfrac{1}{\sqrt{2}}\bar{S}$$

We should point out that our numerical experiments were done at a value of $\omega = \sqrt{0.05}$ which is equivalent to the choice $\bar{\mu} = 0.1$ often used in Nelson potential analyses. Our energies $E = 0.004$ and $E = 0.2$ are equivalent to Nelson energies $\bar{E} = 0.008$ and $\bar{E} = 0.4$.

The form of one useful expression, for the desymmetrized Thomas-Fermi smoothed

density of states, will be given in each of the two scaling schemes. Up to the second term in $\bar{\hbar}$, it has the following form for the Nelson scaling [13]:

$$N(< \bar{E} \text{ or } < (1/\bar{\hbar})) = \frac{\bar{E}^2}{\bar{\hbar}^2}\frac{1}{4\sqrt{2\bar{\mu}}}\left[1 \pm \frac{\sqrt{\bar{\mu}}\,\bar{\hbar}}{\bar{E}} - \frac{\bar{\hbar}^2}{12}\left(\frac{\bar{\mu}+2}{\bar{E}^2} + \frac{2}{\bar{\mu}\bar{E}}\right) + \mathcal{O}(\bar{\hbar}^4)\right].$$

(The + and − correspond, respectively, to the densities for even and odd parity states.) The analogous expression for the Nelson$_2$ rescaling is:

$$N(< E \text{ or } < (1/\hbar)) = \frac{E^2}{4\hbar^2\omega}\left[1 \pm \frac{\hbar\omega}{E} - \frac{\hbar^2}{12}\left(\frac{\omega^2+1}{E^2} + \frac{1}{\omega^2 E}\right) + \mathcal{O}(\hbar^4)\right].$$

B.2 Making $\hbar$ constant again

As mentioned in the text, changing $\hbar$ (in the form of the classicity) is equivalent to a rescaling of the other dynamical variables. In the following we show how it is possible to give $\hbar$ back the constant value that Mother Nature intended (namely 1) by inserting a different parameter, $\tilde{\alpha}$, in the system. The system of equations which we now wish to compare to equation (B.5) is as follows:

$$\tilde{H} = \tfrac{1}{2}\tilde{p_x}^2 + \tfrac{1}{2}\tilde{p_y}^2 + \tfrac{1}{2}\tilde{\omega}^2\tilde{x}^2 + \tfrac{1}{2}\left(\tilde{y} - \tfrac{1}{2}\tilde{\alpha}^2\tilde{x}^2\right)^2 \tag{B.9}$$

$$[\tilde{q}_{x,y}, \tilde{p}_{x,y}] = i \tag{B.10}$$

$$\frac{d\tilde{q}_{x,y}}{d\tilde{t}} = \frac{\partial\tilde{H}}{\partial\tilde{p}_{x,y}} \tag{B.11}$$

$$\frac{d\tilde{p}_{x,y}}{d\tilde{t}} = -\frac{\partial\tilde{H}}{\partial\tilde{q}_{x,y}} \tag{B.12}$$

and we now want to find the connection between the quantities with tildes and the quantities without tildes.

Like before, we isolate the ratios of old to new variables, and solve for the ratios *and now* $\tilde{\alpha}$, *too* in terms of $\hbar$. The process is straightforward, so we only state the results: if Nelson$_2$ (equation (B.5)) has a particular value of $\hbar$, then equation (B.9)

has identical behavior when the following relationships hold:

$$\tilde{q}_{x,y} = q_{x,y}/\sqrt{\hbar}$$

$$\tilde{p}_{x,y} = p_{x,y}/\sqrt{\hbar}$$

$$\tilde{H} = H/\hbar$$

$$\tilde{\omega} = \omega$$

$$\tilde{t} = t$$

$$\tilde{\alpha} = \hbar$$

$$\tilde{\hbar} = 1$$

$$\tilde{S} = S/\hbar$$

Bibliography

[1] M.C. Gutzwiller, *J. Math. Phys.* **8**, 1979 (1967).

[2] M.C. Gutzwiller, *J. Math. Phys.* **10**, 1004 (1969).

[3] M.C. Gutzwiller, *J. Math. Phys.* **11**, 1791 (1970).

[4] M.C. Gutzwiller, *J. Math. Phys.* **12**, 343 (1971).

[5] E.B. Bogomolny, *Nonlinearity* **5**, 805 (1992).

[6] B. Lauritzen, *Chaos* **2**, 409 (1992).

[7] E.B. Bogomolny and M. Carioli, *Physica D* **67**, 88 (1993).

[8] T. Szeredi, J.H. Lefebvre, and D.A. Goodings, to be published.

[9] P.A. Boasman, Ph.D. thesis (1992).

[10] M. Baranger and K.T.R. Davies, *Ann. Phys.* **177**, 330 (1987).

[11] J.M. Robbins, *Nonlinearity* **4**, 343 (1991).

[12] B. Eckhardt and D. Wintgen, *J. Phys. A: Math Gen.* **24**, 4335 (1991).

[13] D. Provost, Ph.D. thesis (1992).